

MODELING AND SOLVING LARGE-SCALE OPTIMIZATION PROBLEMS:
CASE STUDIES IN RENEWABLE ENERGY AND MINING

by
Oluwaseun B. Ogunmodede

Copyright by Oluwaseun B. Ogunmodede 2021

All Rights Reserved

A thesis submitted to the Faculty and the Board of Trustees of the Colorado School of Mines in partial fulfillment of the requirements for the degree of Doctor of Philosophy (Operations Research with Engineering).

Golden, Colorado

Date _____

Signed: _____

Oluwaseun B. Ogunmodede

Signed: _____

Dr. Alexandra Newman
Thesis Advisor

Signed: _____

Dr. Gregory Bogin Jr.
Thesis Advisor

Golden, Colorado

Date _____

Signed: _____

Dr. John Berger
Professor and Head
Department of Mechanical Engineering

ABSTRACT

Large-scale optimization modeling is becoming more prevalent in industry practices. As computational hardware and software continue to improve, the problems practitioners attempt to solve increase in complexity. We explain in detail how to improve the tractability and efficiency of large-scale models with the use of the following techniques: *(i)* Data management, *(ii)* efficient formulations, *(iii)* numerical analysis, *(iv)* heuristics, *(v)* specialized algorithms, and *(vi)* decomposition techniques. We apply these techniques to real-world problems in heavy-industry applications: renewable-energy and mining. The former consists of a design and dispatch model that incorporates renewable energy technologies, combined heat and power, and conventional generation. The latter is an underground production scheduling model that considers ventilation and refrigeration while managing heat load output. We highlight the importance and benefits of the modeling techniques in each of the applications, and discuss improvements with respect to the applications we model. The energy application exhibits savings of millions of dollars using an optimized solution. The underground production scheduling model admits feasible solutions where they had not previously been generated. In both applications, we significantly expedite solutions, allowing for optimization approaches to be used where they would otherwise be considered too slow for operational use.

CONTENTS

Abstract	iii
List of Figures	viii
List of Tables	xi
ACKNOWLEDGMENTS	xiii
Chapter 1 INTRODUCTION	1
Chapter 2 OPTIMIZING DESIGN AND DISPATCH OF A RENEWABLE ENERGY SYSTEM	5
2.1 Introduction	6
2.2 Literature Review	8
2.3 Model Inputs and Structure	13
2.3.1 Model Inputs	13
2.3.2 Model Structure	14
2.4 Optimization Model (\mathcal{R})	16
2.4.1 Sets and Parameters	17
2.4.2 Variables	19
2.4.3 Objective Function	21
2.4.4 Constraints	22
2.4.4.1 Fuel constraints	22
2.4.4.2 Production Constraints	22
2.4.4.3 Storage System Constraints	23
2.4.4.4 Production Incentives	24
2.4.4.5 Power Rating	24
2.4.4.6 Load Balancing and Grid Sales	25
2.4.4.7 Rate Tariff Constraints	26
2.4.4.8 Minimum Utility Charge	28
2.4.4.9 Non-negativity	28

2.4.4.10	Integrality	29
2.5	Case Studies.....	29
2.5.1	Optimization.....	30
2.5.2	Integration	32
2.5.3	Complex Utility Rate Structures	36
2.5.4	Incentives.....	38
2.5.5	Summary	39
2.6	Conclusions and Future Work	40
Chapter 3	OPTIMIZING DESIGN AND DISPATCH OF A RENEWABLE ENERGY SYSTEM WITH COMBINED HEAT AND POWER	41
3.1	Introduction.....	41
3.2	Literature Review.....	43
3.3	Mathematical Formulation	45
3.3.1	Sets and Parameters.....	47
3.3.2	Variables	50
3.3.3	Objective Function	51
3.3.4	Constraints	52
3.3.4.1	Fuel constraints	52
3.3.4.2	Thermal production constraints.....	52
3.3.4.3	Storage System Constraints	53
3.3.4.4	Production Constraints	55
3.4	Solution Methodology	56
3.4.1	Introducing tailored data structures	56
3.4.2	Efficiently handling data	57
3.4.3	Reformulation with streamlined variables	59
3.5	Data and Results	63
3.5.1	Model Statistics.....	63
3.5.2	Model Performance	64

3.5.3	Model Dispatch Strategy.....	66
3.6	Conclusions.....	68
Chapter 4	UNDERGROUND PRODUCTION SCHEDULING WITH VENTILATION AND REFRIGERATION CONSIDERATIONS.....	70
4.1	Introduction.....	71
4.1.1	Mine Planning.....	73
4.1.2	Mine Ventilation.....	74
4.2	Literature Review.....	76
4.2.1	Production Scheduling.....	76
4.3	Underground Mine Ventilation.....	78
4.3.1	Heat from Diesel Equipment.....	81
4.3.2	Heat from Auto-compression.....	83
4.3.3	Heat from Strata Rock.....	83
4.4	Ventilation Formulation (\mathcal{O}).....	84
4.5	Solution Methodology.....	88
4.5.1	Reformulation of (\mathcal{O}).....	89
4.5.2	Propagated Early Start Algorithm.....	91
4.5.3	Optimization-Based Heuristic (\mathcal{H}).....	91
4.6	Results.....	94
4.6.1	Equipment overview.....	95
4.6.2	Computation.....	95
4.6.3	Managerial Insights.....	98
4.7	Conclusions and Future Research Directions.....	100
Chapter 5	CONCLUSION.....	103
	Bibliography.....	105
Appendix A	SUPPLEMENTAL DATA FOR CHAPTER 2.....	117
A.1	117
A.1.1	Renewable Energy.....	118

A.1.2	Load Profile	119
A.1.3	Technical and Economic Parameters	120
Appendix B	SUPPLEMENTAL FORMULATION FOR CHAPTER 3	122
B.1	Appendix	122
B.1.1	Production Incentives	123
B.1.2	Power Rating	123
B.1.3	Load Balancing and Grid Sales	124
B.1.4	Rate Tariff Constraints	125
B.1.5	Minimum Utility Charge	127
B.1.6	Non-negativity	128
B.1.7	Integrality	128
Appendix C	NECESSARY PERMISSIONS FOR REPRODUCTION	130
C.1	Image Permissions	130
C.2	Co-Author Permissions	131
C.3	Publisher Permissions	133

LIST OF FIGURES

Figure 2.1	The REopt Lite system, where the blue boxes above, to the left of and underneath the center box containing the model name are inputs, and the green boxes to the right of center display the outputs (OSTI, 2020).	7
Figure 2.2	Comparison of single and multi-technology system dispatch on peak demand day in San Diego	34
Figure 2.3	Comparison of dispatch under time-of-use and flat rate structures on a peak demand day	38
Figure 3.1	A notional distributed generation system with a collection of technologies (including thermal energy storage (TES)) available for electrical, heating, and cooling loads; the technologies highlighted in blue represent a baseline case without distributed resources. Dashed boxes on the right side of the image represent loads that depend on cooling dispatch decisions when an absorption chiller is available. Image adapted from: Anderson et al. (2021).	42
Figure 3.2	A categorical overview of the decision variables, objective function, and constraints that compose the REopt Lite optimization model, $(\widehat{\mathcal{R}})$, where SOC and O&M denote state of charge, and operations and maintenance, respectively.	46
Figure 3.3	A network flow representation of electrical load balancing in the reformulated model, using a PV system and a battery as the on-site technologies.	62
Figure 3.4	Dispatch summary for one week within Case 9, in which the technologies reduce peak electrical power consumption from the utility while meeting all hourly site loads	67
Figure 4.1	Diagram of Open Pit and Underground Mine (Reused with permission by Epiroc: Hamrin (1980))	72
Figure 4.2	Diagrams of the two different mining methods (Reused with permission by Epiroc: Atlas Copco (2007))	73
Figure 4.3	Diagram of a basic ventilation network (Reused with permission by creator: Larson (2021))	75
Figure 4.4	Respective inputs and outputs modeled in GT-SUITE (Nichols et al., 2019)	82

Figure 4.5	Flowchart of necessary attributes from activities such as loading (bottom-left: Agnor (2017)) and hauling ore (bottom-right: Adwo (2020)) to produce an optimal heat-constrained production schedule considering ventilation and refrigeration	88
Figure 4.6	Percentage of usage for each type of equipment	95
Figure 4.7	The diagram shows the relevant area of the mine, which is comprised of a mixture of sublevel stoping and sublevel caving, in which the former occurs above the black horizontal line, while the latter is executed below the black horizontal line.....	96
Figure 4.8	Comparison of the respective formulations based on daily haulage, where (\mathcal{R}^-) is the standard formulation, (\mathcal{R}) is the simplistic fix to formulation (\mathcal{R}^-) , and (\mathcal{R}^+) is the proposed formulation	99
Figure 4.9	Comparison of the respective formulation types based on end-of-day temperature outputs on the lowest level of the mine, where (\mathcal{R}^-) is the standard formulation, (\mathcal{R}) is the simplistic fix to formulation (\mathcal{R}^-) , and (\mathcal{R}^+) is the proposed formulation	100
Figure 4.10	Comparison of the remaining heat-feasible schedules based on daily heat output on the lowest level in the mine, where (\mathcal{R}) is the simplistic fix to formulation (\mathcal{R}^-) , and (\mathcal{R}^+) is the proposed formulation	100
Figure A.1	San Diego Utility Tariiff Energy TOU period schedule (Ong and McKeel, 2012)	117
Figure A.2	San Diego Utility Tariiff Demand TOU period schedule (Ong and McKeel, 2012)	118
Figure A.3	Each location’s wind and solar production factors over the course of a representative year	119
Figure A.4	Each location’s electric demand for a week in the winter and summer	120
Figure C.1	Permission granted for Figures 4.1, 4.2a, and 4.2b by Epiroc	130
Figure C.2	Permission granted for Figure 4.3 by Dr. Mark Larson	131
Figure C.3	Permission granted for use of Chapter 2 by co-authors Kate Anderson and Dylan Cutler	131
Figure C.4	Permission granted for use of Chapter 3 by co-authors Dr. Alexander Zolan and Jusse Hirwa	132

Figure C.5 Permission granted for use of Chapter 4 by co-authors Dr. Andrea Brickey
and Patricio Lamas132

Figure C.6 Permission not required for use of Chapter 2 by Publisher Elsevier133

LIST OF TABLES

Table 2.3	Characteristics for each location detailing the building type, utility company name and rate structure.....	30
Table 2.4	Comparison of net present value and characteristics of the solution between those provided by (\mathcal{R}) and the rules of thumb estimation.....	32
Table 2.5	Comparison of net present value and characteristics of the solution provided by (\mathcal{R}) considering one and multiple renewable technologies.....	33
Table 2.6	Energy and demand charges by period for each of the two rate structures... ..	36
Table 2.7	Comparison of technology mix produced by (\mathcal{R}) with differing rate structures; recall that the Base Case represents a utility-power-only solution.	37
Table 2.8	Incentives included in each scenario.....	39
Table 2.9	Comparison of technology mix recommended by model (\mathcal{R}) with incentive inclusion.....	39
Table 3.1	Tailored values, i.e., appropriately sized variable bounds and “big-M values,” where those above the dotted line represent explicit right-hand-side “ b ”-values, while those below represent coefficients on binary variables that are either traditional big-M values or are potential replacements for said values based on improvements to user-specified inputs.	59
Table 3.2	Problem statistics for the 12 cases on which we perform computational experiments comparing model $(\bar{\mathcal{R}})$ and model $(\hat{\mathcal{R}})$	64
Table 3.3	Results comparing solution quality obtained from model $(\bar{\mathcal{R}})$ and model $(\hat{\mathcal{R}})$ within a 10-minute time limit. AMPL and Mosel Xpress settings include <code>backtrack = 5</code> , while AMPL settings specifically include <code>lpthreads = 3</code> , and Mosel settings specifically include <code>mipthreads = 2</code>	65
Table 3.4	Model $(\hat{\mathcal{R}})$ ’s technology mix for Case 9	66
Table 4.1	Engine load details for a representative haul truck	81
Table 4.2	Various formulations used to examine the quality of production schedules ..	95
Table 4.3	Problem instances highlighting the number of total activities, stopping activities, caving levels, and horizons lengths	97

Table 4.4	Solution details of the respective cases.....	98
Table 4.5	Comparison of Case 7 formulations and their respective net present value changes	99
Table A.1	Renewable energy parameters used in (\mathcal{R})	121
Table A.2	System-wide parameters used in (\mathcal{R})	121

ACKNOWLEDGMENTS

First, I want to thank my advisor Dr. Alexandra Newman for all of her guidance, teaching, dedication, and support to me and the Operations Research with Engineering program. I also would like to thank my co-advisor Dr. Gregory Bogin Jr., for being a great role model and providing much wisdom on this journey. Thank you to the committee, Dr. Jürgen Brune, Dr. Jason Porter, and Dr. Tülay Flammang for providing guidance in my research. I especially want to thank Dr. Akshay Chowdu. It has been an absolute pleasure working with you on my mining project. Thank you Kate Anderson at the National Renewable Energy Laboratory for your project leadership and Energy insights. Thank you Dr. Alexander Zolan at NREL for your in-depth understanding of energy modeling systems. Thank you Dr. Aditya Juganda, Jusse Hirwa, Eric Smoorenburg, Sam Nichols, and Kieran Lewis from Colorado School of Mines for assistance on the various research tasks that helped complete this dissertation. Thank you to Dr. Marcos Goycoolea, and Patricio Lamas from Universidad Adolfo Ibañez for your modeling expertise.

Thank you to all of my family and friends that encouraged and supported me. Thank you to my loving wife, Jacqueline, for her patience, kindness, and understanding during this time. Finally, I thank God, for without Him none of this is possible. *Nil Sine Numine, Ad Maiorem Dei Gloriam*

CHAPTER 1

INTRODUCTION

Operations research is a field of study that aids in decision making. More specifically, optimization modeling takes known inputs and prescribes values for unknown quantities so as to achieve a goal while satisfying a set of restrictions. This type of modeling is increasingly being implemented in real-world settings owing to improvements in software and hardware that allow larger and more detailed models to be formulated, and solved. The problem size (defined as the number of variables– unknown quantities– and constraints– restrictions) plays a critical role regarding the speed with which an optimization model produces a (near-)optimal solution. However, there are other factors that influence practical implementation, including the nature of the data and the mathematical structure of the model. To aid in the tractability and efficiency of these large-scale models, the following techniques (among others) can be employed: *(i)* Data management, *(ii)* efficient formulations, *(iii)* numerical analysis, *(iv)* heuristics, *(v)* specialized algorithms, and *(vi)* decomposition techniques.

Appropriate data structures eliminate unnecessary constructs and yield formulations that can be read into a solver more efficiently. They can also help to eliminate numerical instability by forcing the practitioner to recognize potential difficulties before the data populates the model. Efficient formulations can eliminate unnecessary variables and/or reveal special mathematical structures that solvers can exploit. Careful numerical analysis ensures that the data are appropriately scaled, and precludes the inclusion of data in a given problem instance with large differences in orders of magnitude. Heuristics, while incapable of providing a proof of optimality in and of themselves, can aid in determining feasible solutions quickly, in some cases, more quickly than state-of-the-art solvers. When combined with a proof of optimality, they can be an effective means of solving a problem. Tailored algorithms can take advantage of special structure, which is sometimes revealed through reformulation or by fixing certain variable values; in the latter case, we say that

the model can be decomposed, and an iterative approach enumerating over the fixed values can expedite solutions with the notion that solving many smaller problems can be more expedient than solving a monolith.

For particularly large problem instances with complicated mathematical structure, the practitioner must often employ multiple techniques to generate high-quality solutions. This dissertation presents three research papers, each of which uses several of the above-mentioned techniques, to generate solutions of acceptable quality and in an acceptable amount of time for heavy-industry applications, specifically: renewable energy with combined heat and power, and mining. The former is an emerging sector, while the latter is an established industry. In fact, the industries are inextricably intertwined in that mining provides materials for many renewable-energy technologies, while renewable energy can help power mines. Both industries can benefit in improvements in efficiency, cost, and worker safety.

The first paper, presented in Chapter 2, documents an efficiently formulated model used to inform commercial building owners regarding optimal renewable energy system designs and corresponding optimal dispatch strategies. This mixed-integer linear program provides an optimal mix of renewable energy technologies, storage devices and conventional generation, and minimizes total life cycle costs while adhering to constraints such as fuel availability, peak demand accounting, load balancing, storage operations, and technology sizing. We explore two case studies—differentiated by location, commercial building type, resource availability, and utility tariffs. We compare results determined by our model against those produced using typical rule-of-thumb estimations. The optimization model solutions generate millions of dollars in savings over a 25-year time horizon. The resulting paper, *Optimizing Design and Dispatch of a Renewable Energy System*, has been accepted in *Applied Energy*. The dissertation writer’s contributions to the paper include: assistance in model development; coding and validation of the optimization model; selection, analysis, and interpretation of results; and writing the paper.

While renewable energy technologies can reduce costs and improve resiliency, they can also be used in conjunction with a combined-heat-and-power system to meet both electricity and heating demands. The National Renewable Energy Laboratory has developed a web application (REopt Lite TM) which extends the work highlighted in Chapter 2 to incorporate combined-heat-and-power technologies (CHP). However, due to the complex mathematical structure resulting from their incorporation, certain model instances require hours of solution time to reach near-optimality. The second paper, which constitutes Chapter 3, highlights the combined-heat-and-power constraints. The paper then describes the data management, variable redefinition, variable elimination, and constraint reformulation techniques necessary to obtain solutions in an operationally acceptable amount of time. We compare results on representative instances using the original model and the reformulated model. On average, our reformulation reduces both the number of variables and the number of constraints by 40%. Our results show an improvement relative to the original formulation in optimality gap of an order of magnitude given the same ten-minute time limit. The resulting paper, *Optimizing Design and Dispatch of a Renewable Energy System with Combined Heat and Power*, has been submitted to *Optimization and Engineering*. The dissertation writer's contributions to the paper include: helping reformulate the existing model; coding and numerical analysis of the reformulation; validation of reformulated model; and writing the paper.

Finally, many mines operate deep below the earth's surface to extract minerals. While providing more targeted access to these minerals in a more environmentally friendly manner than open-pit mining, underground mining operations present significant risks. One such risk is the accumulation of heat underground, which affects mine worker comfort and safety. In particular, the use of large diesel equipment to complete activities generates heat and other unsafe emissions. Typically, appropriately sizing ventilation systems can alleviate build-up of these nuisances. For cases in which ventilation is insufficient to remove heat from the mine, refrigeration units are installed to provide added cooling. Due to the large associated costs, and the desire to balance costs against mine worker safety, it is

critical to determine when to activate refrigeration. The final paper of this dissertation, presented in Chapter 4, examines an optimization-based methodology to schedule pre-determined activities associated with extracting ore in an underground mine. Using mechanical engineering principles, it simultaneously determines a production schedule and the timing of refrigeration to effect this schedule based on heat limits. Due to the large size of these production scheduling problems, generic solvers are unable to solve realistic instances on a standard computer. We therefore reformulate the original model to ensure its suitability for a tailored algorithm, which, in turn: (i) solves the linear-programming relaxation; and, (ii) employs a topological sorting heuristic that operates on the solution to the linear-programming relaxation to generate an integer-feasible solution. We manufacture instances from an existing hard-rock mining operation. On average, we are able to produce a solution with an optimality gap of 7% in 2 hours. The corresponding monolith cannot be solved using a general-purpose solver due to memory issues. The resulting paper, *Underground Production Scheduling with Ventilation and Refrigeration Considerations*, has been submitted to *Optimization and Engineering*. The dissertation writer's contributions to the paper include: developing the original formulation and the reformulation; interfacing engineering software for validation of both formulations; assistance in developing the heuristic; interpretation of results from the problem instances; and writing the paper. Chapter 5 concludes and presents future research.

CHAPTER 2

OPTIMIZING DESIGN AND DISPATCH OF A RENEWABLE ENERGY SYSTEM

This paper has been accepted for publication in *Applied Energy*

Oluwaseun Ogunmodede¹, Kate Anderson^{1,2}, Dylan Cutler², Alexandra Newman^{1,3}

Abstract

Renewable energy technologies are becoming increasingly important due to their cost-competitiveness, and because of enhanced climate concerns. We demonstrate the capabilities of an integer-programming optimization model that minimizes capital (investment) and operational costs, and utility charges, while adhering to system sizing constraints, demand requirements, and interoperability characteristics of the systems chosen. The model recommends an optimally sized mix of renewable energy, conventional generation, and energy storage technologies, while simultaneously optimizing the corresponding dispatch strategy. Our case studies explore several venues, i.e., a small campus and a local hospital, with complex utility rate tariffs, multi-technology integration opportunities, and incentives for renewable power production. Using an optimization model, versus applying rules of thumb, can produce millions of dollars in savings over a 25-year time horizon and result in thousands of kilowatts of installed renewable energy.

¹Colorado School of Mines, Golden, CO 80401

²National Renewable Energy Laboratory, Engineering and Modeling Group, Golden, CO 80401

³Corresponding Author

2.1 Introduction

Distributed energy resources—including solar photovoltaics (PV), battery storage, and wind—are being adopted at an ever-increasing pace, among other reasons, because prices have decreased by 41-73% (depending on the technology) between 2008 and the time of this writing (Donohoo-Vallett et al., 2016). Projections show that as PV deployment grows from 2% to 22% of world electric capacity, 33% of that new capacity will be behind-the-meter (BloombergNEF, 2019). While capital cost reductions have been critical to deployment growth, economic performance of distributed resources is also heavily dependent on system performance, the utility tariff under which the distributed energy resource is operating (e.g., energy costs, demand rates, time-of-use structures), and the economic environment in which the system operates (e.g., incentives and net metering policies). To enable continued, cost-effective deployment, it is critical that developers and building owners are able to size and operate integrated distributed energy resource systems to minimize costs under these considerations (O’Shaughnessy et al., 2018).

As the renewable energy market has grown and matured, determining system design has evolved from simple rules-of-thumb, to step-by-step work flows, to spreadsheet tools, to detailed modeling software. While each of these methods can be useful, an increasingly complex problem setting—including tariff and policy considerations—requires a structured modeling framework to capture economic and operational trade-offs. REopt LiteTM, a mixed-integer programming model, has been developed to help address this need, and offers a subset of technologies and features from the National Renewable Energy Laboratory’s more comprehensive REopt model (Cutler et al., 2017a). This paper describes the corresponding complete mathematical formulation, briefly mentions some techniques to solve problem instances within an acceptable amount of time for deployment purposes, and demonstrates how the corresponding optimization-based solutions navigate the appropriate trade-offs between system sizes and operational strategies.

Specifically, REopt Lite evaluates the economic viability of grid-connected wind, solar,

and battery storage behind a single utility meter using hourly (or sub-hourly) time fidelity over a representative year. The model minimizes discounted cashflow associated with costs and savings while adhering to constraints on fuel use, system operations, system capacities, load balancing, grid sales, rate tariffs, and a variety of other interoperability and logical restrictions. The model recommends an optimally sized mix of renewable energy, conventional generation, and energy storage technologies, while simultaneously optimizing the corresponding dispatch strategy. The model is widely applicable – across residential homes, commercial and industrial sites, university campuses, military installations, and microgrids. In fact, the model is not only applicable to settings in the United States (as demonstrated with our case studies), but, in fact, in African countries such as Tanzania (Booth et al., 2018), and Kenya, Zambia, Ghana, and Niger (Lockhart et al., 2019). Figure 2.1 shows the model’s high-level structure.

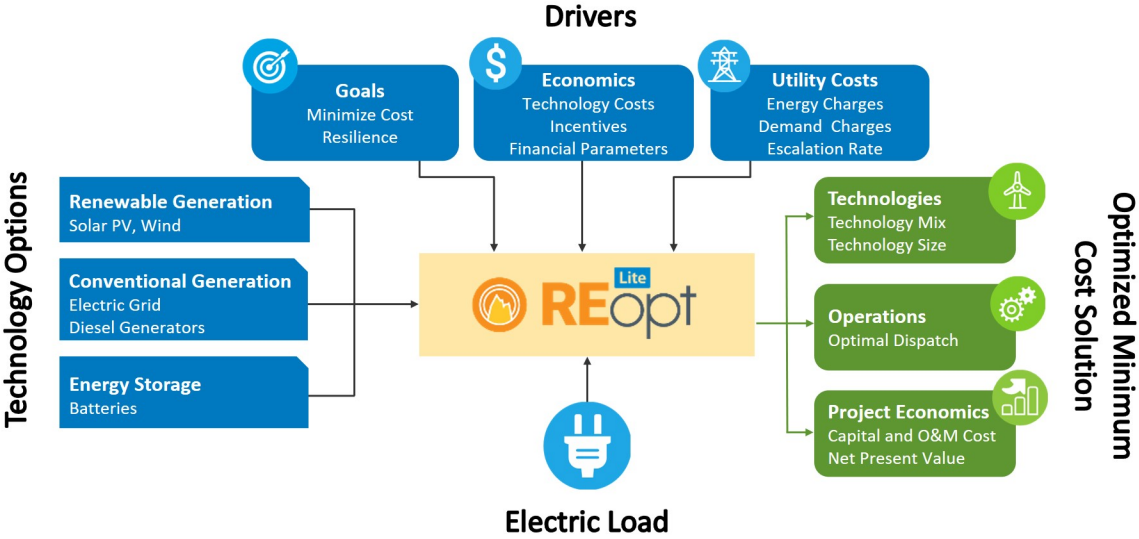


Figure 2.1: The REopt Lite system, where the blue boxes above, to the left of and underneath the center box containing the model name are inputs, and the green boxes to the right of center display the outputs (OSTI, 2020).

The benefits of mathematical optimization for energy design and dispatch problems are numerous: (i) no requirement for the user to pre-select technology types or sizes, (ii) a well-structured problem definition, and (iii) guaranteed global optimality (or some

quantitative measure from it). Despite this, large-scale, comprehensive design and dispatch optimization models have not typically been made available to the wider research and analysis community in a web-based framework, owing primarily to the following: (i) realistic model instances with complex tariff and technology combinations can be time-consuming to solve; and (ii) the model formulations are complex and require intimate knowledge of data input requirements and model operation, thereby restricting the user base to a small team of developers and experts. REopt Lite is a comprehensive model whose instances exhibit operationally feasible run times, but whose access is less limited than that of most academic models owing to its user-friendly web tool, application programming interface, and open-source code (Muratori et al., 2019). The contributions of this paper are: (i) the presentation of a detailed mathematical formulation of a complex design and dispatch model; and, (ii) an analysis of the corresponding solutions through case studies.

The organization of the remainder of this article is as follows: Section 2.2 reviews the extant literature on renewable energy system optimization and associated modeling approaches. Section 2.3 outlines the primary model inputs and the general modeling architecture. Section 2.4 contains the mathematical formulation of the optimization model, with corresponding explanations. Section 3.5 provides the computational setup and presents results that emphasize the capabilities of the model. Section 2.6 concludes with avenues for future work.

2.2 Literature Review

Models that optimally determine design and dispatch simultaneously are NP-hard, and can consist of nonlinear functional forms and/or integrality restrictions on (some of) the decision variables. Common approaches in the literature separate the problem into two. Some authors provide heuristics that yield a good, but not optimal, solution to the design problem using genetic algorithms (Dufo-Lopez and Bernal-Agustin, 2005), or iterative metaheuristic methods (Katsigiannis and Georgilakis, 2008); these take a dispatch strategy

that satisfies load balance as given (Ashari and Nayar, 1999). Problem restrictions such as addressing a shorter time horizon or reducing load variability might compromise the quality of the solution, even if the model itself becomes more tractable (Morais et al., 2010). Conversely, Abbey and Joos (2005) fix design decisions to obtain an optimal dispatch strategy.

An increasing number of models in the literature simultaneously consider the design and dispatch problem. For example, Zhao et al. (2014) optimize system unit size and operating strategy for an island microgrid using a genetic algorithm to minimize lifecycle cost while maximizing renewable energy penetration and minimizing emissions. Buoro et al. (2014) optimize design and operation of an industrial energy system consisting of a cogeneration system, solar thermal plant, and heat storage, to minimize the total annual cost of owning and operating the energy system. Merkel et al. (2015a) optimize the capacity and dispatch of micro-combined heat and power systems for residential applications. However, rather than using an exact solution approach, they rely on simulation, evolutionary algorithms, and/or reduce the scope of the problem (for exact solution approaches). In particular, although Pruitt et al. (2013b) make both design and dispatch decisions for a combined heat and power system, the pricing structure and operational details of the technologies are not as sophisticated as those we consider. Bracco et al. (2016) also present a model, DESOD, to optimize an energy system, with combined heat and power (which is outside the scope of our current work). However, this model ensures that all thermal loads are satisfied by distributed energy, i.e., there is no connection to the utility for thermal energy; it models separate buildings and the pipeline connection between buildings; the load patterns are given by “typical days,” rather than for every hour of the year; and, technology sizes, at least in some cases, are discrete. The authors expedite solutions by shortening the time horizon. Upadhyay and Sharma (2014), Theo et al. (2017) and Wang and Hijazi (2018) provide reviews of the literature associated with hybrid distributed energy resource optimization models.

While many of the optimization techniques described in the literature are implemented

only in research models, a growing number are also available in techno-economic distributed energy optimization tools that provide analysis of project feasibility and decision support to guide energy investments and meet the increasing need for assessment of clean energy investment options. Articles by Connolly et al. (2010), Ringkjøb et al. (2018), and Groissböck (2019) review up to 75 models used for analyzing energy and electricity systems, including short-term operation and long-term energy system planning at the local and national energy scales. The majority of these analyze energy systems at regional, national, and international scales, such as TIMES (Loulou et al., 2004), PyPSA (Brown et al., 2018), OSeMOSYS (Howells et al., 2011), urbs (Dorfner and Hamacher, 2020), oemof (Hilpert et al., 2018), and FINE (Welder et al., 2018), but eight are used for site-specific project identification and analysis: RETScreen, EnergyPro, TRNSYS, HOMER, SAM, iHOGA, DER-CAM, and ficus. Most of these are simulation tools, while iHOGA, DER-CAM, and ficus are based on mathematical optimization.

RETScreen is a clean energy management software system for energy efficiency, renewable energy, and cogeneration project feasibility analysis used to identify and assess the technical and financial viability of clean energy projects (Thevenard et al., 2000). Developed in Excel, it is a free, downloadable tool and, at the time of this writing, has 690,000 users in 222 countries worldwide. RETScreen uses analytical methods to simulate user-specified technology sizes. Each technology is analyzed separately based on five criteria – involving costs, greenhouse gases, finance, sensitivity and risk. RETScreen does not model the integration of multiple technologies nor optimize technology size, though some researchers have used the Excel solver to add an optimization feature for their own research (Lee et al., 2012). EnergyPro is a commercial modeling software package for techno-economic design, analysis, and optimization (Maeng et al., 2002). It is typically used to evaluate cogeneration and tri-generation projects, but can also consider other types of distributed energy and can design systems or optimize the operation of existing systems by dividing the year into calculation periods, and then allocating production through a series of loops according to a set of priority-based rules (Lund and Andersen, 2005). This

technique provides an implementable solution, though not one guaranteed to be globally optimal. TRNSYS is a transient systems simulation program used to assess the performance of thermal and electrical energy systems and to conduct detailed simulations of technology performance based on user-specified technology sizes and other input parameters (Klein et al., 2004). It does not inherently optimize technology size nor economics, but it can be combined with other programs to do so. For example, the TESS Optimization Library couples TRNSYS with Lawrence Berkeley National Lab’s GenOpt program to minimize cost (Asadi et al., 2012). GenOpt allows the user to select from a library of optimization algorithm options including generalized pattern search, particle swarm optimization, hybrid global optimization, discrete Armijo Gradient, Nelder and Mead’s Simplex, and Golden Section and Fibonacci algorithms. HOMER is a piece of software employed for microgrid and distributed generation power system design and analysis (Lambert et al., 2006). It has a broad user base, with over 200,000 users in 190 countries. Analytical methods within HOMER simulate all possible combinations of user-specified technology sizes, and then sort them based on a user-specified metric to demonstrate how the economics change. This approach can be computationally intensive because it requires many simulations, and does not guarantee optimality. The System Advisor Model (SAM) guides renewable energy decisions (Freeman et al., 2018) by providing detailed performance and financial models to evaluate a range of renewable energy technologies and storage through direct purchase, power purchase agreements, or third-party ownership. SAM uses analytical methods to simulate user-specified technology sizes but neither optimizes system size nor models technology integration (with the exception of PV-battery systems).

The software described thus far requires the specification of technology sizes, which are often unknown during early project feasibility assessments. Extensions of these models also determine optimal system size. For example, Improved Hybrid Optimization by Genetic Algorithms (iHOGA) simulates and optimizes hybrid electric systems (Dufo-López and Bernal-Agustín, 2005). iHOGA uses genetic algorithms to determine the number and type

of each technology, an optimal control strategy (selected from load following, cycle charging, or hybrid), and state-of-charge set point. iHOGA optimizes one or multiple objectives using enumeration to evaluate all possible combinations of components. The Distributed Energy Resources-Customer Adoption Model (DER-CAM) is a mixed-integer linear program that determines optimal portfolio, sizing, placement, and dispatch of technologies (Stadler et al., 2014; Mashayekh et al., 2017), while considering load shifting, peak shaving, power export agreements of technologies, and ancillary service markets. Although some renditions of the model account for electrical distribution, loads are not considered at a detailed, e.g., hourly or daily, level, fewer technologies are characterized specifically, and intricate economic incentives are missing. However, DER-CAM’s ability to find a guaranteed optimal solution is unique among the tools reviewed thus far. Ficus is a mixed-integer linear program for capacity expansion and unit commitment that minimizes investment and operations costs (Atabay, 2017), and is primarily used for industrial energy systems.

The existing models in this space provide users with a variety of effective approaches for evaluating energy investment decisions, but do have some limitations. A few (such as RETscreen and SAM) do not assess integrated suites of technologies, despite the complementary properties of distributed energy technologies that can impact system design and dispatch (Neto et al., 2020) and the increasing deployment of integrated systems. With the exceptions of DER-CAM and ficus, many cannot guarantee an optimal solution and fail to provide transparency into the exact model formulation and code, though recent research has highlighted the importance of open access to data and code to facilitate higher quality analysis (Pfenninger et al., 2017). Finally, most of the existing models are oriented toward expert-level users, requiring hours of training. Twaha and Ramli (2018), Lian et al. (2019), and Cuesta et al. (2020) provide reviews of optimum sizing approaches in the literature. REopt Lite attempts to fill the identified gaps by providing a guaranteed optimal solution, while also improving accessibility and ease of use in that it requires just three user inputs, and offers over one hundred optional inputs for advanced users.

2.3 Model Inputs and Structure

This section describes the primary inputs to the optimization model and its general structure to contextualize for the mathematical formulation presented in Section 2.4. (The computational framework is provided in Mishra et al. (2021). The REopt Lite user manual provides complete documentation of input definitions, engineering units, and default values (REopt development team, 2020).)

2.3.1 Model Inputs

We categorize the model inputs as follows: site-related, financial, and technological. Those related to the geographic location of the site include:

- *Resource data*: This encompasses all of the renewable energy resource and climate zone data; the model leverages and integrates open data sets such as the National Solar Radiation Database (Sengupta et al., 2018) and the Wind Integration National Dataset Toolkit (Draxl et al., 2015).
- *Electricity tariff structure*: The utility tariff can either be obtained from the Utility Rate Database (Ong and McKeel, 2012) or by entering a custom rate structure.
- *Load profile*: The load profile can either be simulated based on the appropriate Department of Energy Commercial Reference Building model (Office of Energy Efficiency and Renewable Energy, 2020) and climate zone or by entering energy demand at an hourly fidelity or finer granularity.

The financial inputs cover all of the economic parameters used to escalate and discount costs, thus ensuring that initial costs are weighed appropriately against recurring costs and revenue streams.

- *Financial inputs*: Discount rate, annual electricity cost escalation rate, annual operations and maintenance escalation rate, and analysis period are all considered. Technology inputs include costs, incentives, and technical performance characteristics.
- *Technology costs*: These encompass capital costs, and fixed and variable operating costs.

- *Financial incentives*: These relate to federal, state, local, and utility incentives, both production-based and capacity-based.
- *System characteristics*: These consist of minimum and maximum system sizes, minimum turndown limits (as applicable), fuel consumption curves for generators, module types or turbine size classes, and other technical parameters. For the PV and wind turbine models, REopt Lite uses the System Advisor Model (SAM) simulation core (Freeman et al., 2018) and PVWatts (National Renewable Energy Laboratory, 2020) to combine renewable resource data with technical parameters from which to estimate system performance. Battery energy storage is modeled as a “reservoir,” and includes inverters, rectifiers, and battery round-trip efficiency, as well as minimum state of charge. The energy and power capacity of the system, given minimum and maximum values for both, are optimized independently. Inputs also include replacement year, and expected energy capacity and power costs upon replacement.

2.3.2 Model Structure

We define primary aspects of the model architecture, focusing on system sizing, the way in which size is connected to production, and how that production interfaces with load balancing constraints. Additionally, we outline the tariff structure, including tiers and demand ratchets.

- *System sizing*: Each technology possesses a piecewise linear cost curve that accounts for economies of scale, and incorporates capacity-based incentives, i.e., the base cost curve can be modified to account for a dollar-per-kilowatt or percent-based incentive cost reduction. The system size is indexed on the segments of that curve, and constrained to occupy a single segment with the corresponding price. Additionally, for each technology class (e.g., PV), two technologies are initialized in the model: one is able to benefit from net energy metering by receiving full retail value for export energy, and the other is unable to receive this benefit in that exports are valued at a wholesale rate. The model selects only one technology within a technology class, and

the technology that has net metering available is constrained by a system size capacity equal to the net metering limit for the site.

- *Rated production:* For each technology—excluding storage—the production on a time step-by-time step basis is constrained to be less than the system size, and the rated production is scaled by two correction factors: (i) to account for hourly production of a system of a given capacity due to limited resources, for example, scaling down energy generation from a 100kW wind turbine based on wind resources for the given hour; and (ii) to address any degradation that the system is expected to experience over the analysis period, for example, the degradation of a PV panel over 20 years. Rated production is constrained to operate above a minimum turndown for applicable technologies (e.g., diesel generators) using a switch constraint.
- *Storage system considerations:* These systems are handled separately from the other technologies, and can be charged by the technologies in the model—or the grid—and can discharge to meet the site demand or export to the grid. Energy and power capacities of the battery are constrained to be greater than the stored energy and charge or discharge capacity, respectively, across all time steps.
- *Load balancing constraints:* These restrictions account for all generation (from scaled rated production, grid purchases, and battery discharging) and ensure that it is equal to the demand (from site load, battery charging, and energy exports) across all time steps.
- *Tariff modeling:* The tariff model accounts for three main charges: (i) energy, (ii) demand, and (iii) fixed or minimum-cost thresholds. Central to this modeling are grid purchases, which depend on the time step and energy tier. To capture time-of-use energy charges, grid purchases are accounted for on an hourly basis. Additionally, tiered energy costs are incorporated through the appropriate pricing mechanism in each hour, with binaries ensuring that monthly tier amounts are filled in the correct order. Two types of demand charges are modeled: (i) monthly, that is greater than or equal to any grid purchase (summed over tiers) for the hours in that

month; and, (ii) time-of-use, that can have multiple on- or off-peak periods.

Time-of-use demand is forced to be greater than or equal to grid purchases for the hours in that period for the month. Demand “look-back” levels (e.g., ratchets) can also be applied to a percent of peak demand for a set of months.

- *Time steps*: We model hourly (or sub-hourly) load, weather data, and utility rates for one representative year.

The following section provides the corresponding mathematical formulation and descriptions of the constraints.

2.4 Optimization Model (\mathcal{R})

We define here, in alphabetic order within a group, indices and sets, parameters, and variables, in that order, and then state the objective function and the constraints. We choose as our naming convention calligraphic capital letters to represent sets, lower-case letters to represent parameters, and upper-case letters to represent variables. In the latter case, Z -variables are binary, and represent design and operational decisions; X -variables represent continuous decisions, e.g., quantities of energy. All subscripts denote indices. Names with the same “stem” are related, and superscripts and “decorations” (e.g., hats, tildes) differentiate the names with respect to, e.g., various indices included in the name or maximum and minimum values for the same parameter.

2.4.1 Sets and Parameters

Sets

\mathcal{B}	Storage systems
\mathcal{C}	Technology classes
\mathcal{D}	Time-of-use demand periods
\mathcal{E}	Electrical time-of-use demand tiers
\mathcal{F}	Fuel types
\mathcal{H}	Time steps
\mathcal{K}	Subdivisions of power rating
\mathcal{M}	Months of the year
\mathcal{N}	Monthly peak demand tiers
\mathcal{S}	Power rating segments
\mathcal{T}	Technologies
\mathcal{U}	Total electrical energy pricing tiers
\mathcal{V}	Net metering regimes

Subsets and Indexed Sets

$\mathcal{H}^g \subseteq \mathcal{H}$	Time steps in which grid purchasing is available
$\mathcal{H}_m \subseteq \mathcal{H}$	Time steps within a given month m
$\mathcal{H}_d \subseteq \mathcal{H}$	Time steps within electrical power time-of-use demand tier d
$\mathcal{K}_t \subseteq \mathcal{K}$	Subdivisions applied to technology t
$\mathcal{K}^c \subseteq \mathcal{K}$	Capital cost subdivisions
\mathcal{M}^{lb}	Look-back months considered for ratchet charges
$\mathcal{S}_{tk} \subseteq \mathcal{S}$	Power rating segments from subdivision k applied to technology t
$\mathcal{T}_b \subseteq \mathcal{T}$	Technologies that can charge storage system b
$\mathcal{T}_c \subseteq \mathcal{T}$	Technologies in class c
$\mathcal{T}_f \subseteq \mathcal{T}$	Technologies that burn fuel type f
$\mathcal{T}_u \subseteq \mathcal{T}$	Technologies that may access electrical energy sales pricing tier u
$\mathcal{T}_v \subseteq \mathcal{T}$	Technologies that may access net-metering regime v
$\mathcal{T}^f \subseteq \mathcal{T}$	Fuel-burning, electricity-producing technologies
$\mathcal{T}^{\text{td}} \subseteq \mathcal{T}$	Technologies that cannot turn down, i.e., PV and wind
$\mathcal{U}^c \subseteq \mathcal{U}^s$	Electrical energy curtailment pricing tiers
$\mathcal{U}^{\text{nm}} \subseteq \mathcal{U}^s$	Electrical energy sales pricing tiers used in net metering
$\mathcal{U}^p \subseteq \mathcal{U}$	Electrical energy purchase pricing tiers
$\mathcal{U}^s \subseteq \mathcal{U}$	Electrical energy sales pricing tiers
$\mathcal{U}_t^s \subseteq \mathcal{U}^s$	Electrical energy sales pricing tiers accessible by technology t
$\mathcal{U}^{\text{sb}} \subseteq \mathcal{U}^s$	Electrical energy sales pricing tiers accessible by storage

Scaling Parameters

Δ	Time step scaling	[h]
----------	-------------------	-----

M	Sufficiently large number	[various]
---	---------------------------	-----------

Parameters for Costs and their Functional Forms

c^{afc}	Utility annual fixed charge	[\$]
c^{amc}	Utility annual minimum charge	[\$]
c_{ts}^{cb}	y -intercept of capital cost curve for technology t in segment s	[\$]
c_{ts}^{cm}	Slope of capital cost curve for technology t in segment s	[\$/kW]
c_{uh}^e	Export rate for energy in energy demand tier u in time step h	[\$/kWh]
c_{uh}^g	Grid energy cost in energy demand tier u during time step h	[\$/kWh]
c_b^{kW}	Capital cost of power capacity for storage system b	[\$/kW]
c_b^{kWh}	Capital cost of energy capacity for storage system b	[\$/kWh]
c_b^{omb}	Operation and maintenance cost of storage system b per unit of energy rating	[\$/kWh]
c_t^{omp}	Operation and maintenance cost of technology t per unit of production	[\$/kWh]
$c_t^{om\sigma}$	Operation and maintenance cost of technology t per unit of power rating	[\$/kW]
c_{de}^r	Cost per unit peak demand in time-of-use demand period d and tier e	[\$/kW]
c_{mn}^{rm}	Cost per unit peak demand in tier n during month m	[\$/kW]
c_f^u	Unit cost of fuel type f	[\$/MMBTU]

Demand Parameters

δ_h^d	Electrical load in time step h	[kW]
$\bar{\delta}_u^{gs}$	Maximum allowable sales in electrical energy demand tier u	[kWh]
δ^{lp}	Look-back proportion for ratchet charges	[fraction]
$\bar{\delta}_n^{mt}$	Maximum monthly electrical power demand in peak pricing tier n	[kW]
$\bar{\delta}_e^t$	Maximum power demand in time-of-use demand tier e	[kW]
$\bar{\delta}_u^{tu}$	Maximum monthly electrical energy demand in tier u	[kWh]

Incentive Parameters

\bar{i}_t	Upper incentive limit for technology t	[\$]
i_v^n	Net metering limits in net metering regime v	[kW]
i_t^r	Incentive rate for technology t	[\$/kWh]
\bar{i}_t^σ	Maximum power rating for obtaining production incentive for technology t	[kW]

Technology-Specific Time-series Factor Parameters

f_{th}^{ed}	Electric power de-rate factor of technology t at time step h	[unitless]
f_{th}^p	Production factor of technology t at time step h	[unitless]

Technology-Specific Factor Parameters

f_t^d	Derate factor for turbine technology t	[unitless]
f_t^l	Levelization factor of technology t	[fraction]
f_t^{li}	Levelization factor of production incentive for technology t	[fraction]
f_t^{pf}	Present worth factor for fuel for technology t	[unitless]

f_t^{pi}	Present worth factor for incentives for technology t	[unitless]
f_t^{td}	Minimum turn down for technology t	[unitless]

Generic Factor Parameters

f^e	Energy present worth factor	[unitless]
f^{om}	Operations and maintenance present worth factor	[unitless]
f^{tot}	Tax rate factor for off-taker	[fraction]
f^{tow}	Tax rate factor for owner	[fraction]

Power Rating and Fuel Limit Parameters

b_f^{fa}	Amount of available fuel for type f	[MMBTU]
b_c^σ	Minimum power rating for technology class c	[kW]
\bar{b}_t^σ	Maximum power rating for technology t	[kW]
$b_{tks}^{\sigma s}$	Minimum power rating for technology t , subdivision k , segment s	[kW]
$\bar{b}_{tks}^{\sigma s}$	Maximum power rating for technology t , subdivision k , segment s	[kW]

Efficiency Parameters

η_{bt}^+	Efficiency of charging storage system b using technology t	[fraction]
η_b^-	Efficiency of discharging storage system b	[fraction]
$\eta^{\text{g}+}$	Efficiency of charging electrical storage using grid power	[fraction]

Storage Parameters

$\bar{w}_b^{\text{b kW}}$	Maximum power output of storage system b	[kW]
$\underline{w}_b^{\text{b kW}}$	Minimum power output of storage system b	[kW]
$\bar{w}_b^{\text{b kWh}}$	Maximum energy capacity of storage system b	[kWh]
$\underline{w}_b^{\text{b kWh}}$	Minimum energy capacity of storage system b	[kWh]
$\underline{w}_b^{\text{mcp}}$	Minimum percent state of charge of storage system b	[fraction]
w_b^0	Initial percent state of charge of storage system b	[fraction]

Fuel Burn Parameters

m_t^{fb}	y -intercept of the fuel rate curve for technology t	[MMBTU/h]
m_t^{fm}	Slope of the fuel rate curve for technology t	[MMBTU/kWh]

2.4.2 Variables

Boundary Conditions

$X_{b,0}^{\text{se}}$	Initial state of charge for storage system b	[kWh]
-----------------------	--	-------

Continuous Variables

$X_b^{\text{b kW}}$	Power rating for storage system b	[kW]
$X_b^{\text{b kWh}}$	Energy rating for storage system b	[kWh]

X_{de}^{de}	Peak electrical power demand allocated to tier e and time-of-use demand period d	[kW]
X_{bh}^{dfs}	Power discharged from storage system b during time step h	[kW]
X_{mn}^{dn}	Peak electrical power demand allocated to tier n during month m	[kW]
X_{th}^f	Fuel burned by technology t in time step h	[MMBTU/h]
X_{uh}^g	Power purchased from the grid for electrical load in demand tier u during time step h	[kW]
X_h^{gts}	Electrical power delivered to storage by the grid in time step h	[kW]
X^{mc}	Annual utility minimum charge adder	[\$]
X_t^{pi}	Production incentive collected for technology t	[\$]
X^{plb}	Peak electric demand during look-back period	[kW]
X_{tuh}^{ptg}	Exports from production to the grid by technology t in demand tier u during time step h	[kW]
X_{bth}^{pts}	Power from technology t used to charge storage system b during time step h	[kW]
X_{th}^{rp}	Rated production of technology t during time step h	[kW]
X_t^σ	Power rating of technology t	[kW]
$X_{tks}^{\sigma s}$	Power rating of technology t allocated to subdivision k , segment s	[kW]
X_{bh}^{se}	State of charge of storage system b at the end of time step h	[kWh]
X_{uh}^{stg}	Exports from storage to the grid in demand tier u during time step h	[kW]

Binary Variables

Z_{mn}^{dmt}	1 if tier n has allocated demand during month m ; 0 otherwise	[unitless]
Z_{de}^{dt}	1 if tier e has allocated demand during time-of-use period d ; 0 otherwise	[unitless]
Z_v^{nml}	1 if generation is in net metering limit regime v ; 0 otherwise	[unitless]
Z_t^{pi}	1 if production incentive is available for technology t ; 0 otherwise	[unitless]
$Z_{tks}^{\sigma s}$	1 if technology t in subdivision k , segment s is chosen; 0 otherwise	[unitless]
Z_{th}^{to}	1 if technology t is operating in time step h ; 0 otherwise	[unitless]
Z_{mu}^{ut}	1 if demand tier u is active in month m ; 0 otherwise	[unitless]

2.4.3 Objective Function

$$\begin{aligned}
(\mathcal{R}) \quad & \text{minimize} \quad \underbrace{\sum_{t \in \mathcal{T}, k \in \mathcal{K}^c, s \in \mathcal{S}_{tk}} \left(c_{ts}^{\text{cm}} \cdot X_{tks}^{\sigma s} + c_{ts}^{\text{cb}} \cdot Z_{tks}^{\sigma s} \right)}_{\text{Generating Technology Capital Costs}} + \\
& \underbrace{\sum_{b \in \mathcal{B}} \left(c_b^{\text{kW}} \cdot X_b^{\text{bkW}} + (c_b^{\text{kWh}} + c_b^{\text{omb}}) \cdot X_b^{\text{bkWh}} \right)}_{\text{Storage Capital Costs}} + \\
& (1 - f^{\text{tow}}) \cdot f^{\text{om}} \cdot \left(\underbrace{\sum_{t \in \mathcal{T}} c_t^{\text{om}\sigma} \cdot X_t^\sigma}_{\text{Fixed O\&M Costs}} + \underbrace{\sum_{t \in \mathcal{T}^f, h \in \mathcal{H}} c_t^{\text{omp}} \cdot X_{th}^{\text{rp}}}_{\text{Variable O\&M Costs}} \right) + \\
& \underbrace{(1 - f^{\text{tot}}) \cdot \Delta \cdot \sum_{f \in \mathcal{F}} c_f^{\text{u}} \cdot \sum_{t \in \mathcal{T}_f, h \in \mathcal{H}} f_t^{\text{pf}} \cdot X_{th}^{\text{f}}}_{\text{Fuel Charges}} + \\
& (1 - f^{\text{tot}}) \cdot f^{\text{e}} \cdot \left(\underbrace{\Delta \cdot \sum_{u \in \mathcal{U}^p, h \in \mathcal{H}^g} c_{uh}^{\text{g}} \cdot X_{uh}^{\text{g}}}_{\text{Grid Energy Charges}} + \right. \\
& \underbrace{\sum_{d \in \mathcal{D}, e \in \mathcal{E}} c_{de}^{\text{r}} \cdot X_{de}^{\text{de}}}_{\text{Time-of-Use Demand Charges}} + \underbrace{\sum_{m \in \mathcal{M}, n \in \mathcal{N}} c_{mn}^{\text{rm}} \cdot X_{mn}^{\text{dn}}}_{\text{Monthly Demand Charges}} + \\
& \left. \underbrace{c^{\text{afc}} + X^{\text{mc}}}_{\text{Fixed Charges}} - \right. \\
& \left. \underbrace{\Delta \cdot \left(\sum_{h \in \mathcal{H}^g} \left(\sum_{u \in \mathcal{U}^{\text{sb}}} c_{uh}^{\text{e}} \cdot X_{uh}^{\text{stg}} + \sum_{t \in \mathcal{T}, u \in \mathcal{U}_t^{\text{s}}} c_{uh}^{\text{e}} \cdot X_{tuh}^{\text{ptg}} \right) \right)}_{\text{Energy Export Payment}} \right) - \\
& (1 - f^{\text{tow}}) \cdot \underbrace{\sum_{t \in \mathcal{T}} X_t^{\text{pi}}}_{\text{Production Incentives}}
\end{aligned}$$

The objective function minimizes the life cycle cost of energy, which is the sum of capital costs, operations and maintenance costs, utility costs (including fuel, energy, demand, and fixed charges), and subtracts, i.e., maximizes, energy export payments and incentives. Net present value (NPV) of an investment can be calculated by subtracting the life cycle cost of energy of the base case (where all energy is purchased from the utility) from the life

cycle cost of energy of the optimum case (where distributed energy resources may provide some of the energy). A positive NPV indicates that the investment provides savings, while a negative NPV indicates additional costs.

2.4.4 Constraints

This section contains both mathematical expressions and text descriptions for all constraints in the model. In general, the text descriptions are written to convey the spirit of the constraint and may not address every index in *for all* or *summation* statements when they are not central to how the constraint operates.

2.4.4.1 Fuel constraints

$$\Delta \cdot \sum_{t \in \mathcal{T}_f, h \in \mathcal{H}} X_{th}^f \leq b_f^{\text{fa}} \quad \forall f \in \mathcal{F} \quad (2.1a)$$

$$X_{th}^f = m_t^{\text{fm}} \cdot f_{th}^{\text{p}} \cdot X_{th}^{\text{rp}} + m_t^{\text{fb}} \cdot Z_{th}^{\text{to}} \quad \forall t \in \mathcal{T}^f, h \in \mathcal{H} \quad (2.1b)$$

Constraint (2.1a) restricts fuel consumption (which is a function of (i) total energy produced, and (ii) number of operating hours) to a prespecified limit for each fuel type, and allows different technologies to burn the same type of fuel. Constraint (2.1b) relates the production of a fuel-burning technology to its fuel consumption using a linear function offset from the origin.

2.4.4.2 Production Constraints

$$X_{th}^{\text{rp}} \leq \bar{b}_t^\sigma \cdot Z_{th}^{\text{to}} \quad \forall t \in \mathcal{T}, h \in \mathcal{H} \quad (2.2a)$$

$$\underline{f}_t^{\text{td}} \cdot X_t^\sigma - X_{th}^{\text{rp}} \leq \bar{b}_t^\sigma \cdot (1 - Z_{th}^{\text{to}}) \quad \forall t \in \mathcal{T}, h \in \mathcal{H} \quad (2.2b)$$

Constraint set (2.2) restricts the rated production to an operating window between a system's minimum turn down and its maximum size. Constraint (2.2a) limits a system's output to its maximum power rating if it is on, and 0 otherwise. Constraint (2.2b) forces a lower bound for the minimum power at which a technology can operate if it is on; the constraint is void otherwise.

2.4.4.3 Storage System Constraints

Boundary Conditions and Size Limits

$$X_{b,0}^{\text{se}} = w_b^0 \cdot X_b^{\text{bkWh}} \quad \forall b \in \mathcal{B} \quad (2.3a)$$

$$\underline{w}_b^{\text{bkWh}} \leq X_b^{\text{bkWh}} \leq \bar{w}_b^{\text{bkWh}} \quad \forall b \in \mathcal{B} \quad (2.3b)$$

$$\underline{w}_b^{\text{bkW}} \leq X_b^{\text{bkW}} \leq \bar{w}_b^{\text{bkW}} \quad \forall b \in \mathcal{B} \quad (2.3c)$$

Constraint (2.3a) sets the initial state of charge for each storage system as a fraction of its energy rating, and constraints (2.3b) - (2.3c) restrict the size of the storage system between the lower and upper bounds for energy capacity and power output, respectively. In this sense, we assume that the power and energy rating of each storage system may be optimized separately.

Storage Operations

$$X_{bth}^{\text{pts}} + \sum_{u \in \mathcal{U}_t^s} X_{tuh}^{\text{ptg}} \leq f_{th}^{\text{p}} \cdot f_t^1 \cdot X_{th}^{\text{rp}} \quad \forall b \in \mathcal{B}, t \in \mathcal{T}, h \in \mathcal{H}^{\text{g}} \quad (2.3d)$$

$$X_{bth}^{\text{pts}} \leq f_{th}^{\text{p}} \cdot f_t^1 \cdot X_{th}^{\text{rp}} \quad \forall b \in \mathcal{B}, t \in \mathcal{T}, h \in \mathcal{H} \setminus \mathcal{H}^{\text{g}} \quad (2.3e)$$

$$X_{bh}^{\text{se}} = X_{b,h-1}^{\text{se}} + \Delta \cdot \left(\sum_{t \in \mathcal{T}} (\eta_{bt}^+ \cdot X_{bth}^{\text{pts}}) + \eta_h^{\text{g}+} \cdot X_h^{\text{gts}} - X_{bh}^{\text{dfs}} / \eta_b^- \right) \quad \forall b \in \mathcal{B}, h \in \mathcal{H}^{\text{g}} \quad (2.3f)$$

$$X_{bh}^{\text{se}} = X_{b,h-1}^{\text{se}} + \Delta \cdot \left(\sum_{t \in \mathcal{T}} (\eta_{bt}^+ \cdot X_{bth}^{\text{pts}}) - X_{bh}^{\text{dfs}} / \eta_b^- \right) \quad \forall b \in \mathcal{B}, h \in \mathcal{H} \setminus \mathcal{H}^{\text{g}} \quad (2.3g)$$

$$X_{bh}^{\text{se}} \geq \underline{w}_b^{\text{mcp}} \cdot X_b^{\text{bkWh}} \quad \forall b \in \mathcal{B}, h \in \mathcal{H} \quad (2.3h)$$

Constraints (2.3d) and (2.3e) limit the electrical power dispatched to charge storage and export to the grid (in the former case), or to charge storage only (in the latter case, when grid export is unavailable) from each technology in each time step to no more than the electricity produced. Constraints (2.3f) and (2.3g) provide inventory balance for the state of charge of storage system b at the end of time period h , respectively: (i) for hours in which grid-purchased electricity is available, and (ii) for hours in which grid-purchased electricity is not available, in which case the grid-to-storage decision variable values, X_h^{gts} ,

are zero, i.e., not included in the constraint. Constraint (2.3h) forces the energy in the battery to be greater than or equal to the minimum state of charge.

Charging Rates

$$X_b^{\text{bkW}} \geq \sum_{t \in \mathcal{T}_b} X_{bth}^{\text{pts}} + X_h^{\text{gts}} + X_{bh}^{\text{dfs}} \quad \forall b \in \mathcal{B}, h \in \mathcal{H}^g \quad (2.3i)$$

$$X_b^{\text{bkW}} \geq \sum_{t \in \mathcal{T}_b} X_{bth}^{\text{pts}} + X_{bh}^{\text{dfs}} \quad \forall b \in \mathcal{B}, h \in \mathcal{H} \setminus \mathcal{H}^g \quad (2.3j)$$

$$X_b^{\text{bkWh}} \geq X_{bh}^{\text{se}} \quad \forall b \in \mathcal{B}, h \in \mathcal{H} \quad (2.3k)$$

Constraints (2.3i) and (2.3j) limit the power that can be charged or discharged from the storage system in each time step to the storage system's power rating for grid-connected and non-grid-connected time steps, respectively. Similarly, constraint (2.3k) limits the amount of energy in the storage system in each time step to the storage system's energy rating.

2.4.4.4 Production Incentives

$$X_t^{\text{pi}} \leq \min \left\{ M \cdot Z_t^{\text{pi}}, \sum_{h \in \mathcal{H}} \Delta \cdot i_t^r \cdot f_t^{\text{pi}} \cdot f_{th}^{\text{p}} \cdot f_t^{\text{li}} \cdot X_{th}^{\text{rp}} \right\} \quad \forall t \in \mathcal{T} \quad (2.4a)$$

$$X_t^\sigma \leq \bar{v}_t^\sigma + \bar{b}_t^\sigma \cdot (1 - Z_t^{\text{pi}}) \quad \forall t \in \mathcal{T} \quad (2.4b)$$

Constraint (2.4a) calculates total production incentives, if available, for each technology.

Constraint (2.4b) sets an upper bound on the size of system that qualifies for production incentives, if production incentives are available.

2.4.4.5 Power Rating

$$X_t^\sigma \leq \bar{b}_t^\sigma \cdot \sum_{s \in \mathcal{S}_{tk}} Z_{tks}^{\sigma s} \quad \forall c \in \mathcal{C}, t \in \mathcal{T}_c, k \in \mathcal{K}_t \quad (2.5a)$$

$$\sum_{t \in \mathcal{T}_c, s \in \mathcal{S}_{tk}} Z_{tks}^{\sigma s} \leq 1 \quad \forall c \in \mathcal{C}, k \in \mathcal{K} \quad (2.5b)$$

$$\sum_{t \in \mathcal{T}_c} X_t^\sigma \geq \bar{b}_c^\sigma \quad \forall c \in \mathcal{C} \quad (2.5c)$$

$$X_{th}^{\text{rp}} = X_t^\sigma \quad \forall t \in \mathcal{T}^{\text{td}}, h \in \mathcal{H} \quad (2.5d)$$

$$X_{th}^{\text{rp}} \leq f_{th}^{\text{ed}} \cdot X_t^\sigma \quad \forall t \in \mathcal{T} \setminus \mathcal{T}^{\text{td}}, h \in \mathcal{H} \quad (2.5e)$$

$$\underline{b}_{tk_s}^{\sigma s} \cdot Z_{tk_s}^{\sigma s} \leq X_{tk_s}^{\sigma s} \leq \bar{b}_{tk_s}^{\sigma s} \cdot Z_{tk_s}^{\sigma s} \quad \forall t \in \mathcal{T}, k \in \mathcal{K}_t, s \in \mathcal{S}_{tk} \quad (2.5f)$$

$$\sum_{s \in \mathcal{S}_{tk}} X_{tk_s}^{\sigma s} = X_t^\sigma \quad \forall t \in \mathcal{T}, k \in \mathcal{K}_t \quad (2.5g)$$

Constraint (2.5a) permits nonzero power ratings only for the selected technology and corresponding subdivision in each class. Constraint (2.5b) allows at most one technology to be chosen for each subdivision in each class. Constraint (2.5c) limits the power rating to the minimum allowed for a technology class. Constraint (2.5d) prevents renewable technologies from turning down; rather, they must provide output at their nameplate capacity. Constraint (2.5e) limits rated production from all non-renewable technologies to be less than or equal to the product of the power rating and the derate factor for each time period. Constraint (2.5f) imposes both lower and upper limits on the power rating of a technology, allocated to a subdivision in a segment, and constraint (2.5g) sums the segment sizes to the total for a given technology and subdivision.

2.4.4.6 Load Balancing and Grid Sales

$$\begin{aligned} \sum_{t \in \mathcal{T}} f_{th}^{\text{p}} \cdot f_t^{\text{l}} \cdot X_{th}^{\text{rp}} + \sum_{b \in \mathcal{B}} X_{bh}^{\text{dfs}} + \sum_{u \in \mathcal{U}^{\text{p}}} X_{uh}^{\text{g}} = \sum_{t \in \mathcal{T}} \left(\sum_{b \in \mathcal{B}} X_{bth}^{\text{pts}} + \sum_{u \in \mathcal{U}_t^{\text{s}}} X_{tuh}^{\text{ptg}} \right) \\ + \sum_{u \in \mathcal{U}^{\text{sb}}} X_{uh}^{\text{stg}} + X_h^{\text{gts}} + \delta_h^{\text{d}} \quad \forall h \in \mathcal{H}^g \end{aligned} \quad (2.6a)$$

$$\sum_{t \in \mathcal{T}} f_{th}^{\text{p}} \cdot f_t^{\text{l}} \cdot X_{th}^{\text{rp}} + \sum_{b \in \mathcal{B}} X_{bh}^{\text{dfs}} = \sum_{b \in \mathcal{B}, t \in \mathcal{T}} \left(X_{bth}^{\text{pts}} + \sum_{u \in \mathcal{U}^{\text{c}}} X_{tuh}^{\text{ptg}} \right) + \delta_h^{\text{d}} \quad \forall h \in \mathcal{H} \setminus \mathcal{H}^g \quad (2.6b)$$

$$\sum_{u \in \mathcal{U}^{\text{p}}} X_{uh}^{\text{g}} \geq X_h^{\text{gts}} \quad \forall h \in \mathcal{H}^g \quad (2.6c)$$

$$\sum_{b \in \mathcal{B}} X_{bh}^{\text{dfs}} \geq \sum_{u \in \mathcal{U}^{\text{sb}}} X_{uh}^{\text{stg}} \quad \forall h \in \mathcal{H}^g \quad (2.6d)$$

$$\Delta \cdot \sum_{h \in \mathcal{H}^g} \left(X_{uh}^{\text{stg}} + \sum_{t \in \mathcal{T}_u} X_{tuh}^{\text{ptg}} \right) \leq \bar{\delta}_u^{\text{gs}} \quad \forall u \in \mathcal{U}^{\text{sb}} \quad (2.6e)$$

$$\Delta \cdot \sum_{h \in \mathcal{H}^g, t \in \mathcal{T}_u} X_{tuh}^{\text{ptg}} \leq \bar{\delta}_u^{\text{gs}} \quad \forall u \in \mathcal{U}^{\text{s}} \setminus \mathcal{U}^{\text{sb}} \quad (2.6f)$$

Constraint (2.6a) balances load by requiring that the sum of power (i) produced, (ii) discharged from storage, and (iii) purchased from the grid is equal to the sum of (i) the power charged to storage by on-site generation, (ii) the power sold to the grid from on-site production or storage, (iii) the power charged to storage directly from the grid, and (iv) the electrical load on site. Constraint (2.6b) provides an analogous load-balancing requirement for hours in which the site is disconnected from the grid due to an outage. Constraint (2.6c) restricts charging of storage from grid production to the grid power purchased for each hour. Similarly, constraint (2.6d) restricts the sales from the electrical storage system to its rate of discharge in each time period. Constraints (2.6e) and (2.6f) restrict the annual energy delivered to the grid by pricing tier based on pre-specified limits, such as those imposed by net-metering restrictions; the former allows both storage and production to contribute, whereas the latter restricts the contribution to production.

2.4.4.7 Rate Tariff Constraints

Net Metering

$$\sum_{v \in \mathcal{V}} Z_v^{\text{nmil}} = 1 \quad (2.7a)$$

$$\sum_{t \in \mathcal{T}_v} f_t^d \cdot X_t^\sigma \leq i_v^n \cdot Z_v^{\text{nmil}} \quad \forall v \in \mathcal{V} \quad (2.7b)$$

$$\Delta \cdot \sum_{h \in \mathcal{H}^g} \left(\sum_{u \in \mathcal{U}^{\text{nm}}, t \in \mathcal{T}_u} X_{tuh}^{\text{ptg}} + \sum_{u \in \mathcal{U}^{\text{nm}} \cap \mathcal{U}^{\text{sb}}} X_{uh}^{\text{stg}} \right) \leq \Delta \cdot \sum_{u \in \mathcal{U}^{\text{p}}, h \in \mathcal{H}^g} X_{uh}^g \quad (2.7c)$$

Constraint (2.7a) limits the net metering to a single regime at a time. Constraint (2.7b) restricts the sum of the power rating of all technologies to be less than or equal to the net metering regime. Constraint (2.7c) ensures that energy sales at net-metering rates do not exceed the energy purchased from the grid.

Monthly Total Demand Charges

$$\Delta \cdot \sum_{h \in \mathcal{H}_m} X_{uh}^g \leq \bar{\delta}_u^{\text{tu}} \cdot Z_{mu}^{\text{ut}} \quad \forall m \in \mathcal{M}, u \in \mathcal{U}^{\text{p}} \quad (2.8a)$$

$$Z_{mu}^{\text{ut}} \leq Z_{m,u-1}^{\text{ut}} \quad \forall u \in \mathcal{U}^{\text{p}} : u \geq 2, m \in \mathcal{M} \quad (2.8b)$$

$$\bar{\delta}_{u-1}^{\text{tu}} \cdot Z_{mu}^{\text{ut}} \leq \Delta \cdot \sum_{h \in \mathcal{H}_m} X_{u-1,h}^g \quad \forall u \in \mathcal{U}^{\text{p}} : u \geq 2, m \in \mathcal{M} \quad (2.8c)$$

Constraint (2.8a) limits the quantity of electrical energy purchased from the grid in a given month from a specified pricing tier to the maximum available. Constraint (2.8b) forces pricing tiers to be charged in a specific order, and constraint (2.8c) forces one pricing tier's purchases to be at capacity if any charges are applied to the next tier.

Peak Power Demand Charges: Months

$$X_{mn}^{\text{dn}} \leq \bar{\delta}_n^{\text{mt}} \cdot Z_{mn}^{\text{dmt}} \quad \forall n \in \mathcal{N}, m \in \mathcal{M} \quad (2.9a)$$

$$Z_{mn}^{\text{dmt}} \leq Z_{m,n-1}^{\text{dmt}} \quad \forall n \in \mathcal{N} : n \geq 2, m \in \mathcal{M} \quad (2.9b)$$

$$\bar{\delta}_{n-1}^{\text{mt}} \cdot Z_{mn}^{\text{dmt}} \leq X_{m,n-1}^{\text{dn}} \quad \forall n \in \mathcal{N} : n \geq 2, m \in \mathcal{M} \quad (2.9c)$$

$$\sum_{n \in \mathcal{N}} X_{mn}^{\text{dn}} \geq \sum_{u \in \mathcal{U}^p} X_{uh}^g \quad \forall m \in \mathcal{M}, h \in \mathcal{H}_m \quad (2.9d)$$

Constraint (2.9a) limits the energy demand allocated to each tier to no more than the maximum demand allowed. Constraint (2.9b) forces monthly demand tiers to become active in a prespecified order. Constraint (2.9c) forces demand to be met in one tier before the next demand tier. Constraint (2.9d) defines the peak demand to be greater than or equal to all of the demands across the time horizon, where an equality is actually induced by the sense of the objective function.

Peak Power Demand Charges: Time-of-Use Demand and Ratchet Charges

$$X_{de}^{\text{de}} \leq \bar{\delta}_e^{\text{t}} \cdot Z_{de}^{\text{dt}} \quad \forall e \in \mathcal{E}, d \in \mathcal{D} \quad (2.10a)$$

$$Z_{de}^{\text{dt}} \leq Z_{d,e-1}^{\text{dt}} \quad \forall e \in \mathcal{E} : e \geq 2, d \in \mathcal{D} \quad (2.10b)$$

$$\bar{\delta}_{e-1}^{\text{t}} \cdot Z_{de}^{\text{dt}} \leq X_{d,e-1}^{\text{de}} \quad \forall e \in \mathcal{E} : e \geq 2, d \in \mathcal{D} \quad (2.10c)$$

$$\sum_{e \in \mathcal{E}} X_{de}^{\text{de}} \geq \max \left\{ \sum_{u \in \mathcal{U}^p} X_{uh}^g, \delta^{\text{lp}} \cdot X^{\text{plb}} \right\} \quad \forall d \in \mathcal{D}, h \in \mathcal{H}_d \quad (2.10d)$$

$$X^{\text{plb}} \geq \sum_{n \in \mathcal{N}} X_{mn}^{\text{dn}} \quad \forall m \in \mathcal{M}^{\text{lb}} \quad (2.10e)$$

Constraints (2.10a)-(2.10d) correspond to constraints (2.9a)-(2.9d), respectively, but pertain to a type of charge not related to monthly use, but rather to time of use within a month. These *ratchet charges* are implemented using constraints (2.10d). The charge applied for each time-of-use period is a linearizable function of the greater of the peak

electrical demand during that period (as given by the first term on the right-hand side of (2.10d)) and a fraction of the peak demand that occurs over a collection of months (known as *look-back months*) during the year (as given by the second term on the right-hand side of (2.10d)). Constraint (2.10e) ensures the peak demand over the set of look-back months is no lower than the peak demand for each look-back month. In this way, charges are based not only on use in a given month, but also on a fraction of use over the last several months, and becomes relevant when this latter use is high relative to current use.

2.4.4.8 Minimum Utility Charge

$$\begin{aligned}
X^{\text{mc}} \geq & c^{\text{amc}} - \left(\underbrace{\Delta \cdot \sum_{u \in \mathcal{U}^{\text{p}}, h \in \mathcal{H}^{\text{g}}} c_{uh}^{\text{g}} \cdot X_{uh}^{\text{g}}}_{\text{Grid Energy Charges}} + \underbrace{\sum_{d \in \mathcal{D}, e \in \mathcal{E}} c_{de}^{\text{r}} \cdot X_{de}^{\text{de}}}_{\text{Time-of-Use Demand Charges}} + \right. \\
& \underbrace{\sum_{m \in \mathcal{M}, n \in \mathcal{N}} c_{mn}^{\text{rm}} \cdot X_{mn}^{\text{dn}}}_{\text{Monthly Demand Charges}} - \\
& \left. \underbrace{\Delta \cdot \left(\sum_{h \in \mathcal{H}^{\text{g}}} \left(\sum_{u \in \mathcal{U}^{\text{sb}}} c_{uh}^{\text{e}} \cdot X_{uh}^{\text{stg}} + \sum_{t \in \mathcal{T}, u \in \mathcal{U}_t^{\text{s}}} c_{uh}^{\text{e}} \cdot X_{tuh}^{\text{ptg}} \right) \right)}_{\text{Energy Export Payment}} \right) \quad (2.11)
\end{aligned}$$

Constraint (2.11) enforces a minimum payment to the utility provider, which is a fixed constant less charges incurred from grid energy, time-of-use demand and monthly demand payments, plus sales from exports to the grid.

2.4.4.9 Non-negativity

$$X^{\text{plb}}, X^{\text{mc}} \geq 0 \quad (2.12a)$$

$$X_t^\sigma \geq 0 \quad \forall t \in \mathcal{T} \quad (2.12b)$$

$$X_{th}^{\text{rp}} \geq 0 \quad \forall t \in \mathcal{T}, h \in \mathcal{H} \quad (2.12c)$$

$$X_{tuh}^{\text{ptg}} \geq 0 \quad \forall t \in \mathcal{T}_u, h \in \mathcal{H}, u \in \mathcal{U} \quad (2.12d)$$

$$X_{uh}^{\text{stg}}, X_{uh}^{\text{g}} \geq 0 \quad \forall h \in \mathcal{H}, u \in \mathcal{U} \quad (2.12e)$$

$$X_t^{\text{pi}} \geq 0 \quad \forall t \in \mathcal{T} \quad (2.12\text{f})$$

$$X_{de}^{\text{de}} \geq 0 \quad \forall d \in \mathcal{D}, e \in \mathcal{E} \quad (2.12\text{g})$$

$$X_{mn}^{\text{dn}} \geq 0 \quad \forall m \in \mathcal{M}, n \in \mathcal{N} \quad (2.12\text{h})$$

$$X_h^{\text{gts}} \geq 0 \quad h \in \mathcal{H} \quad (2.12\text{i})$$

$$X_b^{\text{bkW}}, X_b^{\text{bkWh}} \geq 0 \quad b \in \mathcal{B} \quad (2.12\text{j})$$

$$X_{tks}^{\sigma s} \geq 0 \quad \forall t \in \mathcal{T}, k \in \mathcal{K}, s \in \mathcal{S}_{tk} \quad (2.12\text{k})$$

$$X_{bth}^{\text{pts}} \geq 0 \quad \forall b \in \mathcal{B}, t \in \mathcal{T}, h \in \mathcal{H} \quad (2.12\text{l})$$

$$X_{bh}^{\text{se}}, X_{bh}^{\text{dfs}} \geq 0 \quad \forall b \in \mathcal{B}, h \in \mathcal{H} \quad (2.12\text{m})$$

$$X_{th}^{\text{f}}, X_{th}^{\text{fb}} \geq 0 \quad \forall t \in \mathcal{T}, h \in \mathcal{H} \quad (2.12\text{n})$$

2.4.4.10 Integrality

$$Z_v^{\text{nmil}} \in \{0, 1\} \quad \forall v \in \mathcal{V} \quad (2.13\text{a})$$

$$Z_{tks}^{\sigma s} \in \{0, 1\} \quad \forall t \in \mathcal{T}, k \in \mathcal{K}, s \in \mathcal{S}_{tk} \quad (2.13\text{b})$$

$$Z_t^{\text{pi}} \in \{0, 1\} \quad \forall t \in \mathcal{T} \quad (2.13\text{c})$$

$$Z_{th}^{\text{to}} \in \{0, 1\} \quad \forall t \in \mathcal{T}, h \in \mathcal{H} \quad (2.13\text{d})$$

$$Z_{de}^{\text{dt}} \in \{0, 1\} \quad \forall d \in \mathcal{D}, e \in \mathcal{E} \quad (2.13\text{e})$$

$$Z_{mn}^{\text{dmt}} \in \{0, 1\} \quad \forall m \in \mathcal{M}, n \in \mathcal{N} \quad (2.13\text{f})$$

$$Z_{mu}^{\text{ut}} \in \{0, 1\} \quad \forall m \in \mathcal{M}, u \in \mathcal{U} \quad (2.13\text{g})$$

Finally, constraints (2.12) ensure all of the continuous variables in our formulation assume non-negative values. In addition to non-negativity restrictions, constraints (2.13) establish the integrality of the appropriate variables.

2.5 Case Studies

Model (\mathcal{R}) provides an optimal, integrated solution that includes complex economic features – such as rate tariffs and incentives; see Figure 2.1 and the figures contained in Mishra et al. (2021) for schematics. The case studies in this section highlight the

importance of these features by comparing results with and without these capabilities. We focus on four features: (i) optimization; (ii) technology integration; (iii) complex utility rate tariffs; and (iv) incentives.

For these case studies, we use two building type-location combinations. The first is a hospital in San Diego, CA with an average load of 970 kW, served by San Diego Gas and Electric, as shown in Table 2.3. The second is a campus in Cheyenne, WY comprised of five large office buildings with an average load of 3,426 kW, served by Cheyenne Light Fuel and Power. Appendix A provides additional data describing the hourly building load profiles, renewable energy resources, and economic parameters.

Table 2.3: Characteristics for each location detailing the building type, utility company name and rate structure

Location	Building Type	Utility Company Name	Rate Structure
San Diego, CA	Hospital	San Diego Gas & Electric	AL-TOU Primary (Above 500kW)
Cheyenne, WY	Campus	Cheyenne Light, Fuel & Power	Secondary General Service

For each site, the model recommends a technology mix and corresponding dispatch strategy to minimize the life cycle cost over a 25-year horizon. Instances of (\mathcal{R}) are solved on a Dell Power Edge R410 server with two Intel Xeon E5520s at 2.27 GHz, 350 28GB of RAM, and a 1TB HDD using CPLEX 12.10.0.0 (IBM ILOG, 2020). Solution times average about 30 to 60 seconds, and have been significantly reduced, sometimes by as much as two orders of magnitude, using careful modeling constructs such as tailored data structures, specially crafted numerical values (rather than defaults), and reformulation. (See Hirwa et al. (2020) for details.)

2.5.1 Optimization

In simulation-based energy decision tools, the user is typically required to specify a system size for the analysis. However, at the system design stage of the assessment, size may not be known. Therefore, users often rely on rules of thumb. For example, PV may be sized to generate a percent of annual energy consumption (National Renewable Energy

Laboratory, 2002). Batteries may be sized to sustain the load during a grid outage (IEEE, 2020). While rules of thumb produce useful estimates, they may not identify the most economical system sizes.

To demonstrate the impact of optimizing system size rather than using rules of thumb, we use the case study site in San Diego, CA. In the first scenario, we optimize the size of the PV and battery system to minimize life cycle cost of energy. In the following scenarios, we use rules of thumb, sizing PV to generate either 50% or 100% of annual energy consumption and sizing the battery to meet the average load for either 4 or 24 hours. (The four different combinations of these extremes yields the Rules of Thumb 1-4 against which we compare the Base Case and the solution from (\mathcal{R}).) The sizing is computed as follows: The hospital in San Diego consumes 8,498,389 kWh per year. A rooftop PV system in San Diego, facing south and tilted at 10 degrees, produces 1,496 kWh annually for each 1 kW of installed capacity Dobos (2014). Producing 100% of annual energy consumption would require a PV system sized at $\frac{8,498,389 \text{ kWh}}{1,496 \frac{\text{kWh}}{\text{kW}}} = 5,681 \text{ kW}$. Producing 50% of annual energy consumption would require a 2,840 kW PV system.

The hospital consumes on average 23,283 kWh per day, with an average load of $\frac{23,283 \text{ kWh}}{24 \text{ hours}} = 970 \text{ kW}$. A battery sized to meet the average load for 24 hours, assuming a minimum state of charge of 20%, an inverter efficiency of 96%, and a DC-DC round trip efficiency of 97.5%, would require an energy capacity of $\frac{23,283 \text{ kWh}}{0.8 \times 0.96 \times \sqrt{0.975}} = 30,703 \text{ kWh}$ with a power rating of 970 kW to discharge 970 kW of power per hour. A battery sized to meet the average load for 4 hours would require an energy capacity of 5,117 kWh with a power rating of 970 kW. Table 2.4 provides results.

Table 2.4: Comparison of net present value and characteristics of the solution between those provided by (\mathcal{R}) and the rules of thumb estimation

Solution Methodology	PV [kW]	Battery Storage		Life Cycle Cost [\$]	NPV [\$]
		Power [kW]	Capacity [kWh]		
Base Case	-	-	-	15,825,528	-
Model (\mathcal{R})	3,152	728	3,179	13,122,778	2,702,748
Rule of thumb 1	2,840	970	5,117	13,404,475	2,421,053
Rule of thumb 2	5,681	970	5,117	14,199,205	1,626,323
Rule of thumb 3	5,681	970	30,703	22,435,737	-6,610,209
Rule of thumb 4	2,840	970	30,703	22,500,330	-6,674,802

Using rules of thumb results in systems that are less economical at this site. The optimized system sizes would reduce energy costs and save the site \$2.7 million over the 25-year life cycle. The rule of thumb sizes, on the other hand, save the site only \$1.6 to \$2.4 million for systems with the smaller 4-hour battery. Systems with the larger 24-hour battery would cost the site an additional \$6 million, relative to purchasing energy solely from the utility.

While a user could enumerate a large range of system sizes in a simulation tool to find an economical solution, this could require considerable time and computational resources, particularly with hybrid systems for which there exist many different viable combinations. Even then, there is no guarantee that the user selects a size that offers a minimum-cost solution. Optimization techniques, on the other hand, can provide this guarantee.

2.5.2 Integration

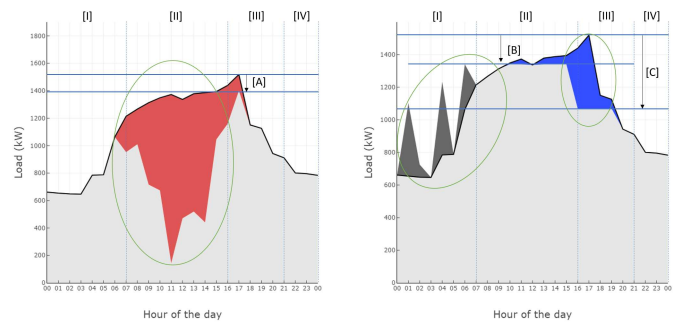
Some energy decision tools fail to consider the interaction between multiple technologies despite the fact they could behave synergistically. Accurate modeling of integrated technologies is especially relevant when evaluating renewable technologies. Complementary technologies such as energy storage or fixed generation can absorb variability in renewable generation and thus are able to deliver more effective demand management or energy resilience as a combined system. Our modeling approach determines technology sizing while delivering combined value through utility-bill-mitigation strategies, such as demand reduction. To demonstrate the impact of integration, we again

use the case study site in San Diego. In the first scenario, we model PV only and optimize the size to minimize life cycle cost of energy to the site. In the second scenario, we model battery only. In the third, we co-optimize the size of a PV and battery system. Table 2.5 provides the recommended technology sizes for each scenario.

Table 2.5: Comparison of net present value and characteristics of the solution provided by (\mathcal{R}) considering one and multiple renewable technologies

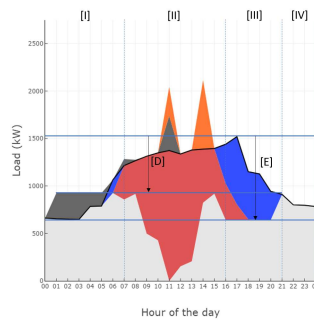
Technology	PV [kW]	Battery Storage		Life Cycle Cost [\$]	NPV [\$]
		Power [kW]	Capacity [kWh]		
Base Case	-	-	-	15,825,528	-
PV	2,308.95	-	-	14,448,559	1,376,969
Battery	-	448.99	1,485.16	15,464,094	361,434
Both	3,152.40	728.07	3,178.81	13,122,780	2,702,748

These results show that PV alone is optimally sized at 2,309 kW, and would provide \$1,376,969 in savings. The battery alone is optimally sized at a power rating of 449 kW and at 1,485 kWh of capacity, and would provide \$361,434 in savings. The integrated system, however, provides savings that are greater than those provided by the sum of the individual systems.



(a) Only PV available

(b) Only battery available



(c) Both technologies available

— Load — PV to Storage — Grid to Storage — Battery Discharge — PV — Utility

Figure 2.2: Comparison of single and multi-technology system dispatch on peak demand day in San Diego

The Roman numerals [I] - [IV] above each graph in Figure 2.2 denote the utility cost for the periods 12am-7am, 7am-4pm, 4pm-9pm, and 9pm-12am for a weekday in April. The energy costs are \$0.09, \$0.11, \$0.12, and \$0.11 per kilowatt-hour, respectively. The demand costs are \$20.87, \$20.87, \$37.75, and \$20.87 per kilowatt-hour, respectively. PV can offset significant daytime utility energy purchases. This is shown in the green circle in Figure 2.2a, where PV serves approximately half of the load from 7am-4pm, reducing energy purchased from the utility. It is not very effective, however, in reducing the peak amount of power purchased from the utility across the day. In Figure 2.2a, we see that peak demand occurs at 4pm, just as PV generation is tailing off. PV provides only a small reduction of about 119 kW in the maximum amount of power drawn from the utility on

this day (indicated by [A]).

Figure 2.2b shows that the battery alone does not provide any reduction in the amount of energy purchased from the utility. Rather, the battery increases the amount of energy purchased from the utility because utility power is used to charge the battery in the early morning hours. Most of the additional energy purchased in the early morning hours is offset by the reduction in energy purchased from the grid in the late afternoon when the battery is discharged to meet the load, but not entirely due to round-trip efficiency losses. However, while more power is purchased from the utility, the cost of this power is less due to the times at which the battery is charging and discharging. By charging in early morning hours when energy costs are lower (\$0.09 per kWh), indicated by [B], and discharging when energy costs are higher (\$0.12 per kWh), indicated by [C], total energy costs are reduced.

Figure 2.2c depicts the benefits of integrating the two technologies to both reduce utility energy purchases and peak demand charges. The maximum amount of power drawn from the utility decreases from about 1,519 kW to 926 kW during the less expensive hours (indicated by [D]), and to as low as 643 kW during the more expensive hours (indicated by [E]). A battery alone could accomplish this, but it would require a size that is prohibitively large and costly. A PV system alone could reduce utility energy purchases, but would not significantly reduce peak demand charges because it does not generate energy during most peak-price times. The combination of the two, however, provides both energy savings and peak demand charge reduction, resulting in overall life cycle savings that are nearly twice as high as those generated by a PV-only system, and seven times greater those generated by a battery-only system. Compared to evaluating each technology individually, considering the complementary properties of PV and batteries results in selecting larger system sizes.

An additional level of integration that could be considered combines demand flexibility with generation-side technologies. While demand flexibility is not explicitly included in the base version of the REopt Lite model, the authors have extended it to evaluate demand flexibility provided by smart thermostats and smart water heaters O'Shaughnessy et al. (2018), Shah et al. (2020). Additionally, research into interruptible service contracts has

shown value to renewable systems and could be considered for future research Sousa et al. (2018). Integration of demand-side flexibility could be incorporated in future analyses by extending the open-source version of the REopt Lite model.

2.5.3 Complex Utility Rate Structures

Upfront investment costs in renewable technologies must be recovered through utility bill savings; therefore, one of the primary factors in determining economic viability is the utility cost they offset. Rate tariffs, which determine economic viability, can be complicated combinations of energy and demand costs that vary by time-of-day, season-of-year, and energy consumed; to simplify, all time-varying demand and energy costs are sometimes averaged into annual rates.

To demonstrate the impact of actual rate structures rather than average rates, we use the case study site in San Diego, CA. For a time-of-use rate, we model the actual rate structure; this includes six energy and three demand time-of-use periods, where the energy and demand rates change based on time-of-day, weekday versus weekend, and season-of-year. Then, for a flat rate structure, we calculate a single average energy rate by dividing annual energy cost by annual energy consumption, and a single average demand rate by dividing the annual demand by the sum across all months in the year of the following two values: (i) the peak demand of each month, and (ii) the peak demand of each time-of-use period within the month. (See Table 2.6, where the periods correspond to the time-of-use schedules in Appendix A.)

Table 2.6: Energy and demand charges by period for each of the two rate structures

	Energy Charges by Period [\$/kWh]						Demand Charges by Period [\$/kW]		
	1	2	3	4	5	6	1	2	3
Time-of-Use	0.1356	0.1045	0.0830	0.1102	0.0979	0.0841	20.87	47.87	37.75
Flat	0.1087						21.08		

Table 2.7 shows the recommended technology mix for each scenario. The simplified flat rate results in smaller PV and battery system sizes than the more complex time-of-use rate; specifically, the PV system is 24% smaller, while the battery power is 63% smaller

and the battery capacity is 80% smaller. Furthermore, the smaller system size induced by the flat rate structure results in a \$1.5 million reduction in net present value.

Table 2.7: Comparison of technology mix produced by (\mathcal{R}) with differing rate structures; recall that the Base Case represents a utility-power-only solution.

Rate	Solution Type	PV [kW]	Battery Storage		Life Cycle Cost [\$]	NPV [\$]
			Power [kW]	Capacity [kWh]		
Time-of-Use	Base Case	-	-	-	15,825,528	-
	Optimal	3,152.40	728.07	3,178.81	13,122,780	2,702,748
Flat	Base Case	-	-	-	12,354,937	-
	Optimal	2,390.77	268.26	626.90	11,126,505	1,228,432

The more complex rate structure increases opportunities for savings from peak demand management. In particular, the system can selectively reduce energy purchased from the utility company during the highest priced time-of-use periods. Figure 2.3 compares the optimum dispatch of PV and battery under a time-of-use rate and flat rate. Roman numerals [I] to [IV] above the graphs denote the energy and demand charges from the utility company; [V] denotes the average flat energy and demand charges of \$0.11 per kWh and \$21.08 per kW, respectively, for the entire 24 hours. Figure 2.3a depicts that most of the battery discharge is in the evening hours, when solar generation is tailing off, but the demand rate is highest. The battery is discharged to reduce the maximum power draw from the utility during the peak price period (4pm-9pm) from 1,519 kW to 643 kW (indicated by [A]). The battery is not discharged to reduce demand at other times of day because the demand charge is lower (\$20.87 per kW instead of \$37.85 per kW), and the potential savings from demand charge reduction during lower price periods would not compensate for the added capital cost of the larger battery that would be required.

When the demand rate is modeled only as a single lower rate of \$21.08 per kW, it is not as lucrative to reduce demand. Figure 2.3b shows that the battery still provides some peak management (indicated as [B] in Figure 2.3b), reducing the maximum power draw from the utility from 1,519 kW to 1,128 kW. The battery is not discharged to reduce the maximum power draw from the utility further because the potential savings from additional demand charge reduction would not make up for the added capital cost of the larger battery that would be required.

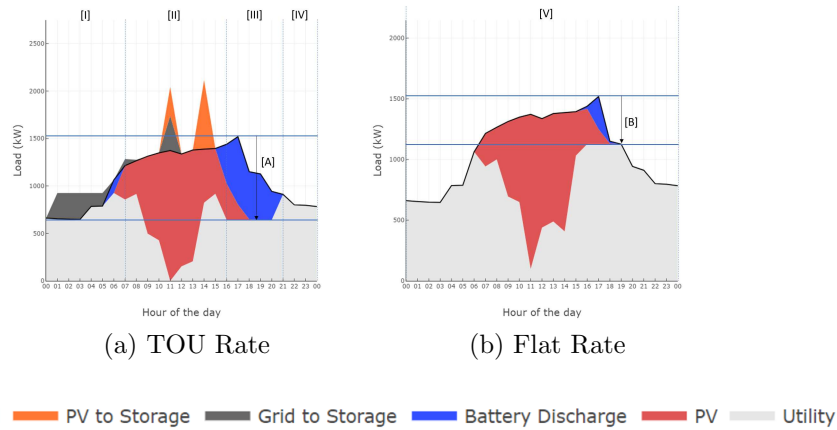


Figure 2.3: Comparison of dispatch under time-of-use and flat rate structures on a peak demand day

2.5.4 Incentives

Typically offered by federal governments, state governments or utilities to meet renewable energy goals, incentives reduce the cost of distributed energy technologies for certain locations. Capital cost incentives reduce the installed system cost on a dollar-per-kilowatt-installed or percentage-of-capital-cost basis; production-based incentives provide the owner with a dollar-per-kilowatt-hour payment for a fixed number of years based on energy produced by the system. Incentives are often limited by a maximum system size or by energy production, which constrains the total incentive value an owner can capture.

The complex rules regarding minimum and maximum sizes that qualify for incentives can preclude them from being considered. Often, incentives are present in cases where other factors such as the rate structures we consider in San Diego are absent. Additionally, different weather patterns suggest the use of different renewable technologies at disparate locations. Therefore, to demonstrate the impact of including incentives, we use a case study site in Cheyenne, WY. The investment tax credit provides a 26% benefit to the owner of a PV system. The use of batteries can also generate this credit if they are installed with a renewable energy system and charged only by that system. Small wind

turbines up to 100 kW are eligible for a 26% credit, and turbines with a capacity greater than 100 kW are eligible for an 18% credit. The credit, if chosen, defers the capital cost of the system. Table 2.8 provides the incentives used in each scenario.

Table 2.8: Incentives included in each scenario

Scenario	PV [%]	Battery [%]	Wind under 100kW [%]	Wind over 100 kW [%]
No Incentives	0	0	0	0
Incentives	26	26*	26	18

*We assume that the battery is charged only from PV or wind.

Table 2.9 shows that without incentives, a 139 kW PV system and a 668; 1,481 kWh battery provide \$169,886 in life cycle cost savings to the site. Wind is not cost-effective. When incentives are included, the optimum PV system size increases 14 times to 1,995 kW, and the battery size doubles in power and triples in capacity. Additionally, a wind system of 143 kW is cost-effective. The life cycle cost savings increase by over \$400,000. This example shows that including incentives in a model can change not only the size of technologies recommended, but also which technologies are included in the solution.

Table 2.9: Comparison of technology mix recommended by model (\mathcal{R}) with incentive inclusion

Type	PV [kW]	Wind [kW]	Battery Storage		Life Cycle Cost [\$]	NPV [\$]
			Power [kW]	Capacity [kWh]		
Base Case	-	-	-	-	34,634,914	-
No Incentives	138.92	-	311.46	443.15	34,465,028	169,886
Incentives	1,995.04	142.86	668.26	1,480.93	34,020,059	614,855

2.5.5 Summary

This model fills a gap in the literature by providing integrated, optimized solutions in an accessible, easy-to-use web interface, as well as through an application programming interface and open-source code Mishra et al. (2021). Not detailed here, yet provided in separate literature Hirwa et al. (2020), are various modeling techniques we employ to significantly reduce solution time, the impetus being not only to enhance the user experience for the current web-based tool, but also to enable in a practical sense the inclusion of additional technologies. Future work will focus on expanding the suite of technologies in the model, such as combined heat and power, geothermal heat pumps, and

thermal storage to provide additional options for reducing energy costs and improving resilience of buildings and campuses. As the size and complexity of the model grows with additional technologies, techniques such as decomposition may be explored to improve model tractability. While (\mathcal{R}) , and the REopt LiteTM tool more broadly, remain deterministic models, incorporating stochasticity, e.g., in renewable resource availability and load profiles, could be incorporated with the use of novel decomposition techniques (Zolan et al., 2020).

2.6 Conclusions and Future Work

As distributed energy resource adoption grows, developers and building owners need increasingly sophisticated tools to size and operate economic and resilient integrated distributed energy resource systems. We provide a detailed integer-programming formulation (\mathcal{R}) of a design and dispatch model that minimizes the life cycle cost of energy, including capital costs, operations and maintenance costs, utility costs, and incentives. Constraints control fuel use, system operations, system capacities, and load balancing, among other interoperability and logical restrictions. We use several case studies to demonstrate the impact of employing an optimization model to determine system size and dispatch over invoking rules of thumb or restricting inputs based on easier-to-navigate subsets of systems and/or rate structures. In all cases, the differences in strategic decisions, i.e., system sizes and even technologies chosen, are significant, sometimes effecting savings that exceed several million dollars over a 25-year time horizon.

CHAPTER 3

OPTIMIZING DESIGN AND DISPATCH OF A RENEWABLE ENERGY SYSTEM WITH COMBINED HEAT AND POWER

This paper has been submitted to *Optimization and Engineering*

Jusse Hirwa¹, Oluwaseun Ogunmodede¹, Alexander Zolan², Alexandra Newman^{1,3}

Abstract

We embellish a mixed-integer program that prescribes a set of renewable energy, conventional generation, and storage technologies to procure, along with a corresponding dispatch strategy. Specifically, we add combined heat and power to this set. The model minimizes fixed and operational costs less incentives for the use of various technologies, subject to a series of component interoperability and system-wide constraints. The resulting mixed-integer linear program contains hundreds of thousands of variables and constraints. We demonstrate how to efficiently formulate and solve the corresponding instances such that we produce near-optimal solutions in minutes. A previous rendition of the model required hours of solution time for the same instances.

3.1 Introduction

Distributed generation is gaining increasing interest in the energy sector owing to its economic, technical, and environmental benefits. As opposed to purchasing power exclusively from the grid, users can invest in on-site generation using technologies of their choice, such as wind, solar photovoltaics (PV) and storage. When integrated with combined heat and power (CHP) technology, a single energy source can simultaneously generate electricity and heat to meet heating and cooling demands (see Figure 3.1). In other words, the process of generating electricity releases waste heat which CHP can capture to produce usable thermal energy, offsetting the consumption of extra fuel for this

¹Colorado School of Mines, 1500 Illinois Street, Golden, CO 80401

²National Renewable Energy Laboratory, Thermal Energy Systems Group, 15013 Denver West Parkway, Golden, CO 80401

³Corresponding Author

purpose. In this way, distributed generation systems achieve greater energy efficiency relative to that of conventional generators that separate electrical and thermal production (Kerr, 2008). The use of renewable technologies and the efficiency gains of CHP lead to significant reduction in emissions, which promote the world’s initiative to reduce global pollution and meet climate change goals. Additionally, research shows that distributed generation systems offer energy savings and play a major role in reducing investments in transmission and distribution capacity (El-Khattam and Salama, 2004; Gumerman et al., 2003). Benefits also include peak shaving, as well as improved system reliability and resiliency (Chiradeja and Ramakumar, 2004). Our research informs the optimal design (i.e., size and mix) and dispatch of renewable technologies with combined heat and power to reduce costs for representative commercial buildings.

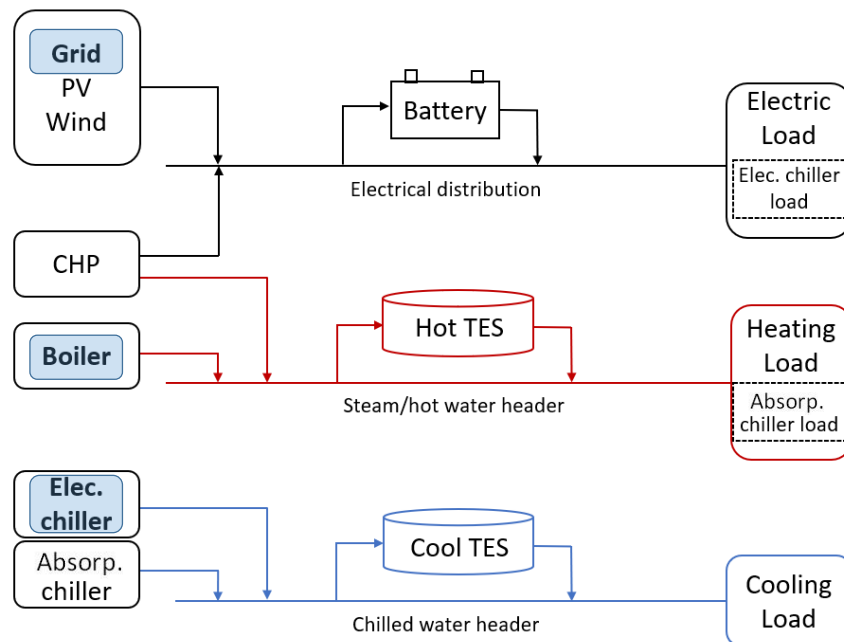


Figure 3.1: A notional distributed generation system with a collection of technologies (including thermal energy storage (TES)) available for electrical, heating, and cooling loads; the technologies highlighted in blue represent a baseline case without distributed resources. Dashed boxes on the right side of the image represent loads that depend on cooling dispatch decisions when an absorption chiller is available. Image adapted from: Anderson et al. (2021).

The National Renewable Energy Laboratory has developed REopt Lite, a model that helps energy planners assess the economic feasibility of using renewable energy technologies, combined heat and power, conventional generators, and storage (Mishra et al., 2021; Anderson et al., 2021). This model determines the system sizes and dispatch decisions, includes an option to assess grid resilience in case of an outage, and incorporates sophisticated pricing structures. For the purpose of this paper, we refer to this model as the original formulation ($\bar{\mathcal{R}}$). Ogunmodede et al. (2021) improve the performance of the mathematical formulation without CHP, but omit implementation details. Our model ($\hat{\mathcal{R}}$) extends the reformulation in Ogunmodede et al. (2021) to include the option of CHP technologies and thermal energy storage,. This involves the addition of: (i) fuel constraints, (ii) thermal production restrictions, (iii) storage operations, (iv) charging rates, (v) cold and hot thermal loads, (vi) load balancing and grid sales, and (vii) standby charges. We correspondingly provide implementation details.

In aggregate, the contributions of our paper are as follows: (i) the extension of an existing energy design and dispatch model (Ogunmodede et al., 2021) to accommodate combined heat and power technologies, (ii) an improvement in the tractability of this (and the Ogunmodede et al. (2021)) model through the use of appropriate data handling and data structures, and thorough reformulation; and, (iii) the presentation of managerial insights gained from solutions to realistic instances of this complicated system. The remainder of the paper is organized as follows: §3.2 reviews the relevant literature. §3.3 presents the notation and corresponding mathematical formulation. §3.4 provides the solution methodology we employ to increase tractability of the model. §3.5 describes the data we use and corresponding results, including performance characteristics and solution analysis. Finally, §3.6 concludes and proposes future work.

3.2 Literature Review

Models that optimally determine design and dispatch simultaneously are NP-hard, and can consist of nonlinear functional forms (Pruitt et al., 2014; Zakrzewski, 2017; De Mel

et al., 2020) and/or integrality restrictions on (some of) the decision variables (Merkel et al., 2015b). Problem simplifications, such as shortening the time horizon (Gopalakrishnan and Kosanovic, 2014, 2015; Fuentes-Cortés and Flores-Tlacuahuac, 2018), aggregating time periods (Oluleye et al., 2018), or scaling down the entire system (Merkel et al., 2015b; Adam et al., 2015) might compromise the quality of the solution, even if the model itself becomes more tractable.

An increasing number of models in literature simultaneously address the design and dispatch problem. Specifically, there have been those that consider dispatching microgrids (Zhao et al., 2014; Scioletti et al., 2017; Goodall et al., 2019), concentrated solar power (Hamilton et al., 2020), and oxidized fuel cells (Anyenya et al., 2018). Some optimization models incorporate combined heat and power. For example, Krug et al. (2020) provide a nonlinear model whose solution dispatches district heating networks, and Rong and Lahdelma (2007) weigh the cost of investing in such technologies against CO₂ emissions in a multi-period stochastic optimization model. Literature demonstrates alternative solutions to design and dispatch with CHP using multi-objective optimization (Perera et al., 2017; Huster et al., 2019; Hollermann et al., 2020). Other models addressing simultaneous design and dispatch with combined heat and power tend to produce sub-optimal solutions to the monolith (Blackburn et al., 2019), or optimal solutions to a problem with reduced scope (Burer et al., 2003; Weber et al., 2006; Pruitt et al., 2013b; Buoro et al., 2014; Silvente et al., 2015). In particular, although Pruitt et al. (2013b,a) make optimal design and dispatch decisions for a combined heat and power system, the pricing structure and operational details of the technologies are not as sophisticated as those we consider.

The Distributed Energy Resources-Customer Adoption Model (DER-CAM) is a mixed-integer linear program. Authors such as Siddiqui et al. (2005), Stadler et al. (2014), Braslavsky et al. (2015), and Mashayekh et al. (2017) report on its capabilities, which consist of generating an optimal design and dispatch strategy for a suite of technologies, subject to constraints on load shifting, peak shaving, power export agreements, and ancillary service markets. Some versions of this model consider detailed electrical

distribution, but loads are not incorporated at a level as fine as hourly, the technologies are dispatched in a coarser manner, and the model lacks certain economic nuances, such as tiered monthly demand charges, minimum required utility payments, and offtake agreements. DESOD (Bracco et al., 2016) optimizes an energy system with CHP for independent buildings, omitting connections to the utility for thermal energy. Dispatch is also on a coarser level, e.g., by considering “typical-day” loads. A shortened time horizon expedites solutions. BALMOREL (Wiese et al., 2018) is an open-source model that considers thermal-producing and distributed energy generation (Nasution et al., 2019; Koivisto et al., 2019; Karlsson and Meibom, 2008). Although the model possesses hourly fidelity, it fails to include resiliency and investment incentives. Connolly et al. (2010) and Ringkjøb et al. (2018) provide significant reviews of energy and electricity system analysis.

3.3 Mathematical Formulation

We introduce the monolith mixed-integer linear programming formulation of our design and dispatch problem, which we term $(\widehat{\mathcal{R}})$. This model is an extension of that given in Ogunmodede et al. (2021), which we term (\mathcal{R}) , and introduces combined heat and power into the system. Figure 3.2 summarizes the variables, objectives, and constraints of the monolith, which seeks design and dispatch decisions for a system of distributed energy resources that minimizes the cost of capital, operations and maintenance, fuel and utility costs, net of production incentives and energy exports. Constraints ensure that: *(i)* system sizing and fuel consumption fall within user-specified limits, *(ii)* valid production and load balance in each time period, and *(iii)* production incentives, utility charges, and other policy structures are accurately accounted for.

This section presents contributions to the model that involve additional or significantly altered constraints. We provide first notation used for these additions, in alphabetic order, and categorized as: *(i)* indices and sets, *(ii)* parameters, and *(iii)* variables. We state for ease of exposition the objective function, and then give the sets of constraints that were significantly modified from (\mathcal{R}) . Finally, we point to the appendix for the remainder, which

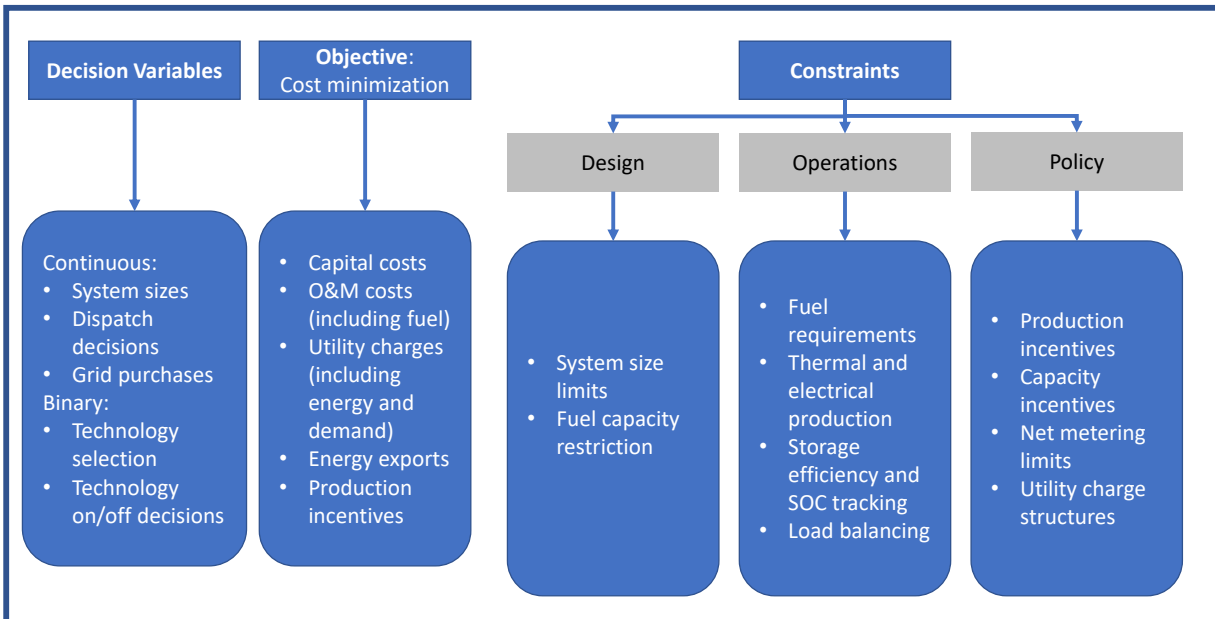


Figure 3.2: A categorical overview of the decision variables, objective function, and constraints that compose the REopt Lite optimization model, $(\hat{\mathcal{R}})$, where SOC and O&M denote state of charge, and operations and maintenance, respectively.

we include for completeness. Our naming convention represents sets using calligraphic capital letters, parameters employing lower-case letters, and variables invoking upper-case letters. Subscripts denote indices, whereas superscripts and other “decorations” represent similar constructs with the same “stem.”

3.3.1 Sets and Parameters

Sets

\mathcal{B}	Storage systems
\mathcal{C}	Technology classes
\mathcal{D}	Time-of-use demand periods
\mathcal{E}	Electrical time-of-use demand tiers
\mathcal{F}	Fuel types
\mathcal{H}	Time steps
\mathcal{M}	Months of the year
\mathcal{N}	Monthly peak demand tiers
\mathcal{T}	Technologies
\mathcal{U}	Total electrical energy pricing tiers

Subsets and Indexed Sets

$\mathcal{B}^c \subseteq \mathcal{B}^{\text{th}}$	Cold thermal energy storage systems
$\mathcal{B}^e \subseteq \mathcal{B}$	Electrical storage systems
$\mathcal{B}^h \subseteq \mathcal{B}^{\text{th}}$	Hot thermal energy storage systems
$\mathcal{B}^{\text{th}} \subseteq \mathcal{B}$	Thermal energy storage systems
$\mathcal{H}^g \subseteq \mathcal{H}$	Time steps in which grid purchasing is available
$\mathcal{H}_m \subseteq \mathcal{H}$	Time steps within a given month m
$\mathcal{H}_d \subseteq \mathcal{H}$	Time steps within electrical power time-of-use demand tier d
$\mathcal{K}_t \subseteq \mathcal{K}$	Subdivisions applied to technology t
$\mathcal{K}^c \subseteq \mathcal{K}$	Capital cost subdivisions
$\mathcal{S}_{tk} \subseteq \mathcal{S}$	Power rating segments from subdivision k applied to technology t
$\mathcal{T}_b \subseteq \mathcal{T}$	Technologies that can charge storage system b
$\mathcal{T}_c \subseteq \mathcal{T}$	Technologies in class c
$\mathcal{T}_f \subseteq \mathcal{T}$	Technologies that burn fuel type f
$\mathcal{T}_v \subseteq \mathcal{T}$	Technologies that may access net-metering regime v
$\mathcal{T}^{\text{ac}} \subseteq \mathcal{T}^{\text{cl}}$	Absorption chillers
$\mathcal{T}^{\text{CHP}} \subseteq \mathcal{T}^{\text{f}}$	CHP technologies
$\mathcal{T}^{\text{cl}} \subseteq \mathcal{T}$	Cooling technologies
$\mathcal{T}^e \subseteq \mathcal{T}$	Electricity-producing technologies
$\mathcal{T}^{\text{ec}} \subseteq \mathcal{T}^{\text{cl}}$	Electric chillers
$\mathcal{T}^{\text{f}} \subseteq \mathcal{T}^e$	Fuel-burning, electricity-producing technologies
$\mathcal{T}^{\text{ht}} \subseteq \mathcal{T}$	Heating technologies
$\mathcal{T}^{\text{td}} \subseteq \mathcal{T}$	Technologies that cannot turn down, i.e., PV and wind
$\mathcal{U}^p \subseteq \mathcal{U}$	Electrical energy purchase pricing tiers
$\mathcal{U}_t^s \subseteq \mathcal{U}^s$	Electrical energy sales pricing tiers accessible by technology t
$\mathcal{U}^{\text{sb}} \subseteq \mathcal{U}^s$	Electrical energy sales pricing tiers accessible by storage

Scaling Parameters

Γ	Number of time periods within a day	[-]
Δ	Time step scaling	[h]
Θ	Peak load oversizing factor	[-]
M	Sufficiently large number	[various]

Parameters for Costs and their Functional Forms

c^{afc}	Utility annual fixed charge	[\$]
c_{ts}^{cb}	y -intercept of capital cost curve for technology t in segment s	[\$]
c_{ts}^{cm}	Slope of capital cost curve for technology t in segment s	[\$/kW]
c_{uh}^e	Export rate for energy in energy demand tier u in time step h	[\$/kWh]
c_{uh}^g	Grid energy cost in energy demand tier u during time step h	[\$/kWh]
c_b^{kW}	Capital cost of power capacity for storage system b	[\$/kW]
c_b^{kWh}	Capital cost of energy capacity for storage system b	[\$/kWh]
c_b^{omb}	Operation and maintenance cost of storage system b per unit of energy rating	[\$/kWh]
c_t^{omp}	Operation and maintenance cost of technology t per unit of production	[\$/kWh]
$c_t^{\text{om}\sigma}$	Operation and maintenance cost of technology t per unit of power rating, including standby charges	[\$/kW]
c_{de}^r	Cost per unit peak demand in time-of-use demand period d and tier e	[\$/kW]
c_{mn}^{rm}	Cost per unit peak demand in tier n during month m	[\$/kW]
c_f^{u}	Unit cost of fuel type f	[\$/MMBTU]

Demand Parameters

δ_h^c	Cooling load in time step h	[kW]
δ_h^d	Electrical load in time step h	[kW]
$\bar{\delta}_u^{\text{gs}}$	Maximum allowable sales in electrical energy demand tier u	[kWh]
δ_h^h	Heating load in time step h	[kW]
δ^{lp}	Look-back proportion for ratchet charges	[fraction]
$\bar{\delta}_n^{\text{mt}}$	Maximum monthly electrical power demand in peak pricing tier n	[kW]
$\bar{\delta}_e^t$	Maximum power demand in time-of-use demand tier e	[kW]
$\bar{\delta}_u^{\text{tu}}$	Maximum monthly electrical energy demand in tier u	[kWh]

Incentive Parameters

\bar{i}_t	Upper incentive limit for technology t	[\$]
i_v^{n}	Net metering limits in net metering regime v	[kW]
i_t^r	Incentive rate for technology t	[\$/kWh]
\bar{i}_t^{σ}	Maximum power rating for obtaining production incentive for technology t	[kW]

Technology-Specific Time-Series Factor Parameters

f_{th}^{ed}	Electrical power de-rate factor of technology t at time step h	[unitless]
f_{th}^{fa}	Fuel burn ambient correction factor of technology t at time step h	[unitless]
f_{th}^{ha}	Hot water ambient correction factor of technology t at time step h	[unitless]

f_{th}^{ht}	Hot water thermal grade correction factor of technology t at time step h	[unitless]
f_{th}^p	Production factor of technology t during time step h	[unitless]

Technology-Specific Factor Parameters

f_t^d	Derate factor for turbine technology t	[unitless]
f_t^l	Levelization factor of technology t	[fraction]
f_t^{li}	Levelization factor of production incentive for technology t	[fraction]
f_t^{pf}	Present worth factor for fuel for technology t	[unitless]
f_t^{pi}	Present worth factor for incentives for technology t	[unitless]
f_t^{td}	Minimum turn down for technology t	[unitless]

Generic Factor Parameters

f^e	Energy present worth factor	[unitless]
f^{om}	Operations and maintenance present worth factor	[unitless]
f^{tot}	Tax rate factor for off-taker	[fraction]
f^{tow}	Tax rate factor for owner	[fraction]

Power Rating and Fuel Limit Parameters

b_f^{fa}	Amount of available fuel for fuel type f	[MMBTU]
\bar{b}_t^σ	Maximum power rating for technology t	[kW]

Efficiency Parameters

η_{bt}^+	Efficiency of charging storage system b using technology t	[fraction]
η_b^-	Efficiency of discharging storage system b	[fraction]
η^{ac}	Absorption chiller efficiency	[fraction]
η^b	Boiler efficiency	[fraction]
η^{ec}	Electric chiller efficiency	[fraction]
η^{g+}	Efficiency of charging electrical storage using grid power	[fraction]

Storage Parameters

\bar{w}_b^{kW}	Maximum power output of storage system b	[kW]
\underline{w}_b^{kW}	Minimum power output of storage system b	[kW]
\bar{w}_b^{kWh}	Maximum energy capacity of storage system b	[kWh]
\underline{w}_b^{kWh}	Minimum energy capacity of storage system b	[kWh]
w_b^d	Decay rate of storage system b	[1/h]
\underline{w}_b^{mcp}	Minimum percent state of charge of storage system b	[fraction]
w_b^0	Initial percent state of charge of storage system b	[fraction]

Fuel Burn Parameters

m_t^{fb}	y -intercept of the fuel rate curve for technology t	[MMBTU/h]
m_t^{fbm}	Fuel burn rate y -intercept per unit size for technology t	[MMBTU/kWh]
m_t^{fm}	Slope of the fuel rate curve for technology t	[MMBTU/kWh]

CHP Thermal Performance Parameters

k_t^{te}	Thermal energy production of CHP technology t per unit electrical output	[unitless]
k_t^{tp}	Thermal power production of CHP technology t per unit power rating	[unitless]

3.3.2 Variables

Boundary Conditions

$X_{b,0}^{se}$	Initial state of charge for storage system b	[kWh]
----------------	--	-------

Continuous Variables

X_b^{bkW}	Power rating for storage system b	[kW]
X_b^{bkWh}	Energy rating for storage system b	[kWh]
X_{de}^{de}	Peak electrical power demand allocated to tier e and time-of-use demand period d	[kW]
X_{bh}^{dfs}	Power discharged from storage system b during time step h	[kW]
X_{mn}^{dn}	Peak electrical power demand allocated to tier n during month m	[kW]
X_{th}^f	Fuel burned by technology t in time step h	[MMBTU/h]
X_{th}^{fb}	y -intercept of fuel burned by technology t in time step h	[MMBTU/h]
X_{uh}^g	Power purchased from the grid for electrical load in demand tier u during time step h	[kW]
X_h^{gts}	Electrical power delivered to storage by the grid in time step h	[kW]
X^{mc}	Annual utility minimum charge adder	[\$]
X_t^{pi}	Production incentive collected for technology t	[\$]
X^{plb}	Peak electrical demand during look back periods	[kW]
X_{tuh}^{ptg}	Exports from production to the grid by technology t in demand tier u during time step h	[kW]
X_{bth}^{pts}	Power from technology t used to charge storage system b during time step h	[kW]
X_{th}^{ptw}	Thermal power from technology t sent to waste or curtailed during time step h	[kW]
X_{th}^{rp}	Rated production of technology t during time step h	[kW]
X_t^σ	Power rating of technology t	[kW]
$X_{tks}^{\sigma s}$	Power rating of technology t allocated to subdivision k , segment s	[kW]
X_{bh}^{se}	State of charge of storage system b at the end of time step h	[kWh]
X_{uh}^{stg}	Exports from storage to the grid in demand tier u during time step h	[kW]
X_{th}^{tp}	Thermal production of technology t in time step h	[kW]
X_{th}^{tpb}	y -intercept of thermal production of CHP technology t in time step h	[kW]

Binary Variables

$Z_{tks}^{\sigma s}$	1 If technology t in subdivision k , segment s is chosen; 0 otherwise	[unitless]
Z_{th}^{to}	1 If technology t is operating in time step h ; 0 otherwise	[unitless]

3.3.3 Objective Function

$$\begin{aligned}
(\widehat{\mathcal{R}}) \quad & \text{minimize} \quad \underbrace{\sum_{t \in \mathcal{T}, k \in \mathcal{K}^c, s \in \mathcal{S}_{tk}} \left(c_{ts}^{\text{cm}} \cdot X_{tks}^{\sigma s} + c_{ts}^{\text{cb}} \cdot Z_{tks}^{\sigma s} \right)}_{\text{Generating Technology Capital Costs}} + \\
& \underbrace{\sum_{b \in \mathcal{B}} \left(c_b^{\text{kW}} \cdot X_b^{\text{bkW}} + (c_b^{\text{kWh}} + c_b^{\text{omb}}) \cdot X_b^{\text{bkWh}} \right)}_{\text{Storage Capital Costs}} + \\
& (1 - f^{\text{tow}}) \cdot f^{\text{om}} \cdot \left(\underbrace{\sum_{t \in \mathcal{T}} c_t^{\text{om}\sigma} \cdot X_t^\sigma}_{\text{Fixed O\&M Costs}} + \underbrace{\sum_{t \in \mathcal{T}^f, h \in \mathcal{H}} c_t^{\text{omp}} \cdot X_{th}^{\text{rp}}}_{\text{Variable O\&M Costs}} \right) + \\
& \underbrace{(1 - f^{\text{tot}}) \cdot \Delta \cdot \sum_{f \in \mathcal{F}} c_f^{\text{u}} \cdot \sum_{t \in \mathcal{T}_f, h \in \mathcal{H}} f_t^{\text{pf}} \cdot X_{th}^{\text{f}}}_{\text{Fuel Charges}} + \\
& (1 - f^{\text{tot}}) \cdot f^{\text{e}} \cdot \underbrace{\left(\Delta \cdot \sum_{u \in \mathcal{U}^p, h \in \mathcal{H}^g} c_{uh}^{\text{g}} \cdot X_{uh}^{\text{g}} \right)}_{\text{Grid Energy Charges}} + \\
& \underbrace{\sum_{d \in \mathcal{D}, e \in \mathcal{E}} c_{de}^{\text{r}} \cdot X_{de}^{\text{de}}}_{\text{Time-of-Use Demand Charges}} + \underbrace{\sum_{m \in \mathcal{M}, n \in \mathcal{N}} c_{mn}^{\text{rm}} \cdot X_{mn}^{\text{dn}}}_{\text{Monthly Demand Charges}} + \\
& \underbrace{c^{\text{afc}} + X^{\text{mc}}}_{\text{Fixed Charges}} - \\
& \underbrace{\Delta \cdot \left(\sum_{h \in \mathcal{H}^g} \left(\sum_{u \in \mathcal{U}^{\text{sb}}} c_{uh}^{\text{e}} \cdot X_{uh}^{\text{stg}} + \sum_{t \in \mathcal{T}, u \in \mathcal{U}_t^{\text{s}}} c_{uh}^{\text{e}} \cdot X_{tuh}^{\text{ptg}} \right) \right)}_{\text{Energy Export Payment}} - \\
& (1 - f^{\text{tow}}) \cdot \underbrace{\sum_{t \in \mathcal{T}} X_t^{\text{pi}}}_{\text{Production Incentives}}
\end{aligned}$$

The objective function is the same as that in (\mathcal{R}) and minimizes energy life cycle cost, i.e., capital costs, operations and maintenance costs, and utility costs; it maximizes (by subtracting) payments for energy exports and other incentives.

3.3.4 Constraints

We mathematically present and describe the constraints that we modify from Ogunmodede et al. (2021) to account for combined heat and power. For ease of presentation, we exclude initial conditions and other minor exceptions.

3.3.4.1 Fuel constraints

$$\Delta \cdot \sum_{t \in \mathcal{T}_f, h \in \mathcal{H}} X_{th}^f \leq b_f^{\text{fa}} \quad \forall f \in \mathcal{F} \quad (3.1a)$$

$$X_{th}^f = m_t^{\text{fm}} \cdot f_{th}^{\text{p}} \cdot X_{th}^{\text{rp}} + m_t^{\text{fb}} \cdot Z_{th}^{\text{to}} \quad \forall t \in \mathcal{T}^f \setminus \mathcal{T}^{\text{CHP}}, h \in \mathcal{H} \quad (3.1b)$$

$$X_{th}^f = m_t^{\text{fm}} \cdot X_{th}^{\text{tp}} \quad \forall t \in \mathcal{T}^{\text{ht}} \setminus \mathcal{T}^{\text{CHP}}, h \in \mathcal{H} \quad (3.1c)$$

$$X_{th}^f = f_{th}^{\text{fa}} \cdot (X_{th}^{\text{fb}} + f_{th}^{\text{p}} \cdot m_t^{\text{fm}} \cdot X_{th}^{\text{rp}}) \quad \forall t \in \mathcal{T}^{\text{CHP}}, h \in \mathcal{H} \quad (3.1d)$$

$$m_t^{\text{fbm}} \cdot X_t^\sigma - M \cdot (1 - Z_{th}^{\text{to}}) \leq X_{th}^{\text{fb}} \quad \forall t \in \mathcal{T}^{\text{CHP}}, h \in \mathcal{H} \quad (3.1e)$$

Constraints (3.1) enforce the fuel requirements for the combustion-powered technologies in REopt Lite. Constraint (3.1a) limits the available quantity of each fuel type per annum; we assume that while multiple technologies (e.g., natural gas boilers and CHP systems) may share the same fuel type, each technology may burn at most one type of fuel.

Constraint (3.1b) enforces both a fixed consumption rate per hour of operational time and a variable burn rate per unit of energy produced for each electric, non-CHP technology.

Constraint (3.1c) applies logic similar to that in constraint (3.1b) for non-CHP heating technologies, but removes the fixed fuel consumption rate during operation.

Constraint (3.1d) defines fuel consumption for CHP systems using both a per-operating-hour rate and a per-unit-production rate, but, unlike constraint (3.1b), the hourly burn rate is a decision variable; constraint (3.1e) sets this decision variable to a fixed proportion of the system's power rating if it is operating, and to zero otherwise.

3.3.4.2 Thermal production constraints

$$X_{th}^{\text{tpb}} \leq \min \{ k_t^{\text{tp}} \cdot X_t^\sigma, M \cdot Z_{th}^{\text{to}} \} \quad \forall t \in \mathcal{T}^{\text{CHP}}, h \in \mathcal{H} \quad (3.2a)$$

$$X_{th}^{\text{tpb}} \geq k_t^{\text{tp}} \cdot X_t^\sigma - M \cdot (1 - Z_{th}^{\text{to}}) \quad \forall t \in \mathcal{T}^{\text{CHP}}, h \in \mathcal{H} \quad (3.2b)$$

$$f_{th}^{\text{ha}} \cdot f_{th}^{\text{ht}} \cdot \left(k_t^{\text{te}} \cdot f_{th}^{\text{p}} \cdot X_{th}^{\text{rp}} + X_{th}^{\text{tpb}} \right) = X_{th}^{\text{tp}} \quad \forall t \in \mathcal{T}^{\text{CHP}}, h \in \mathcal{H} \quad (3.2c)$$

Constraints (3.2a)-(3.2b) limit the fixed component of thermal production of CHP technology t in time step h to the product of the thermal power production per unit of power rating and the power rating itself if the technology is operating, and 0 if it is not. Constraint (3.2c) relates the thermal production of a CHP technology to its constituent components, where the relationship includes a term that is proportional to electrical power production in each time step.

3.3.4.3 Storage System Constraints

Boundary Conditions and Size Limits

$$X_{b,0}^{\text{se}} = w_b^0 \cdot X_b^{\text{bkWh}} \quad \forall b \in \mathcal{B} \quad (3.3a)$$

$$\underline{w}_b^{\text{bkWh}} \leq X_b^{\text{bkWh}} \leq \bar{w}_b^{\text{bkWh}} \quad \forall b \in \mathcal{B} \quad (3.3b)$$

$$\underline{w}_b^{\text{bkW}} \leq X_b^{\text{bkW}} \leq \bar{w}_b^{\text{bkW}} \quad \forall b \in \mathcal{B} \quad (3.3c)$$

Constraint (3.3a) initializes a storage system's state of charge using a fraction of its energy rating; constraints (3.3b) and (3.3c) limit the storage system size under the implicit assumption that a storage system's power and energy ratings are independent. These constraints are identical to those given in (\mathcal{R}) , but work in conjunction with significantly modified storage constraints that directly follow.

Storage Operations

$$X_{bth}^{\text{pts}} + \sum_{u \in \mathcal{U}_t^{\text{s}}} X_{tuh}^{\text{ptg}} \leq f_{th}^{\text{p}} \cdot f_t^{\text{l}} \cdot X_{th}^{\text{rp}} \quad \forall b \in \mathcal{B}^{\text{e}}, t \in \mathcal{T}^{\text{e}}, h \in \mathcal{H}^{\text{g}} \quad (3.3d)$$

$$X_{bth}^{\text{pts}} \leq f_{th}^{\text{p}} \cdot f_t^{\text{l}} \cdot X_{th}^{\text{rp}} \quad \forall b \in \mathcal{B}^{\text{e}}, t \in \mathcal{T}^{\text{e}}, h \in \mathcal{H} \setminus \mathcal{H}^{\text{g}} \quad (3.3e)$$

$$X_{bth}^{\text{pts}} \leq f_{th}^{\text{p}} \cdot X_{th}^{\text{tp}} \quad \forall b \in \mathcal{B}^{\text{th}}, t \in \mathcal{T}_b \setminus \mathcal{T}^{\text{CHP}}, h \in \mathcal{H} \quad (3.3f)$$

$$X_{bth}^{\text{pts}} + X_{th}^{\text{ptw}} \leq X_{th}^{\text{tp}} \quad \forall b \in \mathcal{B}^{\text{h}}, t \in \mathcal{T}^{\text{CHP}}, h \in \mathcal{H} \quad (3.3g)$$

$$X_{bh}^{\text{se}} = X_{b,h-1}^{\text{se}} + \Delta \cdot \left(\sum_{t \in \mathcal{T}^{\text{e}}} (\eta_{bt}^+ \cdot X_{bth}^{\text{pts}}) + \eta^{\text{g}+} \cdot X_h^{\text{gts}} - X_{bh}^{\text{dfs}} / \eta_b^- \right) \quad \forall b \in \mathcal{B}^{\text{e}}, h \in \mathcal{H}^{\text{g}} \quad (3.3h)$$

$$X_{bh}^{\text{se}} = X_{b,h-1}^{\text{se}} + \Delta \cdot \left(\sum_{t \in \mathcal{T}^e} (\eta_{bt}^+ \cdot X_{bth}^{\text{pts}}) - X_{bh}^{\text{dfs}} / \eta_b^- \right) \quad \forall b \in \mathcal{B}^e, h \in \mathcal{H} \setminus \mathcal{H}^g \quad (3.3i)$$

$$X_{bh}^{\text{se}} = X_{b,h-1}^{\text{se}} + \Delta \cdot \left(\sum_{t \in \mathcal{T}_b} \eta_{bt}^+ \cdot X_{bth}^{\text{pts}} - X_{bh}^{\text{dfs}} / \eta_b^- - w_b^d \cdot X_{bh}^{\text{se}} \right) \quad \forall b \in \mathcal{B}^{\text{th}}, h \in \mathcal{H} \quad (3.3j)$$

$$X_{bh}^{\text{se}} \geq \underline{w}_b^{\text{mcp}} \cdot X_b^{\text{bkWh}} \quad \forall b \in \mathcal{B}, h \in \mathcal{H} \quad (3.3k)$$

Constraints (3.3d) and (3.3e) restrict the electrical power that charges storage and is exported to the grid (in the former case), or that charges storage only (in the latter case, when grid export is unavailable) from each technology in each time step relative to the amount of electricity produced. Constraint (3.3f) provides an analogous restriction to that of constraint (3.3e) for thermal production, and constraint (3.3g) provides the same restriction for the thermal production of CHP systems. Constraints (3.3h), (3.3i), and (3.3j) balance state of charge for each storage system and time period for three specific cases, respectively: (i) available grid-purchased electricity, (ii) lack of grid-purchased electricity, and (iii) thermal storage, in which we account for decay. Constraint (3.3k) ensures that minimum state-of-charge requirements are not violated.

Charging Rates

$$X_b^{\text{bkW}} \geq \sum_{t \in \mathcal{T}_b} X_{bth}^{\text{pts}} + X_h^{\text{gts}} + X_{bh}^{\text{dfs}} \quad \forall b \in \mathcal{B}^e, h \in \mathcal{H}^g \quad (3.3l)$$

$$X_b^{\text{bkW}} \geq \sum_{t \in \mathcal{T}_b} X_{bth}^{\text{pts}} + X_{bh}^{\text{dfs}} \quad \forall b \in \mathcal{B}^e, h \in \mathcal{H} \setminus \mathcal{H}^g \quad (3.3m)$$

$$X_b^{\text{bkW}} \geq \sum_{t \in \mathcal{T}_b} X_{bth}^{\text{pts}} + X_{bh}^{\text{dfs}} \quad \forall b \in \mathcal{B}^{\text{th}}, h \in \mathcal{H} \quad (3.3n)$$

$$X_{bh}^{\text{se}} \leq X_b^{\text{bkWh}} \quad \forall b \in \mathcal{B}, h \in \mathcal{H} \quad (3.3o)$$

Constraints (3.3l) and (3.3m) require that a battery's power rating must meet or exceed its rate of charge or discharge; the latter constraint considers the case in which the grid is not available. Constraint (3.3n) reflects the power requirements for the thermal system. Constraint (3.3o) requires a storage system's energy level to be at or below the corresponding rating.

Cold and hot thermal loads

$$\sum_{t \in \mathcal{T}^{cl}} f_{th}^p \cdot X_{th}^{tp} + \sum_{b \in \mathcal{B}^c} X_{bh}^{dfs} = \delta_h^c \cdot \eta^{ec} + \sum_{b \in \mathcal{B}^c, t \in \mathcal{T}^{cl}} X_{bth}^{pts} \quad \forall h \in \mathcal{H} \quad (3.4a)$$

$$\begin{aligned} \sum_{t \in \mathcal{T}^{CHP}} X_{th}^{tp} + \sum_{t \in \mathcal{T}^{ht} \setminus \mathcal{T}^{CHP}} f_{th}^p \cdot X_{th}^{tp} + \sum_{b \in \mathcal{B}^h} X_{bh}^{dfs} &= \delta_h^h \cdot \eta^b \\ + \sum_{t \in \mathcal{T}^{CHP}} X_{th}^{ptw} + \sum_{b \in \mathcal{B}^h, t \in \mathcal{T}^{ht}} X_{bth}^{pts} + \sum_{t \in \mathcal{T}^{ac}} X_{th}^{tp} / \eta^{ac} &\quad \forall h \in \mathcal{H} \end{aligned} \quad (3.4b)$$

Constraints (3.4a) and (3.4b) balance cold and hot thermal loads, respectively, by equating the power production and the power from storage with the sum of the demand, the power to storage, and, in the case of cold loads, from the absorption chillers as well. Here, for legacy reasons, we have scaled the power by the efficiency of the respective technology; based on our variable definitions, we could have equivalently adjusted these by a coefficient of performance.

3.3.4.4 Production Constraints

$$X_{th}^{rp} \leq \bar{b}_t^\sigma \cdot Z_{th}^{to} \quad \forall t \in \mathcal{T}, h \in \mathcal{H} \quad (3.5a)$$

$$\underline{f}_t^{td} \cdot X_t^\sigma - X_{th}^{rp} \leq \bar{b}_t^\sigma \cdot (1 - Z_{th}^{to}) \quad \forall t \in \mathcal{T}, h \in \mathcal{H} \quad (3.5b)$$

$$X_{th}^{tp} \leq X_t^\sigma \quad \forall t \in \mathcal{T} \setminus \mathcal{T}^e, h \in \mathcal{H} \quad (3.5c)$$

Constraint set (3.5) ensures that the rated production lies between a minimum turn-down threshold and a maximum system size; constraints (3.5a) and (3.5b) are copied from Ogunmodede et al. (2021), while constraint (3.5c) is new. Constraint (3.5a) restricts system power output to its rated capacity when the technology is operating, and to 0 otherwise. Constraint (3.5b) ensures a minimum power output while a technology is operating; otherwise, the constraint is dominated by simple bounds on production. Constraint (3.5c) ensures that the thermal production of non-CHP heating and cooling technologies does not exceed system size.

The remainder of the formulation largely mimics that of (\mathcal{R}) given in Ogunmodede et al. (2021), and is provided in the appendix (along with additional notation).

3.4 Solution Methodology

The mathematical formulation in §3.3 extends the model given in Ogunmodede et al. (2021) to incorporate combined heat and power, which entails the introduction of more technologies and the corresponding constraints to control them, including balancing multiple loads, i.e., cold thermal, hot thermal, and electrical. As such, instances of $(\widehat{\mathcal{R}})$ are more difficult to solve. In order to improve tractability and to enable the model’s use in the web-based tool described in Mishra et al. (2021), we reformulate the model by: (i) introducing tailored data structures; (ii) efficiently handling data; and, (iii) reformulating with a more streamlined set of variables. The improvements are made relative to the implementation of the formulation given in Cutler et al. (2017b), and which we term $(\bar{\mathcal{R}})$.

3.4.1 Introducing tailored data structures

Reducing the instantiation of parameters and variables through the judicious use of sets is critical to mitigating otherwise large instances whose size would preclude them from being solved in a practical amount of time. Brown and Dell (2007) (§4) point towards small examples, while Klotz and Newman (2013b) explain theoretical and computational difficulties associated with large models. Formulation $(\widehat{\mathcal{R}})$ employs subsets and indexed sets to ensure that only appropriate decision variables appear in the objective function and in the constraints, either as a sum and/or according to a constraint qualifier. This reduces the size of the model, both in terms of the number of variables and in terms of the number of constraints an instance contains.

For example, the set \mathcal{T} represents all available technologies; the subset \mathcal{T}^e contains only electricity producing technologies. Similarly, \mathcal{B} represents the set of storage systems; the subset \mathcal{B}^e contains only electrical energy storage systems. Constraint (3.3d) highlights the efficiency of using subsets to limit electrical power dispatched to charge storage and export to the grid for electricity-producing technologies and storage systems.

$$X_{bth}^{\text{pts}} + \sum_{u \in \mathcal{U}_t^s} X_{tuh}^{\text{ptg}} \leq f_{th}^p \cdot f_t^l \cdot X_{th}^{\text{rp}} \quad \forall b \in \mathcal{B}^e, t \in \mathcal{T}^e, h \in \mathcal{H}^s \quad (3.3d)$$

The original formulation used sets, rather than subsets, controlling the terms that appeared in the constraints using binary indicator parameters. Not only did this introduce unnecessary parameters, it induced more terms in the constraint, and an increased number of constraints overall.

A construct similar to subsets that also limits the number of variables and constraints appearing in a model instance are *indexed sets* that restrict the size of a set to relevant elements based on another set. Constraint (3.3f), reformulated from the original model, provides an example in which the set of technologies considered is restricted to those associated with storage, resulting in a qualifier \mathcal{T}_b , rather than a constraint based on each element in the entire set of technologies, \mathcal{T} :

$$X_{bth}^{\text{pts}} \leq f_{th}^{\text{p}} \cdot X_{th}^{\text{tp}} \quad \forall b \in \mathcal{B}^{\text{th}}, t \in \mathcal{T}_b \setminus \mathcal{T}^{\text{CHP}}, h \in \mathcal{H} \quad (3.3f)$$

Similar to the case in which subsets replace larger sets, the case in which indexed sets replace larger sets precludes the need for binary parameters, and reduces both the number of terms a constraint contains, and the number of constraints overall in a given formulation instance.

3.4.2 Efficiently handling data

Data used to populate $(\widehat{\mathcal{R}})$ are drawn from myriad sources, including user-specified inputs, and had been introduced into the original model at disjoint stages during its development, resulting in (i) complex calculations to determine various parameter values; (ii) superfluous variables representing calculations consisting of both parameters and variables; and, (iii) arbitrarily high variable bounds, resulting in potential numerical stability issues (in the case of simple bounds, see Klotz and Newman (2013a)), and in weak linear programming relaxations (in the case of big-M values, see Camm et al. (1990)). In order to preclude variables with unnecessarily and arbitrarily high bounds, we reduce the values using physical limitations, appropriate for a given model instance.

Constraint (3.1a) provides an example of a simple variable bound on X_{th}^f :

$$\Delta \cdot \sum_{t \in \mathcal{T}_f, h \in \mathcal{H}} X_{th}^f \leq b_f^{\text{fa}} \quad \forall f \in \mathcal{F} \quad (3.1a)$$

The maximum fuel limit, b_f^{fa} , had been an arbitrarily large value by default in the original formulation. In order to reduce the size of the feasible region and to control the discrepancy in the orders of magnitude between the largest and smallest non-zero values in a problem instance (thus, reducing the potential for numerical stability issues), we suggest a reasonable default value based on physical attributes of the system:

$$\begin{aligned} b_f^{\text{fa}} &= \sum_{h \in \mathcal{H}} f_{th}^{\text{fa}} \cdot m_t^{\text{fbm}} \cdot \bar{b}_t^\sigma + f_{th}^{\text{fa}} \cdot f_{th}^P \cdot m_t^{\text{fm}} \cdot \bar{b}_t^\sigma \quad t \in \mathcal{T}^{\text{CHP}} \\ b_f^{\text{fa}} &= |\mathcal{H}| \cdot m_t^{\text{fm}} \cdot \bar{b}_t^\sigma \quad \forall t \in \mathcal{T}^{\text{ht}} \setminus \mathcal{T}^{\text{CHP}} \\ b_f^{\text{fa}} &= \sum_{h \in \mathcal{H}} m_t^{\text{fm}} \cdot f_{th}^P \cdot \bar{b}_t^\sigma + m_t^{\text{fb}} \quad \forall t \in \mathcal{T}^f \setminus (\mathcal{T}^{\text{ht}} \cup \mathcal{T}^{\text{CHP}}) \end{aligned}$$

where the first constraint pertains to a CHP technology, the second to a boiler, and third to a diesel generator, respectively.

An example that illustrates a reduction in big-M values follows. Constraint (B.2a) permits nonzero power ratings only for the selected technology and corresponding subdivision in each class:

$$X_t^\sigma \leq M \cdot \sum_{s \in \mathcal{S}_{tk}} Z_{tks}^{\sigma s} \quad \forall c \in \mathcal{C}, t \in \mathcal{T}_c, k \in \mathcal{K}_t \quad (B.2a)$$

Here, the big-M value for the system size can be given by the product of the number of hours in a day and the peak hourly load, assuming there is no economic incentive for exporting energy greater than the peak hourly load; this quantity would conservatively meet daily load, i.e., in the absence of other technologies, including storage devices:

$$M = \bar{b}_t^\sigma = \max_{h \in \mathcal{H}} \{24 \cdot \delta_h^d\}$$

Table 3.1 highlights the list of values we tailor throughout formulation ($\widehat{\mathcal{R}}$).

Table 3.1: Tailored values, i.e., appropriately sized variable bounds and “big-M values,” where those above the dotted line represent explicit right-hand-side “ b ”-values, while those below represent coefficients on binary variables that are either traditional big-M values or are potential replacements for said values based on improvements to user-specified inputs.

Constraints	Input Parameter	Tailored Value	Bound Rationale
(3.1a)	b_f^{fa}	$\Delta \cdot \sum_{h \in \mathcal{H}} (f_{th}^{\text{fa}} \cdot m_t^{\text{fbm}} \cdot \bar{b}_t^\sigma + f_{th}^{\text{fa}} \cdot f_{th}^{\text{p}} \cdot m_t^{\text{fm}} \cdot \bar{b}_t^\sigma)$ $\Delta \cdot \mathcal{H} \cdot m_t^{\text{fm}} \cdot \bar{b}_t^\sigma$ $\Delta \cdot (\sum_{h \in \mathcal{H}} m_t^{\text{fm}} \cdot f_{th}^{\text{p}} \cdot \bar{b}_t^\sigma + \mathcal{H} \cdot m_t^{\text{fb}})$	Per (3.1d) and (3.1e) [†] Per (3.1c) [†] Per (3.1b) [†]
(3.3b)	\bar{w}_b^{bkW}	$\frac{\bar{w}_b^{\text{bkW}}}{\Delta}$	Practical
(3.3c)	\bar{w}_b^{bkWh}	$\sum_{h \in \mathcal{H}} \delta_h^{\text{d}} \quad \forall b \in \mathcal{B}^{\text{e}}$ $\sum_{h \in \mathcal{H}} \delta_h^{\text{h}} \quad \forall b \in \mathcal{B}^{\text{h}}$ $\sum_{h \in \mathcal{H}} \delta_h^{\text{c}} \quad \forall b \in \mathcal{B}^{\text{c}}$	Practical Practical Practical
(B.1b)	\bar{b}_t^σ	\bar{b}_t^σ	Practical
(B.3e), (B.3f)	$\bar{\delta}_u^{\text{gs}}$	$\Delta \cdot \sum_{h \in \mathcal{H}} \delta_h^{\text{d}}$	Practical
(3.1e)	M	$m_t^{\text{fbm}} \cdot \bar{b}_t^\sigma$	Practical
(3.2a), (3.2b)	M	$\bar{b}_t^\sigma \cdot k_t^{\text{tp}}$	Practical
(3.5a), (3.5b), (B.2a)	\bar{b}_t^σ	$\max_{h \in \mathcal{H}} \{\Gamma \cdot \delta_h^{\text{d}}\} \quad \forall t \in \mathcal{T}^{\text{e}}$ $\max_{h \in \mathcal{H}} \{\Theta \cdot \delta_h^{\text{h}}\} \quad \forall t \in \mathcal{T}^{\text{ht}} \setminus \mathcal{T}^{\text{CHP}}$ $\max_{h \in \mathcal{H}} \{\Theta \cdot \delta_h^{\text{c}}\} \quad \forall t \in \mathcal{T}^{\text{ec}}$ $\sum_{h \in \mathcal{H}} \delta_h^{\text{c}} + \frac{\bar{w}_b^{\text{bkWh}}}{\Delta} \quad \forall t \in \mathcal{T}^{\text{ac}}$	Practical Practical Practical Practical
(B.1a)	\bar{i}_t	$\sum_{h \in \mathcal{H}} \Delta \cdot i_t^{\text{r}} \cdot f_t^{\text{pi}} \cdot f_{th}^{\text{p}} \cdot f_t^{\text{li}} \cdot \bar{b}_t^\sigma$	Practical
(B.1b)	M	$\bar{b}_t^\sigma - \bar{i}_t^\sigma$	Practical
(B.4b)	i_v^{n}	$\sum_{t \in \mathcal{T}_v} f_t^{\text{d}} \cdot \bar{b}_t^\sigma$	Per net metering limit
(B.5a)	$\bar{\delta}_{ \mathcal{U} }^{\text{tu}}$	$\max_{m \in \mathcal{M}} \{ \sum_{h \in \mathcal{H}_m} \delta_h^{\text{d}} \}$	Practical
(B.6a)	$\bar{\delta}_{ \mathcal{N} }^{\text{mt}}$	$\max_{m \in \mathcal{M}} \{ \sum_{h \in \mathcal{H}_m} \delta_h^{\text{d}} \}$	Practical
(B.7a)	$\bar{\delta}_{ \mathcal{E} }^{\text{t}}$	$\max_{d \in \mathcal{D}} \{ \sum_{h \in \mathcal{H}_d} \delta_h^{\text{d}} \}$	Practical

[†]The tailored values hold for all relevant instances as given by the constraint qualifiers, e.g., the first expression in the third column of the table is valid $\forall t \in \mathcal{T}^{\text{CHP}}$, the second $\forall t \in \mathcal{T}^{\text{ht}} \setminus \mathcal{T}^{\text{CHP}}$ and the third $\forall t \in \mathcal{T}^{\text{f}} \setminus (\mathcal{T}^{\text{ht}} \cup \mathcal{T}^{\text{CHP}})$. Constraint qualifiers for the other expressions are either explicitly stated or are self-explanatory; some tailored values may be invariant by one or more indices, e.g., the tailored value for (B.3e) and (B.3f) holds $\forall u \in \mathcal{U}$.

3.4.3 Reformulation with streamlined variables

Mixed-integer programs can assume a variety of mathematically equivalent formulations. However, some render instances that are more easily solved than others, in large part owing not to obvious theoretical characteristics, but to a practitioner’s understanding of a solver’s ability to exploit certain mathematical structures (Trick, 2005). It is in this spirit that we examine $(\bar{\mathcal{R}})$ for possible improvements in the mathematical formulation. Specifically, in the original formulation, $(\bar{\mathcal{R}})$, a set $j \in \mathcal{J}$ informed destinations for electrical power, e.g., site demand, storage, curtailment, or the grid, and

determined the relevance of a technology for a particular constraint. Correspondingly, a decision variable, $\hat{Y}_{tjhsu}^{\text{rp}}$, appearing in the original model represented the rated production of technology t at destination j during time step h in segment s from pricing tier u , in which elements t in the set \mathcal{T} represented all dispatchable technologies, including electricity from the grid. Separately, the decision variable $\hat{Y}_{jheun}^{\text{g}}$ was defined as electrical power from the grid dispatched to destination j , in time step h , for demand bin e , in pricing tier u , and monthly peak demand tier n , and a constraint ensured that rated production by the utility was equal to grid purchases:

$$\sum_{s \in \mathcal{S}} \hat{Y}_{tjhsu}^{\text{rp}} = \sum_{e \in \mathcal{E}, n \in \mathcal{N}} \hat{Y}_{jheun}^{\text{g}} \quad \forall j \in \mathcal{J}, u \in \mathcal{U}, h \in \mathcal{H}, t \in \mathcal{T} : t = \text{'Grid'}$$

Formulation $(\hat{\mathcal{R}})$ assumes that electricity from the grid has unlimited availability, removing the need for the above-mentioned constraint. In turn, we note that we can eliminate sets \mathcal{U} , \mathcal{S} , and \mathcal{J} from a variable representing production for the following reasons, respectively: (i) grid purchases are represented by a separate decision variable, so we can excise the utility from the collection of technologies \mathcal{T} , and we can remove the utility-specific pricing tier index u from rated production; (ii) the set of segments $s \in \mathcal{S}$ is only utilized for system sizing decisions; and, (iii) the set of destinations is now informed solely by the technology type. This results in the transformation of the more complicated variable $\hat{Y}_{tjhsu}^{\text{rp}}$ into the much simplified rated production variable, X_{th}^{rp} , where the latter variable is related to system size as follows:

$$X_t^\sigma \leq \bar{b}_t^\sigma \cdot \sum_{s \in \mathcal{S}_{tk}} Z_{tks}^{\sigma s} \quad \forall c \in \mathcal{C}, t \in \mathcal{T}_c, k \in \mathcal{K}_t \quad (\text{B.2a})$$

$$X_{th}^{\text{rp}} = X_t^\sigma \quad \forall t \in \mathcal{T}^{\text{td}}, h \in \mathcal{H} \quad (\text{B.2d})$$

$$X_{th}^{\text{rp}} \leq f_{th}^{\text{ed}} \cdot X_t^\sigma \quad \forall t \in \mathcal{T} \setminus \mathcal{T}^{\text{td}}, h \in \mathcal{H} \quad (\text{B.2e})$$

We replace the set of destinations \mathcal{J} with variables that represent power flows to the grid (X_{tuh}^{ptg}) and to storage (X_{bth}^{pts}). The relationships between these variables are enforced as follows:

$$X_{bth}^{\text{pts}} + \sum_{u \in \mathcal{U}_t^s} X_{tuh}^{\text{ptg}} \leq f_{th}^{\text{p}} \cdot f_t^1 \cdot X_{th}^{\text{rp}} \quad \forall b \in \mathcal{B}^e, t \in \mathcal{T}^e, h \in \mathcal{H}^g \quad (3.3d)$$

$$X_{bth}^{\text{pts}} \leq f_{th}^{\text{p}} \cdot f_t^1 \cdot X_{th}^{\text{rp}} \quad \forall b \in \mathcal{B}^e, t \in \mathcal{T}^e, h \in \mathcal{H} \setminus \mathcal{H}^g \quad (3.3e)$$

And to remove destination j from the original variable \hat{Y}_{jheun}^g containing it, we employ a decision variable for the flow of electricity from the grid to storage (X_h^{gts}):

$$\sum_{u \in \mathcal{U}^p} X_{uh}^g \geq X_h^{\text{gts}} \quad \forall h \in \mathcal{H}^g \quad (B.3c)$$

Without the indices e and n , we enforce peak demand by billing period via constraints (B.6d) and (B.7d):

$$\sum_{n \in \mathcal{N}} X_{mn}^{\text{dn}} \geq \sum_{u \in \mathcal{U}^p} X_{uh}^g \quad \forall m \in \mathcal{M}, h \in \mathcal{H}_m \quad (B.6d)$$

$$\sum_{e \in \mathcal{E}} X_{de}^{\text{de}} \geq \max_{h \in \mathcal{H}_d} \left\{ \sum_{u \in \mathcal{U}^p} X_{uh}^g, \delta^{\text{lp}} \cdot X^{\text{plb}} \right\} \quad \forall d \in \mathcal{D} \quad (B.7d)$$

Finally, constraints (B.3a) and (B.3b) balance load using the rated production and grid purchasing variables described above. Figure 3.3 provides a network flow representation of electrical load balancing under the reformulation, with PV and storage as the technologies, and a grid connection.

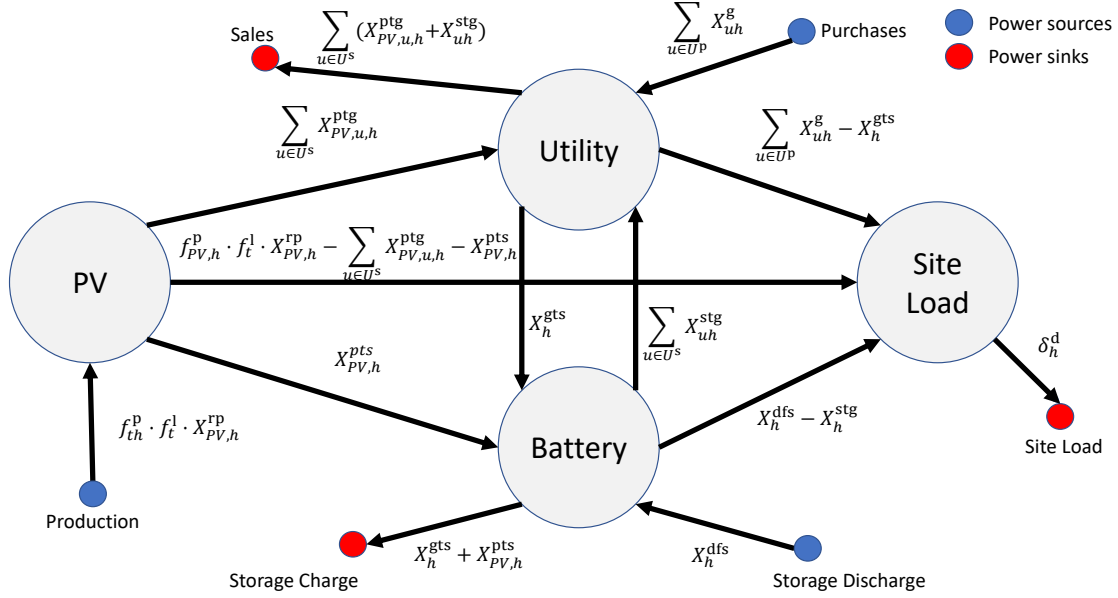


Figure 3.3: A network flow representation of electrical load balancing in the reformulated model, using a PV system and a battery as the on-site technologies.

The revised formulation contains significantly fewer variables. In Figure 3.3, the blue nodes represent sources and the red nodes represent destinations. While inflows and outflows are balanced for the technologies and utility, constraints (B.3a) and (B.3b) enforce flow balance for the node labeled “Site Load” in periods with utility connectivity and with an outage, respectively. Constraints (3.3d) and (3.3e) enforce nonnegative flows from PV to site load with and without a grid connection, respectively. Constraints (B.3c) and (B.3d) provide an analogous restriction on flows to site load from the utility and the battery, respectively.

One demonstration of the increased efficiency of our reformulation is the presence of at most one arc between each pair of nodes in Figure 3.3, whereas in a representation of the previous formulation, each arc departing from PV would have had one copy for each segment s , and each arc departing from the utility would have had at least one additional copy due to the presence of both rated-production and grid-purchase decision variables for the utility, regardless of the number of redundant copies due to additional sets in both cases.

3.5 Data and Results

We derive data for the 12 cases against which we evaluate our performance-enhancing techniques from a test set developed by the National Renewable Energy Laboratory. Each case contains combined heat and power and a boiler, and also some combination of solar photovoltaics, electric chillers, absorption chillers, along with different forms of energy storage such as batteries and thermal (hot and cold) energy storage; we solve for a year’s worth of dispatch decisions at hourly fidelity. In order to fully exercise the model attributes formulated mathematically and explained in §3.3, the case studies differ in the building type, total electrical energy pricing tiers ($|\mathcal{U}|$), monthly peak demand tiers ($|\mathcal{N}|$), time-of-use demand periods ($|\mathcal{D}|$), and whether standby charges apply. (We note that standby charges occur only if CHP technologies are not allowed to reduce peak demand; see constraint (B.6d) and constraint (B.7d).)

We first present the results by comparing models $(\widehat{\mathcal{R}})$ and $(\bar{\mathcal{R}})$ in terms of their problem statistics. Secondly, we compare run-time performance. Finally, we showcase our model’s ability to minimize the users’ dependency on the grid, especially during peak demand, by highlighting aspects of a solution to one case.

3.5.1 Model Statistics

Because of the complicated mathematical structure of our model and the size of our cases, we reformulate model $(\bar{\mathcal{R}})$ as $(\widehat{\mathcal{R}})$ using the methods described in §3.4. Table 3.2 shows the improvements in reformulation $(\widehat{\mathcal{R}})$ as a percent reduction in the number of variables and constraints. We concede that this reduction comes at the expense of a denser A matrix, owing to a more “compact” set of constraints, but the reduction in problem size more than offsets the increased density. That is, the approximately 40% reduction in both the number of variables and in the number of constraints in the reformulated model more than offsets the approximately same increase in the density of the constraint matrix when comparing solve times of the two models; this can be attributed to our use of simplex-based (versus interior point) methods. Furthermore, our reformulated model contains data that is

much better scaled than that of the original model, where the decrease between the largest and smallest non-zero values is five (or more) orders of magnitude.

Table 3.2: Problem statistics for the 12 cases on which we perform computational experiments comparing model $(\bar{\mathcal{R}})$ and model $(\hat{\mathcal{R}})$

Case	Model $(\bar{\mathcal{R}})$		Model $(\hat{\mathcal{R}})$		Density of A -matrix $\cdot 10^3$ (%)		$^1 \log_{10}(k/k')$
	Number of variables	constraints	Reduction (%) in variables	constraints	Model $(\bar{\mathcal{R}})$	Model $(\hat{\mathcal{R}})$	Model $(\bar{\mathcal{R}})$ - Model $(\hat{\mathcal{R}})$
1	333,030	481,914	31.6	36.3	1.03	1.37	5
2	333,030	481,914	28.9	36.3	1.03	1.35	5
3	333,030	481,914	28.9	36.3	1.03	1.35	5
4	490,738	665,255	33.9	43.4	0.72	1.06	5
5	701,038	691,661	55.0	46.8	0.53	1.09	5
6	841,148	691,817	61.5	46.8	0.58	1.09	5
7	1,471,910	735,731	76.2	50.0	0.55	1.15	5
8	490,738	665,255	35.7	43.4	0.72	1.11	5
9	578,366	857,993	30.3	45.9	0.57	0.83	5
10	333,030	481,914	31.6	36.3	1.03	1.37	5
11	333,030	481,914	31.6	36.3	1.03	1.37	5
12	333,030	481,914	31.6	36.3	1.03	1.37	6

¹ Represents the difference in orders of magnitude between the largest and smallest non-zero entries in the data, i.e., across the A -matrix, b -vector and c -vector, as calculated using $\log_{10}(k/k')$, where $k = \max \{ \text{all entries in } A\text{-matrix, } b\text{-vector, } c\text{-vector} \}$ and $k' = \min \{ \text{all entries in } A\text{-matrix, } b\text{-vector, } c\text{-vector} \}$

3.5.2 Model Performance

Model $(\bar{\mathcal{R}})$ is implemented in MOSEL while model $(\hat{\mathcal{R}})$ is implemented in AMPL. They are both solved in Xpress V8.8.0 on a Dell Power Edge R410 server with two Intel Xeon E5520s at 2.27 GHz 28GB RAM, and 1TB HDD. Both models were tuned to achieve the best average performance across cases. Specifically, both AMPL and Mosel use a breadth-first search, while AMPL specifically parallelizes the linear programming solves and Mosel the integer programming solves.

We display problem characteristics associated with each case, and provide the corresponding performance in terms of percent optimality gap achieved within a 10-minute time limit, which was deemed to be appropriate given that our model is embedded in a web-based tool. In each case, model $(\hat{\mathcal{R}})$ performs better than $(\bar{\mathcal{R}})$ by achieving a tighter optimality gap. For each case in which the model finds a feasible solution, the gaps average more than 28% for model $(\bar{\mathcal{R}})$, whereas the corresponding average gap is slightly greater than 2% for these same cases with model $(\hat{\mathcal{R}})$. For Case 9, the only one that exercises

every possible technology combined with both hot and cold thermal energy storage, $(\bar{\mathcal{R}})$ cannot find a feasible solution within the time limit, while $(\hat{\mathcal{R}})$ finds a solution with a 2.65 % optimality gap. Case 7 is another extreme that reaches only a 99.3 % gap using $(\bar{\mathcal{R}})$, whereas $(\hat{\mathcal{R}})$ is able to reach a 1.16 % optimality gap within the time limit. On average (excluding case 9), the overall gap improves by about 98 % using formulation $(\hat{\mathcal{R}})$.

Because our formulation is an extension of model (\mathcal{R}) in Ogunmodede et al. (2021), we also test those cases (i.e., without CHP) and find that our implementation outperforms the original with solution times that average between 30 and 60 seconds – amounting to a reduction of as much as two orders of magnitude (using the same software and hardware).

Table 3.3: Results comparing solution quality obtained from model $(\bar{\mathcal{R}})$ and model $(\hat{\mathcal{R}})$ within a 10-minute time limit. AMPL and Mosel Xpress settings include `backtrack = 5`, while AMPL settings specifically include `lpthreads = 3`, and Mosel settings specifically include `mipthreads = 2`.

Case	¹ Technologies included	$ \mathcal{U} $	$ \mathcal{N} $	$ \mathcal{D} $	Standby charges	Building type	² Gap (%)	
							$\bar{\mathcal{R}}$	$\hat{\mathcal{R}}$
1	CHP, BOIL, EC	1	1	30	No	Hospital	12.5	0.01
2	CHP, BOIL	1	1	30	No	Hospital	15.7	2.98
3	CHP, BOIL, TES	1	1	30	No	Hospital	17.6	4.30
4	CHP, BOIL, BES	1	1	30	No	Hospital	15.8	4.32
5	CHP, BOIL, PV, BES	1	5	12	No	Hospital	35.1	1.31
6	CHP, BOIL, PV, BES	2	2	12	No	Hospital	46.6	0.47
7	CHP, BOIL, PV, BES	5	1	12	No	Hospital	99.3	1.16
8	CHP, BOIL, PV, BES	1	1	30	Yes	Hospital	8.70	0.16
9	CHP, BOIL, PV, BES, TES, AC	1	1	30	No	Hospital	–	2.65
10	CHP, BOIL	1	1	30	No	Large office	11.2	0.13
11	CHP, BOIL	1	1	30	No	Large hotel	26.8	0.38
12	CHP, BOIL	1	1	30	No	Apartment	22.5	6.37

¹ BOIL: Boiler, EC: Electric Chiller, TES: Thermal Energy Storage, BES: Battery Electrical Storage, AC: Absorption Chiller, PV: Solar photovoltaics.

² The gap is reported within a 10-minute time limit and is calculated as: $(\frac{\text{Upper bound} - \text{Lower bound}}{\text{Upper bound}}) \cdot 100$.

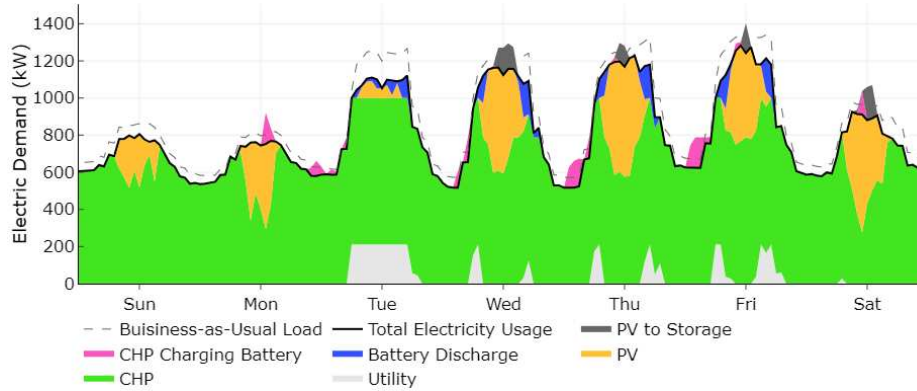
3.5.3 Model Dispatch Strategy

We examine the solution determined by $(\hat{\mathcal{R}})$ for Case 9 which prescribes the systems shown in Table 3.4.

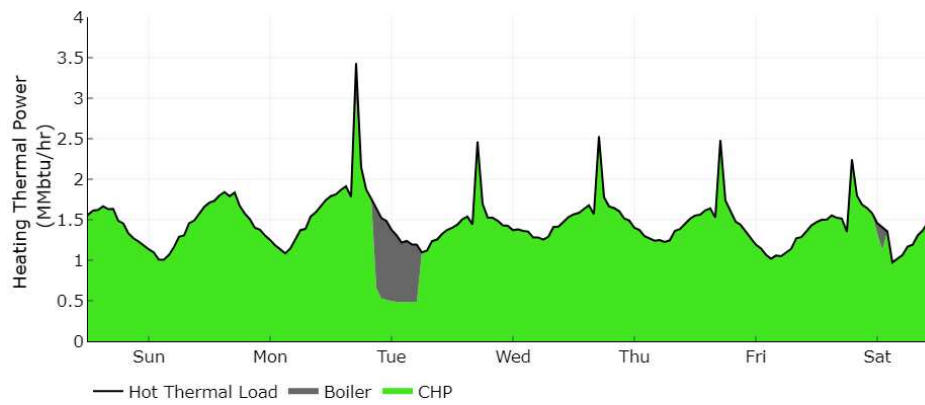
Table 3.4: Model $(\hat{\mathcal{R}})$'s technology mix for Case 9

Technology	Power	Energy	
	[kW]	[kWh]	[gal]
CHP	789	-	-
PV	1,400	-	-
Boiler	1,696	-	-
Absorption Chiller	512	-	-
Electric Chiller	324	-	-
Battery Energy Storage	180	616	-
Chilled Water Thermal Energy Storage	-	-	19

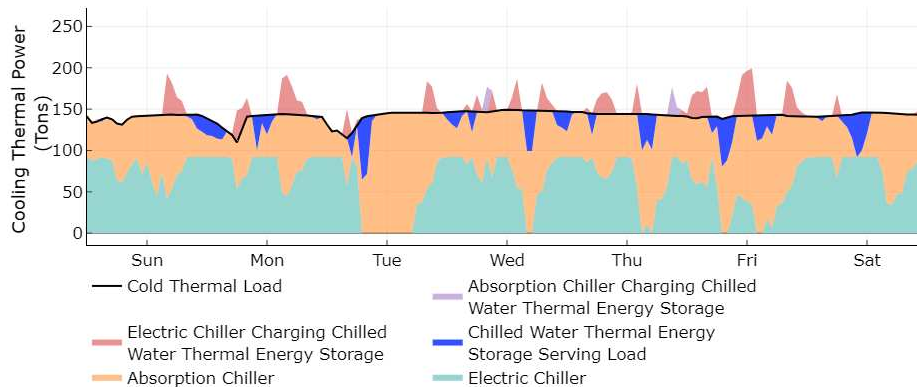
Figure 3.4 displays how the technologies are dispatched to meet hourly site requirements while reducing electrical power consumption from the utility relative to the business-as-usual scenario, which only employs the utility, the boiler, and the electric chiller to meet the electrical, heating, and cooling loads, respectively.



(a) Case 9 Electrical Demand



(b) Case 9 Heating Demand



(c) Case 9 Cooling Demand

Figure 3.4: Dispatch summary for one week within Case 9, in which the technologies reduce peak electrical power consumption from the utility while meeting all hourly site loads

Typically, in an electrical demand graph (see Figure 3.4a), there are five high-demand periods representing the afternoon and evening of each weekday. However, due to Christmas day occurring on Monday of the respective week, there are four. The dashed

line highlights the business-as-usual scenario in which the hospital’s cooling load is entirely met by the electric chiller. The optimized solution for Case 9 exhibits battery discharge, PV, and CHP – reducing the peak utility consumption to 212 kW to meet the majority of the electrical load. Figure 3.4b highlights the dispatch strategy of the CHP and the boiler systems. As part of peak-shaving, the absorption chiller is used instead of the electric chiller, and CHP is run at capacity. The heat provided by CHP cannot meet both the load consumed by the absorption chiller and the site heating load; therefore, the boiler makes up the difference. Figure 3.4c demonstrates the dispatch strategies of the absorption chiller, electric chiller and the chilled water thermal storage system serving the cooling demand. The use of the absorption chiller reduces the dependence of the system on the existing electric chiller, thereby reducing the total electricity usage. The solution associated with model ($\widehat{\mathcal{R}}$) represents a 22% savings over business-as-usual.

3.6 Conclusions

We examine a mixed-integer program that designs and dispatches renewable energy technologies and combined heat and power with a grid option. Instances of our mixed-integer program contain hundreds of thousands of variables and constraints, rendering an initial instantiation of our model intractable. To improve performance, we tailor data structures, efficiently handle data, and streamline the formulation through variable redefinition. These enhancements result in solutions within about 2% of optimality, on average, for the cases we test within a ten-minute time limit, rendering use of the model appropriate for a web-based tool. Without the enhancements, instances generally remain at optimality gaps well above 10% within the same time limit.

Future work could entail implementing a decomposition procedure to further expedite solutions, and employing the model in international settings such as emerging markets of sub-Saharan Africa where opportunities for combined heat and power could enhance economic growth. Additionally, experimental work in thermal science might reveal that a more detailed combined heat and power representation might better reflect the operations

of this technology. Finally, domestic implementation calls for myriad variations of the model and its output, such as considering alternate objective functions that would encompass resiliency and efficiency, and examining a diversity of solutions that would capture intangibles.

CHAPTER 4
UNDERGROUND PRODUCTION SCHEDULING WITH VENTILATION AND REFRIGERATION
CONSIDERATIONS

This paper has been submitted to *Optimization and Engineering*
Oluwaseun Ogunmodede¹, Patricio Lamas², Andrea Brickey³, Gregory Bogin Jr.¹,
Alexandra Newman^{1,4}

Abstract

Mine production scheduling determines when, if ever, notional three-dimensional blocks of ore should be extracted. The accumulation of heat in the mine where operators are extracting ore is a major concern when designing a ventilation system. At the time of this writing, production scheduling and ventilation decisions are not made in concert. Correspondingly, heat limitations from activities are largely ignored. Our model maximizes net present value subject to constraints on precedence, and mill and extraction capacities with the consideration of heat. The model produces more realistic schedules that could increase revenue by determining when, if ever, refrigeration is needed underground. Mine-planning models that fail to consider ventilation and heat produce solutions that are untenable from a health-and-safety standpoint. Our proposed model and corresponding solution methodology provide solutions that maintain a safe working environment for the mine operators. For the realistic instances we test, solution times range between 10 and 25,000 seconds and are provable to within 7% of optimality on average. A conventional approach to solving the monolith of our optimization model with ventilation considerations is otherwise intractable.

¹Colorado School of Mines, Golden, CO 80401

²Universidad Adolfo Ibañez, Santiago, Chile

³South Dakota School of Mines and Technology, Rapid City, SD, 57701

⁴Corresponding Author

4.1 Introduction

Underground mining is a method of extracting deep crustal rock containing economic quantities of metal or minerals, called ore. Rock without sufficient economic value is referred to as waste. Underground mining is most often used when costs or safety factors prohibit accessing the ore deposit from the surface (Hartman and Mutmanský, 2002). Although more expensive on a unit-cost basis than surface mining, most underground mining methods provide greater ore selectivity with reduced waste extraction. Bulk underground mining methods, such as block caving, have limited selectivity; therefore, these methods are associated with much lower unit operating cost. Underground mines use shafts or declines, i.e., a ramp, to provide access from the surface. Connected to the main access infrastructure, drifts and haulage ways provide ingress to the ore deposit. Once mining has begun, ore is transported, i.e., via trucks, trains, or conveyor belts, to the shaft or decline and then to the surface. Most metallic ores require some processing to extract the desired metal, or to remove unwanted minerals or metals contained in the rock, before the final product can be sold. Figure 4.1 shows common underground mine design elements, such as: *(i)* major access infrastructure; *(ii)* production stopes, i.e., areas within the orebody where ore is extracted, leaving a void after extraction; *(iii)* drifts and haulage levels, which are underground openings that provide access for mining equipment to transport material throughout the mine; and, *(iv)* backfilled stopes, which are previously mined areas that are filled with waste or a processing by-product used to maintain the structural integrity of the mine.

Many factors influence the size and scale of an underground mine including: geology, deposit type, geotechnical characteristics, and economics. Through mine planning processes, engineers must determine how the deposit will be: *(i)* accessed, e.g., via a vertical shaft or decline; *(ii)* mined, i.e., according to which mining method; *(iii)* transported, e.g., employing equipment and/or hoists; and, *(iv)* remediated, e.g., by using backfill. These decisions are based on economic factors, e.g., commodity price and mining

costs, physical limitations, operational parameters, and health and safety regulations (Gertsch and Bullock, 1998).

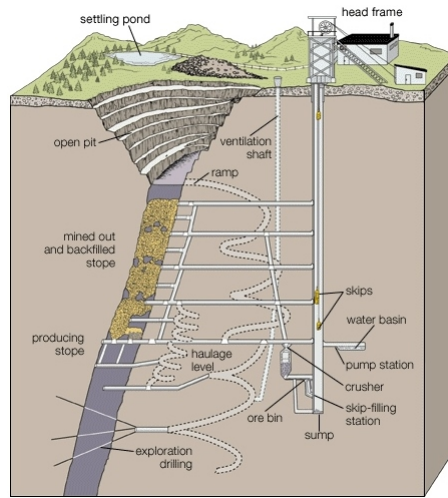


Figure 4.1: Diagram of Open Pit and Underground Mine (Reused with permission by Epiroc: Hamrin (1980))

There are many different underground mining methods, categorized broadly as: unsupported, supported, and caving. Unsupported methods utilize the surrounding rock and sequencing rules dictating the order in which activities are executed to provide stability to mined-out areas. Although unsupported methods may use artificial support systems, e.g., pastefill, to provide structural support, it is not a requirement. Supported methods, such as stull stoping and cut-and-fill, use artificial support structures. Caving methods share the characteristic that some or all of the deposit is allowed to cave by gravitational forces or with the assistance of explosives. The higher productivity associated with caving methods is offset by limited selectivity in the extracted rock. The selection of a mining method is based on numerous factors such as ore strength, depth, shape, and size among other characteristics unique to each deposit (Nieto, 2011).

For this study, we focus on an operation that utilizes sublevel stoping and sublevel caving as their primary mining methods. For both methods, mining areas are defined using economic and engineering factors. Stope size, layout, and number of active mining areas can have a positive correlation with production rates, i.e., larger stopes often result in

higher production rates (Hustrulid and Bullock, 2001). For the areas using sublevel stoping, see Figure 4.2a, the mined out areas, i.e., voids, may be filled with broken waste rock, or waste rock mixed with cement or other binding agents, to provide support to surrounding mining areas. For areas in which sublevel caving is employed, the ore is blasted but the surrounding rock is allowed to cave (Figure 4.2b).

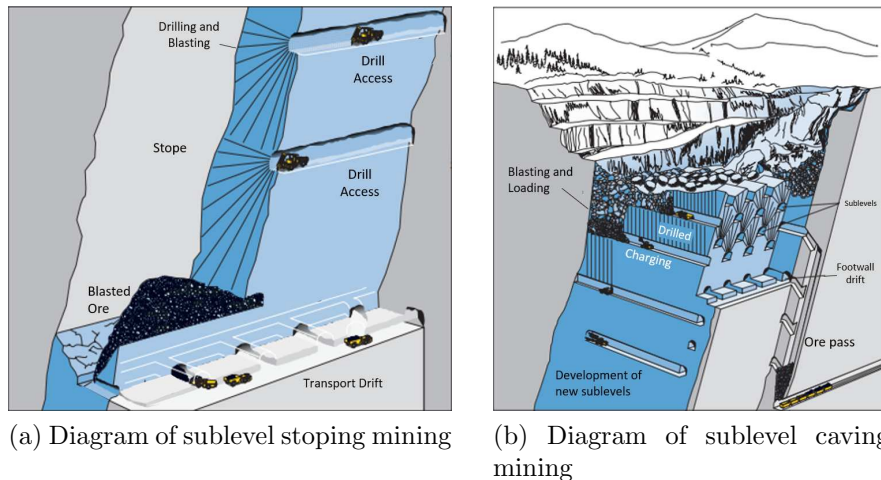


Figure 4.2: Diagrams of the two different mining methods (Reused with permission by Epiroc: Atlas Copco (2007))

4.1.1 Mine Planning

The process of determining how a deposit is mined and operated is termed *mine planning* and includes deposit models, resource and reserve calculations, mining method selection, mine layout, infrastructure design, costs and revenue economics, and production scheduling. The process of mine planning is iterative, often beginning during the exploration stage with a series of studies to determine the technical and economic feasibility of the deposit. If the deposit is viable and proceeds into operation, the design, layout, and infrastructure are continually revised as more information is acquired. This process continues throughout the life of the mine. Using a given mine design, a mine sequence is defined by long-, mid-, and short-term production schedules. As with the mine design, schedules are frequently updated as parameters or conditions of the mine change, e.g., commodity price or deposit definition.

Long-term, i.e., strategic, schedules are used to make high-level decisions regarding the mine, and often span a time horizon of years to decades. Mid-term (tactical) schedules reflect greater detail and a time horizon of one to three years. Short-term schedules provide the operational guidance for day-to-day operations with a time horizon ranging from a few days to a few months. To assist mine engineers with these tasks, some commercial tools are available, such as MineRP's EPS Schedule Optimization Tool (EPSOT) (MineRP, 2015), Datamine's Enhanced Production Scheduler (EPS) (Datamine, 2015), and Deswik.SOT (Deswik Mining Consultants (Australia) Pty Ltd, 2014), yet many underground mine schedules are developed manually, i.e., using spreadsheets. These commercial programs use heuristics to determine solutions whose proximity to optimality cannot be quantified. Despite the availability of these tools, many underground mining operations continue to utilize manual methods, i.e., spreadsheets, to produce production schedules.

4.1.2 Mine Ventilation

Underground mining presents many occupational hazards (Donoghue, 2004), which operators must eliminate or reduce through various control methods. One such hazard is the accumulation of heat and diesel particulate matter. As mines extend deeper underground, naturally occurring heat from geothermal sources, equipment, auto-compression (resulting from the fact that air at lower elevations is more dense), and other sources cause the air temperature to rise. Heat from internal combustion engines, i.e., mining equipment used to transport rock from the mining area to the surface, can add both heat and humidity to the mine air (Hartman et al., 2012; McPherson, 2012). When the human body is exposed to high heat and humidity, there is an increased chance of heat stress and even heat stroke. These physiological effects create a health hazard and must be controlled to protect working miners. Lazaro and Momayez (2020) provide a thorough review of the impacts of heat stress in underground mines.

Ventilation mitigates these nuisances by using mechanical fans to push or pull air through the mine, thereby providing oxygen, flushing out harmful gases, e.g., carbon

monoxide, and diluting particulates, e.g., diesel particulate matter (Hartman et al., 2012). These systems consist of one or more primary fans, which can be located on the surface or underground on a semi-permanent basis. Auxiliary fans, unlike main fans, can be installed for temporary use to direct air to specific (often active) areas of the mine, then moved to other locations when they are no longer needed. Once a ventilation system is constructed and operational, it becomes challenging to modify. Achieving additional airflow can require large capital investments and may necessitate construction of additional infrastructure, e.g., additional fans, ventilation shafts. There are other control methods that can be used to reduce or eliminate these challenges, for example, the use of bio-diesel or Tier 4 engines (Mischler and Colinet, 2009).

Refrigeration, a supplement to mine ventilation, cools air prior to its presence in an active mining area. Refrigeration may be required depending on the depth of the mine and other geological characteristics, and provides support in the removal of heat and/or humidity in the mine. Refrigeration plants tend to be expensive and inflate the already-high costs of mine ventilation.

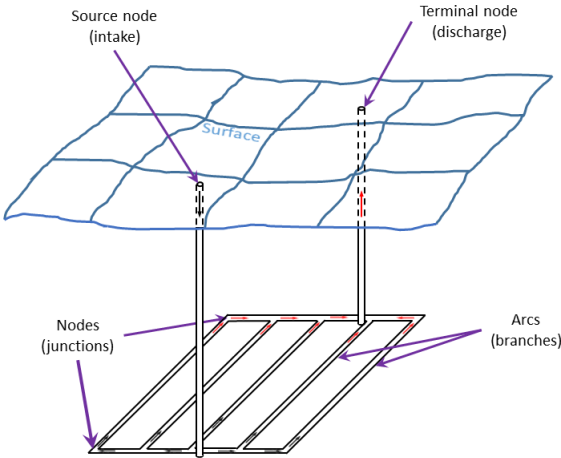


Figure 4.3: Diagram of a basic ventilation network (Reused with permission by creator: Larson (2021))

Ventilation in underground mines can be modeled as a network, where the source node marks the intake and the terminal node signifies the outlet. The workings, e.g., tunnels, of

the underground mine are represented by arcs in the network diagram and the junctions correspond to nodes. Figure 4.3 provides a simplified diagram of an underground mine ventilation network. Numerous commercial software packages are used to evaluate and plan ventilation network systems (Chasm Consulting, 2015; Bluhm et al., 2001; Mine Ventilation Services Inc., 2014).

4.2 Literature Review

Operations research has been used in mining since the 1960's, with most early research directed towards the open pit variant (Lerchs and Grossmann, 1965; Johnson, 1968). Overall, underground mines are much more difficult to schedule than their open-pit counterparts, because of difficulties such as heterogeneous activities (with respect to duration, precedence relationships and resources required for their execution), increased geotechnical risk associated with accessing the ore, and additional protocols necessary for safe operations (O'Sullivan et al., 2015). As demands for more detailed mine plans increase, commensurate advances in algorithms and computational power provide more accurate and more robust production schedules.

4.2.1 Production Scheduling

Until the early 2000s, academic production scheduling models were specific to a given mine. Trout (1995) provides one of the first templates of underground production scheduling for a sublevel stoping operation known as Mt. Isa in Australia. Studies such as Carlyle and Eaves (2001) adapt Trout's work to a hard rock mine in Stillwater, Montana in which development, drilling, and other preparation activities are scheduled. Smith et al. (2003) implement a mixed integer program for a life-of-mine schedule at Mt. Isa that significantly reduces solution times by aggregating time periods; the result, while not provably optimal, demonstrates significant improvement in net present value over those generated via traditional spreadsheet-based methods. LKAB's Kiruna sublevel caving mine in Sweden has used models that implement variable reduction, aggregation, and decomposition techniques to improve tractability (Kutcha et al., 2003; Kuchta et al., 2004;

Newman and Kuchta, 2007; Martinez and Newman, 2011b). These consider details of the operation such as electric tethered load-haul-dump trucks, which limit the amount of equipment with power cables operating in a given area, as well as precedence constraints between so-called machine placements, to minimize the deviation between iron ore produced in each time period and that set by long-term contracts. In particular, a decomposition heuristic provides good solutions by splitting the monolith into sub-problems based on spatial fidelity (Martinez and Newman, 2011b).

Researchers are increasingly solving medium- and short-term models with a commensurate level of detail. Nehring et al. (2010) provide a production scheduling model that integrates long- and short-term scheduling by: (i) considering the net present value of activities, and (ii) taking into account the deviation between when these activities start relative to a predetermined target date. Similarly, Nehring et al. (2012) explore the integration of medium- and short-term planning in underground mining. Although Nehring et al. use a small test case to evaluate the model, such tests highlight the importance of incorporating an increased level of detailed information into the production schedule. As of this writing, this detail includes uncertainty of human and technical factors, such as number of teams, team efficiencies, and team size, that can affect productivity (Sebutsoe and Musingwini, 2017); geological uncertainty (Carpentier et al., 2016); active mining levels available for simultaneous extraction or advancement (Huang et al., 2020); ore mixed near adjacent drawpoint columns (Khodayari and Pourrahimian, 2019); and the availability of mining equipment as a resource (Campeau and Gamache, 2020).

Sotoudeh et al. (2020) provide an overview in which sublevel stoping is the primary underground mining method. The authors encourage researchers to focus on expanding the optimization models to include more detail, thereby increasing the operational feasibility and accuracy of the resulting solutions. Sotoudeh et al. suggest that ventilation is considered by only a few researchers, e.g., Brickey (2015); Sharma (2015); Zhang et al. (2017). Brickey and Sharma both treat airflow as a resource which is limited per time period. Brickey extends this concept by assigning domains based on the location of the

respective activities. Zhang et al. explore the effects that certain activities have on air flow availability in a long-term schedule. While there is significant literature on ventilation and production scheduling in underground mining, there is sparse literature integrating the two topics.

Marks (1980) and Brake and Fulker (2000) examine ventilation, and the refrigeration layout, using economic cost-benefit analysis; although their studies advance the understanding of ventilation, they fail to consider operational factors or the integration of refrigeration and production scheduling. Magri and Unsted (1976) and Anderson and Longson (1986) provide numerical methods to appropriately size ventilation and refrigeration for an underground mine. Specifically, the former research introduces a mixed integer programming model to evaluate ventilation and refrigeration costs for a given production schedule; the latter work is a simulation model. However, neither of the models considers all heat sources; specifically, they omit that from diesel machinery. More detail regarding state-of-the-art modeling in underground production scheduling can be found in Newman et al. (2010), Acuña and Lowndes (2014), and Chowdu et al. (2021).

We show the impact of incorporating ventilation and refrigeration constraints on production schedules and, in so doing, extend Brickey’s work, which focuses on ventilation with respect to the dilution of diesel particulate matter in an airway. Specifically, we consider heat in a detailed computational analysis used to inform the constraint set of our integer program. Section 4.3 highlights the heat considerations in underground mining. Section 4.4 details the initial model formulation. Section 4.5 explains the solution methodology, which, inter alia, involves model reformulation. Section 4.6 analyzes results, and Section 4.7 concludes and suggests future work.

4.3 Underground Mine Ventilation

Heat build-up can be problematic in underground mines, both from a human safety standpoint and also because failure to consider it when planning operations results in compromised schedules. In order to mitigate the unacceptable work conditions associated

with high temperatures, and to better approximate realistic production schedules, we first develop a framework in which we can characterize heat sources in underground mines.

Heat dissipates both temporally and spatially during mining operations; as an activity is executed in one section of the mine, heat is emitted; this heat then travels to other sections over time, increasing the ambient air temperature. A *heat load* is defined as the heat transfer rate from one body to another. The three main sources are the following: *(i)* diesel equipment, *(ii)* auto-compression, and *(iii)* strata rock. We discuss how each of these sources is modeled, calculated, and handled, given the following assumptions: *(i)* the model into which the heat is incorporated is solved at steady state, implying that heat from the previous time period does not inform the heat output for the current time period; *(ii)* the mass flow rate, \dot{m} , is constant on each mine level n ; *(iii)* the air flow velocity is constant, provided that there are auxiliary fans on each level; *(iv)* the relative humidity is constant throughout the mine; and, *(v)* sensible heat from equipment is absorbed into the air of the mine via convection on any given mine level. We note that the greatest mode of heat transfer is convection (relative to conduction and radiation). We use the following notation to mathematically model the heat in the mine:

Symbol	Explanation	Units
Sets		
\mathcal{A}	Activities	
\mathcal{C}	Cycle stages	
\mathcal{E}	Equipment	
\mathcal{N}	Mine levels	
Indexed Sets		
$\tilde{\mathcal{A}}_n \subset \mathcal{A}$	Activities occurring in mine level n	
$\mathcal{C}_e \subset \mathcal{C}$	Cycle stages for equipment e	
$\mathcal{E}_a \subset \mathcal{E}$	Equipment required for activity a	
Parameters		
c_p	Specific heat capacity of the air	$[\frac{J}{kg \cdot ^\circ C}]$
k	Thermal conductivity of the mine rock	$[\frac{W}{m \cdot ^\circ C}]$
l_n	Length of mine level n	$[m]$
\hat{p}_{ea}	Proportion of time equipment e is used for activity a	$[-]$
\hat{p}_{ec}	Proportion of time equipment e is used for cycle stage c	$[-]$
p_n	Perimeter along the length of mine level n	$[m]$
\dot{q}_a	Heat load for activity a	$[W]$
\ddot{q}_{en}	Heat load for equipment e in mine level n	$[W]$
\ddot{q}_{ecn}	Heat load for equipment e during cycle stage c in mine level n	$[W]$
\dot{q}_n^v	Virgin rock heat load on mine level n	$[W]$
r_n	Hydraulic radius of mine level n	$[m]$
z_n	Elevation of mine level n	$[m]$
τ_n^{air}	Air temperature on mine level n	$[^\circ C]$
α	Thermal diffusivity of the mine rock	$[\frac{m^2}{s}]$
ϵ_n	Thermal emissivity coefficient of mine level n	$[-]$
η_n	Age of airway for mine level n	$[s]$
τ_n^v	Virgin rock temperature on mine level n	$[^\circ C]$
ω_n	Goch-Patterson coefficient of mine level n	$[-]$
Physical Constants		
g	Acceleration due to gravity	$[\frac{m}{s^2}]$
∇^T	Thermal gradient	$[\frac{^\circ C}{m}]$

4.3.1 Heat from Diesel Equipment

Much of the heavy machinery necessary for ore extraction consumes diesel fuel and, correspondingly, emits a significant amount of heat into the air. In fact, diesel equipment can account for more than 50% of the heat production in underground operations, causing a non-trivial increase in the ambient air temperature (Bascompta et al., 2016).

Hot exhaust gases from the diesel equipment contain a significant portion of water vapor that impacts both the dry-bulb and the wet-bulb temperatures, the latter of which is calculated based on dry-bulb temperature and relative humidity. Government safety regulations for mine workers stipulate the monitoring of wet-bulb air temperature. Due to the effects of heat on the human body, operations must be halted when the wet-bulb temperature reaches $32.5^{\circ}C$ (Howes, 2011). Each piece of diesel equipment has a specific set of cycle stages associated with the execution of an activity underground. (See Table 4.1 for an example related to a haul truck.) The heat load is estimated as the heat transfer rate from the diesel equipment to the environment and is determined by the engine motor load and the proportion of time the diesel equipment is running at each cycle stage.

Table 4.1: Engine load details for a representative haul truck

Cycle Stage	Engine Power Load [%]	Proportion of Time [%]
Up Ramp	100	40
On Surface	0	5
Down Ramp	10	35
Loading or Idling	10	20

The heat load of the associated diesel equipment can be estimated using a modeling software such as GT-SUITE (Gamma Technologies, 2017), which is a one-dimensional simulation tool that uses fully unsteady nonlinear Navier-Stokes equations based on engine specifications and ambient conditions (see, e.g., Figure 4.4a for a haul truck). Figure 4.4b illustrates the effect of ambient temperature, humidity, and pressure on the heat load, using the haul truck as an example. As the diesel equipment operates deeper in the mine, the air temperature increases. Additionally, due to gravity, traveling deeper in the mine causes increased pressure. The combination of these factors, and changes in humidity,

lower the performance of the engine, and increase the heat released into the environment, assuming a fixed mass of fuel consumed based on the maximum power calculations at standard temperature and pressure conditions (25°C and 101 kPa , respectively).

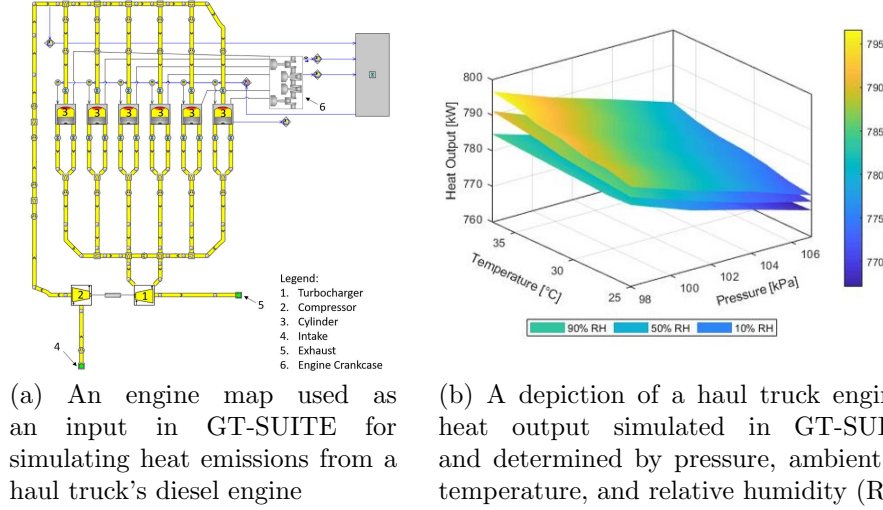


Figure 4.4: Respective inputs and outputs modeled in GT-SUITE (Nichols et al., 2019)

The output from GT-SUITE results in the heat load emitted from any given piece of equipment e in cycle stage c and based on the ambient environment conditions on mine level n , \ddot{q}_{ecn} . Calculating the total heat load associated with a piece of equipment e on a mine level, \ddot{q}_{en} , requires the proportion of time equipment e spends performing cycle stage c , \hat{p}_{ec} , and is given as follows:

$$\ddot{q}_{en} \equiv \sum_{c \in \mathcal{C}_e} \hat{p}_{ec} \cdot \ddot{q}_{ecn} \quad \forall e \in \mathcal{E}, n \in \mathcal{N} \quad (4.1)$$

Due to the variability in activity type and duration, a proportion, \hat{p}_{ea} , is assigned to each piece of equipment e used for activity a to account for the appropriate amount of heat for each respective activity that could occur underground. Therefore, the heat load for each activity a is defined as follows:

$$\dot{q}_a \equiv \sum_{e \in \mathcal{E}_a} \hat{p}_{ea} \cdot \ddot{q}_{en} \quad \forall n \in \mathcal{N}, a \in \tilde{\mathcal{A}}_n \quad (4.2)$$

4.3.2 Heat from Auto-compression

Underground mining operations can exist at depths of up to 4,000 meters below the surface. Auto-compression indicates an increased temperature with this depth, and is caused by the conversion of potential energy into enthalpy directly linked to the elevation, z_n (Wagner, 2013). Equation (4.3) relates the air temperature to the depth, provided the initial surface conditions are known:

$$\tau_n^{\text{air}} = \tau_{n-1}^{\text{air}} + g \cdot \frac{z_{n-1} - z_n}{c_p} \quad \forall n \in \mathcal{N} \quad (4.3)$$

Due to the six-degree change in temperature exhibited in the underground mine we use in our case study, implying that the change in specific heat capacity of air is less than 0.05%, we assume a constant value of $1,005 \frac{J}{kg \cdot ^\circ C}$ based on initial surface dry-bulb temperature of $25^\circ C$. The air temperature due to auto-compression is calculated a priori and provided as a parameter, further discussed in §4.4.

4.3.3 Heat from Strata Rock

As new airways are created in an underground mine, the mine cavity itself gives off heat. Hartman et al. (2012) provide an equation calculating the heat load based on the excavated area for each mine level n :

$$\dot{q}_n^v = l_n \cdot p_n \cdot \frac{k}{r_n} \cdot (\tau_n^v - \tau_n^{\text{air}}) \cdot \omega_n \quad \forall n \in \mathcal{N} \quad (4.4)$$

Thermal rock properties, such as k , are assumed to be known a priori and to be constant throughout the mine; the values are based on mine layout and infrastructure necessary for the geotechnical stability of the operation. Knowledge of the area and volumetric properties, such as length, perimeter and hydraulic radius of the mine level (l_n , p_n , and r_n , respectively), are provided by mine planners a priori and used in software such as Deswik (Deswik Mining Consultants (Australia) Pty Ltd, 2018). The product of l_n and p_n produces the daily area advancement on mine level n . To calculate the virgin rock temperature, τ_n^v , the thermal gradient (∇^T) constant is necessary for all mine levels. The virgin rock temperature increases as elevation (denoted by z_n) decreases – similar to its

relationship with auto-compression:

$$\tau_n^v = \tau_{n-1}^v + (z_{n-1} - z_n) \cdot \nabla^T \quad \forall n \in \mathcal{N} \quad (4.5)$$

The Goch-Patterson coefficient, ω_n , is derived by interpolating the thermal emissivity coefficient, ϵ_n . Hartman et al. (2012) calculate ϵ_n using a collection of airway and thermal rock properties for each level n :

$$\epsilon_n = \frac{\alpha \cdot \eta_n}{r_n^2} \quad \forall n \in \mathcal{N} \quad (4.6)$$

Heat load from virgin rock, \dot{q}_n^v , in equation (4.4), is used as a parameter and discussed further in §4.4. In our mathematical formulation of production scheduling that considers the presence of heat, we also allow for an option to mitigate it, namely through the use of refrigeration, which lowers the initial ambient air temperature and increases the maximum heat load allowed with respect to each mine level.

4.4 Ventilation Formulation (\mathcal{O})

We address the problem of determining, for an underground mine with a set of activities, which are selected, and when they are executed, to yield a production schedule that maximizes discounted net present value. The production schedule adheres to temperature conditions, precedence between activities, and resource constraints such as mill and extraction capacities. The following production-scheduling formulation considers heat in a mine by level while limiting the number of activities simultaneously executed in various active parts of a mine, as necessary. Our *original* formulation, (\mathcal{O}), subscribes to the following optimization modeling assumptions in addition to the thermal science assumptions in §4.3: (*i*) Each activity requires at least one time period to execute; (*ii*) there is a constant mining rate; (*iii*) resources are consumed equally by a given activity over its duration; and, (*iv*) once refrigeration is activated, it must remain on for the remainder of the time horizon. Assumptions (*i*), (*ii*) and (*iii*) can be justified by ensuring that the mining operation is appropriately partitioned both temporally and spatially, respectively, while assumption (*iv*) suffices for tactical mine planning; the concluding section discusses an extension in which this is relaxed.

Symbol	Definition	Units
Sets		
\mathcal{A}	Activities	
\mathcal{N}	Mine levels	
\mathcal{R}	Production resources	
\mathcal{S}	Stages of refrigeration	
\mathcal{T}	Time periods	
Indexed Sets		
$\tilde{\mathcal{A}}_n \subset \mathcal{A}$	Activities that occur on mine level n	
$\hat{\mathcal{A}}_r \subset \mathcal{A}$	Activities that consume production resource r	
$\mathcal{P}_a \subset \mathcal{A}$	Precedence activities for activity a	
Parameters		
c_p	Specific heat capacity of air	$\left[\frac{J}{kg \cdot ^\circ C} \right]$
\hat{d}_a	Duration of activity a	[days]
$\bar{d}_{a'a}$	Delay between finishing activity a' and starting activity a	[days]
f	Fixed cost of refrigerated air	[\$]
\dot{m}_n	Mass flow rate of air on mine level n	$\left[\frac{kg}{s} \right]$
p_a	Net present value derived from performing activity a	[\$]
\dot{q}_a	Heat load for activity a	[W]
\dot{q}_n^v	Virgin rock heat load on mine level n	[W]
r_{ar}	Amount of production resource r required for activity a	[tons, meters, -]
\hat{r}_{rt}	Amount of production resource r available in time period t	[tons, meters, -]
δ	Daily discount rate	[-]
κ	Operation and maintenance cost of refrigeration	[\$]
$\bar{\tau}_n$	Maximum air temperature allowed on mine level n	[$^\circ C$]
τ_n^{air}	Air temperature on mine level n based on auto-compression	[$^\circ C$]
τ_s^{cold}	Refrigerated air temperature at the surface for stage s	[$^\circ C$]
τ_{sn}^{mix}	Air temperature with refrigeration at stage s on level n	[$^\circ C$]
ϕ^{air}	Volumetric portion of ambient air mixed at the surface	[-]
ϕ^{cold}	Volumetric portion of refrigerated air mixed at the surface	[-]
Continuous Variables		
\tilde{H}_{nt}	Net heat load on mine level n during time period t	[W]
F_{nt}	Final air temperature on mine level n at time period t	[$^\circ C$]
Binary Variables		
Y_{at}	1 if activity a starts in time period t , 0 otherwise	[binary]
\hat{Z}_{st}	1 if refrigerated air of stage s is activated by time period t , 0 otherwise	[binary]

$$(\mathcal{O}) \max \left(\frac{1}{1 + \delta} \right)^t \cdot \left(\sum_{a \in \mathcal{A}} \sum_{t \in \mathcal{T}} p_a \cdot Y_{at} - \sum_{s \in \mathcal{S}} \sum_{t \in \mathcal{T}} (f \cdot (\hat{Z}_{st} - \hat{Z}_{s,t-1}) + \kappa \cdot \hat{Z}_{st}) \right) \quad (4.7a)$$

subject to:

$$\sum_{t' \leq t} Y_{at'} \leq \sum_{t'=1}^{t-\bar{d}_{a'}-\hat{d}_{a'}} Y_{a't'} \quad \forall a \in \mathcal{A}, a' \in \mathcal{P}_a, t \in \mathcal{T} \quad (4.7b)$$

$$\sum_{t \in \mathcal{T}} Y_{at} \leq 1 \quad \forall a \in \mathcal{A} \quad (4.7c)$$

$$\sum_{a \in \hat{\mathcal{A}}_r} \sum_{t'=t-\hat{d}_a+1}^t \frac{r_{ar}}{\hat{d}_a} \cdot Y_{at'} \leq \hat{r}_{rt} \quad \forall r \in \mathcal{R}, t \in \mathcal{T} \quad (4.7d)$$

$$\tilde{H}_{nt} = \dot{q}_n^v + \sum_{a \in \hat{\mathcal{A}}_n} \sum_{t'=t-\hat{d}_a+1}^t \dot{q}_a \cdot Y_{at'} \quad \forall n \in \mathcal{N}, t \in \mathcal{T} \quad (4.7e)$$

$$\begin{aligned} \tilde{H}_{nt} = \dot{m}_n \cdot \hat{c}_p \cdot & \left(F_{nt} - \tau_n^{\text{air}} \cdot (1 - \hat{Z}_{1t}) \right. \\ & \left. - \sum_{s \in \mathcal{S}: s > 1} \tau_{s-1,n}^{\text{mix}} \cdot (\hat{Z}_{s-1,t} - \hat{Z}_{st}) - \tau_{|S|n}^{\text{mix}} \cdot \hat{Z}_{|S|t} \right) \quad \forall n \in \mathcal{N}, t \in \mathcal{T} \end{aligned} \quad (4.7f)$$

$$\hat{Z}_{st} \leq \hat{Z}_{s-1,t} \quad \forall s \in \mathcal{S} : s > 1, t \in \mathcal{T} \quad (4.7g)$$

$$\hat{Z}_{s,t-1} \leq \hat{Z}_{st} \quad \forall s \in \mathcal{S}, t \in \mathcal{T} : t > 1 \quad (4.7h)$$

$$0 \leq F_{nt} \leq \bar{\tau}_n \quad \forall n \in \mathcal{N}, t \in \mathcal{T} \quad (4.7i)$$

$$\tilde{H}_{nt} \text{ unrestricted} \quad \forall n \in \mathcal{N}, t \in \mathcal{T} \quad (4.7j)$$

$$Y_{at} \text{ binary} \quad \forall a \in \mathcal{A}, t \in \mathcal{T} \quad (4.7k)$$

$$\hat{Z}_{st} \text{ binary} \quad \forall s \in \mathcal{S}, t \in \mathcal{T} \quad (4.7l)$$

The objective function (4.7a) maximizes the discounted net present value based on the execution time of an activity a and the cost of refrigerated air. Constraint (4.7b) ensures precedence activities, $a' \in \mathcal{P}_a$, of activity a are completed before said activity can start. Constraint (4.7c) restricts all activities $a \in \mathcal{A}$ to at most one start time across the entire horizon $t \in \mathcal{T}$. Constraint (4.7d) limits the number of activities, $a \in \hat{\mathcal{A}}_r$, that can start in time period t based on each production resource limit \hat{r}_{rt} . Constraint (4.7e) monitors the net heat load present from the strata and activities occurring on mine level n . Constraint (4.7f) computes the net heat load from the temperature of the air flowing in and out of a mine level while also considering refrigeration, where the “by” definition of variable \hat{Z}_{st} simplifies the expression on the right-hand side owing to the requirement that, once

activated, refrigeration remains on for the duration of the mine life. The initial mixed air temperature at the surface is calculated as follows:

$$\tau_{s,\text{surface}}^{\text{mix}} = \phi^{\text{air}} \cdot \tau_{\text{surface}}^{\text{air}} + \phi^{\text{cold}} \cdot \tau_s^{\text{cold}} \quad \forall s \in \mathcal{S} \quad (4.8)$$

We assume the volumetric portion of refrigerated air and ambient air is mixed equally ($\phi^{\text{air}} = \phi^{\text{cold}} = 0.50$) at the surface and is sent down to the corresponding levels. The temperature of the mixed air increases as the air travels deeper into the mine due to auto-compression. The corresponding temperature is calculated similar to the way in which the ambient air temperature for mine level n is computed in equation (4.3):

$$\tau_{sn}^{\text{mix}} = \tau_{s,n-1}^{\text{mix}} + g \cdot \frac{z_{n-1} - z_n}{c_p} \quad \forall s \in \mathcal{S}, n \in \mathcal{N} \quad (4.9)$$

Constraint (4.7g) enforces precedence structure of the refrigeration stages. Constraint (4.7h) maintains refrigeration for the remainder of the horizon once active. Constraint (4.7i) ensures non-negativity and an upper bound on the final temperature at time period t on mine level n , while constraints (4.7k) and (4.7l) enforce binary requirements. Figure 4.5 provides a visual depiction of how all of the components are needed to produce an optimal schedule.

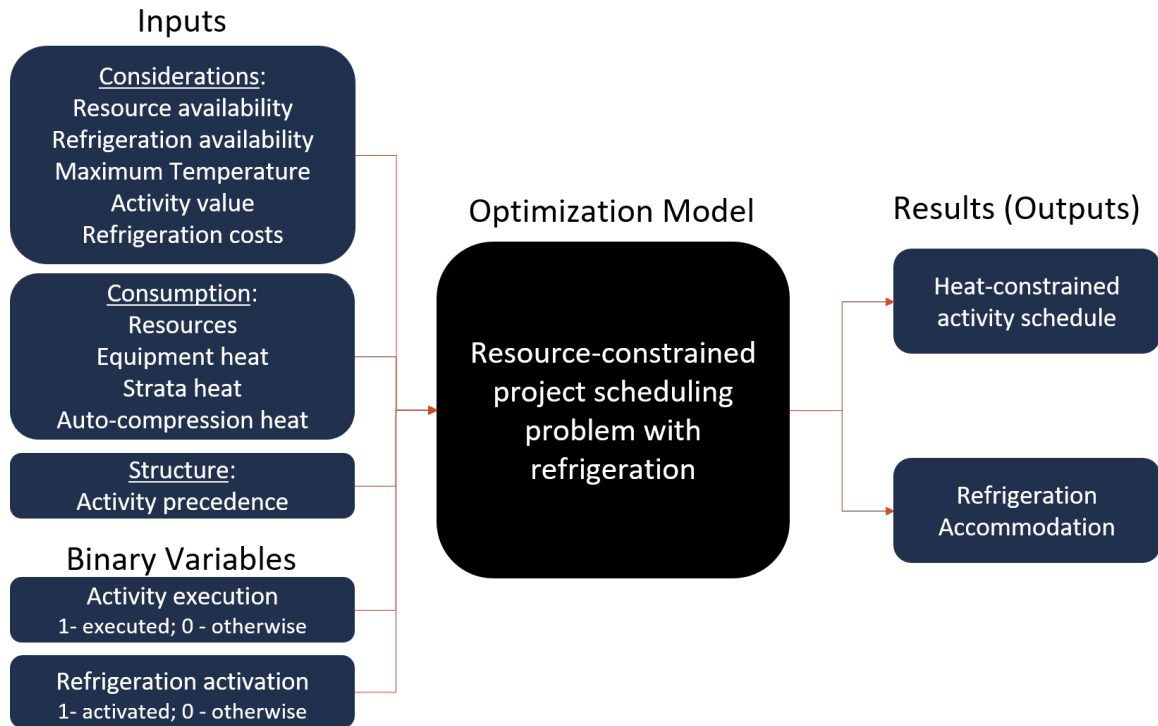


Figure 4.5: Flowchart of necessary attributes from activities such as loading (bottom-left: Agnor (2017)) and hauling ore (bottom-right: Adwo (2020)) to produce an optimal heat-constrained production schedule considering ventilation and refrigeration

4.5 Solution Methodology

State-of-the-art integer-programming solvers such as CPLEX (IBM ILOG, 2020) have difficulty generating solutions for realistic instances of formulation (\mathcal{O}), even to within 10% of optimality in a reasonable amount of time. Many heuristics have been applied to mine planning problems with mathematical structure similar to ours. For example, O’Sullivan and Newman (2014) separate the monolith into several sub-problems associated with the

value of ore, and solve these sub-problems, decreasing by block size. An alternative divides the problem temporally, rather than spatially, using a sliding time window that can accommodate discrete decisions in the shorter term while relaxing variables representing decisions more distant in time to be continuous, and/or not considering them at all (Lopes, 2017). However, there is no guarantee of optimality using either of these approaches; in fact, a monolithic solve that would provide a bound on the solution quality is elusive using standard approaches. However, by reformulating our model as a *Resource Constrained Project Scheduling Problem* (RCPSP), we can exploit its special structure not only to obtain a solution to the linear programming relaxation of the problem (Bienstock and Zuckerberg, 2010) but also to use this solution to generate a good, integer-feasible solution to the monolith. See Muñoz (2012) for details.

4.5.1 Reformulation of (\mathcal{O})

The RCPSP contains three types of constraints: *(i)* precedence (constraint (4.7b)), *(ii)* unique activity start time (constraint (4.7c)), and *(iii)* resource knapsacks (constraint (4.7d)). For ease of implementation in the solver, i.e., OMP (Rivera et al., 2016), we use the “at” (rather than the “by”) variable definitions. To this end, we define the following additional notation for reformulation (\mathcal{R}^+):

Symbol	Definition	Units
Parameters		
\bar{h}_n	Upper heat load limit for level n	[kW]
g_{sn}	Cooling load of stage s for level n	[kW]
Binary Variable		
Z_{st}	1 if refrigerated air of stage s is activated at time period t , 0 otherwise	[binary]

$$(\mathcal{R}^+) \quad \mathbf{max} \quad \left(\frac{1}{1 + \delta} \right)^t \cdot \left(\sum_{a \in \mathcal{A}} \sum_{t \in \mathcal{T}} p_a \cdot Y_{at} - \sum_{s \in \mathcal{S}} \sum_{t \in \mathcal{T}} (f + \kappa \cdot (|\mathcal{T}| - t)) \cdot Z_{st} \right) \quad (4.10a)$$

subject to:

(4.7b), (4.7c), and (4.7d)

$$\sum_{s \in \mathcal{S}} \sum_{\hat{t}=1}^t g_{s\hat{t}} \cdot Z_{s\hat{t}} + \sum_{a \in \tilde{\mathcal{A}}_n} \sum_{t'=\hat{t}-\hat{d}_a+1}^t \dot{q}_a \cdot Y_{at'} \leq \bar{h}_n \quad \forall n \in \mathcal{N}, t \in \mathcal{T} \quad (4.10b)$$

$$\sum_{\hat{t}=1}^t Z_{s\hat{t}} \leq \sum_{\hat{t}=1}^t Z_{s-1,\hat{t}} \quad \forall s \in \mathcal{S} : s > 1, t \in \mathcal{T} \quad (4.10c)$$

$$\sum_{t \in \mathcal{T}} Z_{1t} \leq 1 \quad (4.10d)$$

(4.7k) and (4.7l)

In formulation (\mathcal{R}^+), the variable Z_{st} undergoes a structural change (see, e.g., Lambert et al. (2014) for more detail). Constraints (4.7b), (4.7c), and (4.7d) are retained.

Constraints (4.7e) and (4.7f) are reformulated, eliminating variables \tilde{H}_{nt} and F_{nt} .

Constraint (4.10b) is a relaxed heat resource knapsack that incorporates parameters \bar{h}_n and g_{sn} to account for refrigeration for any given mine level n . Specifically, the upper heat load limit, \bar{h}_n , is defined as:

$$\bar{h}_n = \dot{m}_n \cdot \hat{c}_p \cdot (\bar{\tau}_n - \tau_n^{\text{air}}) - \dot{q}_n^v \quad \forall n \in \mathcal{N} \quad (4.11)$$

where the expression follows from algebraic manipulations on (4.7e) and (4.7f) and the substitution of $\bar{\tau}_n$ for F_{nt} , valid because of the inequality in (4.10b). Equation (4.11) considers the heat load from the virgin rock, \dot{q}_n^v , and uses the ambient air temperature due to auto-compression as an initial temperature on mine level n to inform the maximum allowable heat load on any given level. The cooling load, g_{sn} , for each stage s and mine level n is calculated as:

$$g_{1n} = \dot{m}_n \cdot \hat{c}_p \cdot (\tau_{1n}^{\text{mix}} - \tau_n^{\text{air}}) \quad \forall n \in \mathcal{N} \quad (4.12)$$

$$g_{sn} = \dot{m}_n \cdot \hat{c}_p \cdot (\tau_{sn}^{\text{mix}} - \tau_{s-1,n}^{\text{mix}}) \quad \forall n \in \mathcal{N}, s \in \mathcal{S} : s > 1 \quad (4.13)$$

where the expressions follow owing to algebraic manipulations similar to those used to derive (4.11).

Due to the transformation of Z_{st} , constraints (4.7g) and (4.7h) are transformed into constraints (4.10c) and (4.10d) to represent the precedence structure of refrigeration stages $s \in \mathcal{S}$ for all time periods $t \in \mathcal{T}$. Constraints (4.7i) and (4.7j) are removed due to the excision of F_{nt} and \tilde{H}_{nt} . The revised formulation (\mathcal{R}^+) is structured as an RCPSP. Therefore, we can use the special-purpose, fast solver OMP to generate solutions to its linear programming relaxation.

4.5.2 Propagated Early Start Algorithm

The propagated early start algorithm is an in-built feature of the software we use, and reduces the number of activity-start time combinations (and, hence, Y_{at} variables) based on the precedence structure between activities (including lag times between the completion of one activity and the start time of a successor), and their durations. The set of activities can be visualized as nodes on a graph, and the arcs connecting them denote precedence. Given this, it is possible to traverse the graph in a topologically sorted order and assign to each activity an earliest start time. Any activity without predecessors possesses an early start time corresponding to the first period in the horizon. For any activity with one or more predecessors, the early start is determined by the most constraining time of any predecessor, given as the sum of: (i) the earliest time at which said predecessor can finish and any lag time between the end of that predecessor activity and (ii) the start time of a successor. The propagated early start algorithm helps enhance tractability; variants of this algorithm relying on precedence and resource constraints have been employed in other mining settings, e.g., Martinez and Newman (2011a).

4.5.3 Optimization-Based Heuristic (\mathcal{H})

Given a solution to the linear programming relaxation, (Y', Z') , of formulation (\mathcal{R}^+), we construct a corresponding integer-feasible solution by sequentially running the simple

sorting algorithm (ALGORITHM 1), and the topological sorting algorithm (ALGORITHM 2).

First, ALGORITHM 1 determines the set of activities $\mathcal{A}' \subseteq \mathcal{A}$ that should potentially be scheduled. Specifically, set \mathcal{A}' is defined as follows:

$$\mathcal{A}' \equiv \{a \in \mathcal{A} : \sum_{t \in \mathcal{T}} Y'_{at} \geq \beta\} \quad (4.14)$$

where $\beta \in \mathbb{R}$ is a parameter such that $0 \leq \beta \leq 1$. Larger values of β imply that fewer activities are potentially scheduled.

Then, ALGORITHM 1 sorts activities, non-decreasing by their respective *mean start times*. We define the mean start time M_a for each activity $a \in \mathcal{A}$ as follows:

$$M_a \equiv \sum_{t \in \mathcal{T}} t \cdot Y'_{at} \quad (4.15)$$

Second, ALGORITHM 2 determines, for each stage, at what period refrigeration is activated, and then schedules the activities in topological order. Given a stage s , the time period \tilde{t}_s at which the refrigeration starts is determined as follows:

$$\tilde{t}_s \equiv \min_{t \in \mathcal{T}} \left\{ \sum_{t'=1}^t Z'_{st'} \geq \alpha \right\} \quad (4.16)$$

where $\alpha \in \mathbb{R}$ is a parameter such that $0 \leq \alpha \leq 1$. This parameter represents a threshold value associated with refrigeration start time; larger values for α correspond to later start times.

ALGORITHM 2 repeatedly determines the refrigeration and activity start times for different values of α , and then chooses the best solution. For example, let us assume three alternative values for α : 0.85, 0.9, or 0.95. In this case, ALGORITHM 2 determines three solutions, each of which corresponds to a given value of α ; it then chooses the best solution among the three determined by their respective objective function value. The list that contains the values of α corresponds to α -*points*.

Algorithm 1: SIMPLE SORT

Data: Solution Y' from having solved the linear relaxation of formulation (\mathcal{R}^+)

Result: Sorted list of activities L

1 construct set \mathcal{A}' of activities that will potentially be executed:

$$\mathcal{A}' \leftarrow \{a \in \mathcal{A} : \sum_{t \in \mathcal{T}} Y'_{at} \geq \beta\};$$

2 compute mean starting time M_a of each activity $a \in \mathcal{A}'$: $M_a \leftarrow \sum_{t \in \mathcal{T}} t \cdot Y'_{at}$;

3 sort activities in set \mathcal{A}' , non-decreasing by M_a and assign to ordered list L ;

4 return list L ;

Algorithm 2: TOPOLOGICAL SORT

Data: List of activities L and solution (Y', Z') from having solved the linear relaxation of formulation

(\mathcal{R}^+)

Result: Feasible solution $(Y^{\text{best}}, Z^{\text{best}})$ to formulation (\mathcal{R}^+)

```
1  $v^* \leftarrow -\infty$ ;
2 foreach  $\alpha \in \alpha\_points$  do
3    $Y_{at} \leftarrow 0$  for each activity  $a \in \mathcal{A}$ , time period  $t \in \mathcal{T}$ ;
4   foreach stage  $s \in \mathcal{S}$  do
5      $Z_{st} \leftarrow 0$  for time period  $t \in \mathcal{T}$ ;
6      $\tilde{t}_s \leftarrow \min_{t \in \mathcal{T}} \{\sum_{t'=1}^t Z'_{st'} \geq \alpha\}$ ;
7      $Z_{s\tilde{t}_s} \leftarrow 1$ ;
8   end
9   while list  $L$  is not empty do
10    select the first activity  $a$  in list  $L$  and delete it from  $L$ ;
11    foreach time period  $t \in \mathcal{T}$  do
12      if assigning  $Y_{at}$  to 1 is precedence-, resource-, and heat-feasible then
13         $Y_{at} \leftarrow 1$ ;
14        break;
15      end
16    end
17  end
18  compute objective function value of solution  $(Y, Z)$  and save it in  $v$ ;
19  if  $v > v^*$  then
20     $v^* \leftarrow v$ ;
21     $(Y^{\text{best}}, Z^{\text{best}}) \leftarrow (Y, Z)$ ;
22  end
23 end
24 return feasible solution  $(Y^{\text{best}}, Z^{\text{best}})$ ;
```

4.6 Results

We use data from a large-scale underground hard-rock mining operation in which ore is extracted via a combination of sublevel stoping and sublevel caving. We solve formulation (\mathcal{R}^+) using a direct interface of our model with OMP v20190809 on a Dell Poweredge R610 with Two Hex Core Intel Xeon x5670s running at 2.93 GHz, using 128 GB RAM, and possessing 1 TB HDD. The computational results: (i) illustrate the usage of diesel equipment; (ii) enhance model tractability in terms of solution time and quality of

solutions found; and, (iii) demonstrate the practical benefits of and economic trade-offs associated with the exclusion of heat constraints, and the incorporation of refrigeration as a means to recover production when heat constraints are imposed. Table 4.2 defines the different formulations we test.

Table 4.2: Various formulations used to examine the quality of production schedules

Formulation	Mathematical Description	Characteristics
(\mathcal{R}^-)	(\mathcal{R}^+) without constraint (4.10b)	Omits consideration of heat (typical formulation)
(\mathcal{R})	(\mathcal{R}^+) without variable Z_{st}	Constrains heat while precluding refrigeration (simplistic fix to typical formulation)
(\mathcal{R}^+)	Our formulation	Constrains heat while allowing for refrigeration (proposed)

4.6.1 Equipment overview

The underground mining operation we model utilizes an assortment of diesel and electric equipment. Figure 4.6 shows the percentage of operational hours for equipment associated with activities operating underground. The mine uses a mixed equipment fleet of 70% diesel and 30% electric, averaged across all the operational hours of the anticipated set of activities to be scheduled over the planning horizon.

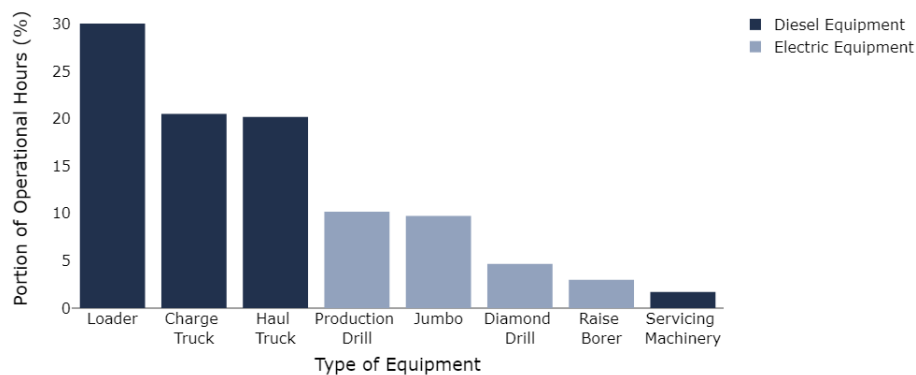


Figure 4.6: Percentage of usage for each type of equipment

4.6.2 Computation

The activity layout of the hard rock mining operation is produced by the mining software DESWIK (Deswik Mining Consultants (Australia) Pty Ltd, 2018); see Figure 4.7. Information regarding the (i) resource, e.g., grade, tons, linear feet, (ii) precedence, and

(iii) location of each individual activity is exported for use in (\mathcal{R}^+) . The heat modeled by GT-SUITE is entered as data for the respective activities in DESWIK. As a means to simplify the formulation (\mathcal{R}^+) and due to the mathematical structure required by OMP at the time of this writing, we assume an initial surface temperature of $25^\circ C$ and 80% relative humidity to be constant for the time horizons we consider based on weather station data provided by industry partners at the mining location. This assumption is considered sufficient for tactical scheduling.

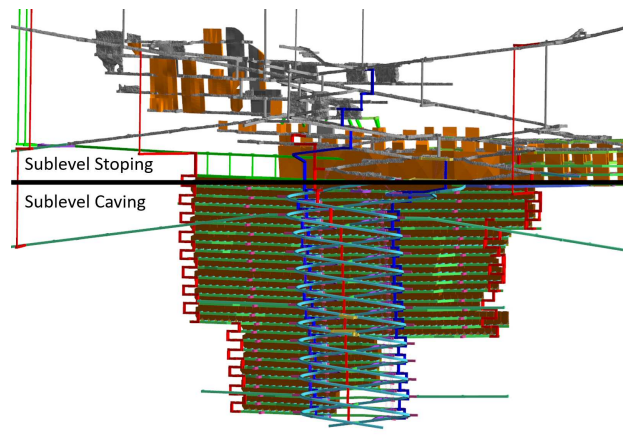


Figure 4.7: The diagram shows the relevant area of the mine, which is comprised of a mixture of sublevel stopping and sublevel caving, in which the former occurs above the black horizontal line, while the latter is executed below the black horizontal line.

Table 4.3 highlights the ten instances we schedule, which contain between 895 and 7,356 activities over a horizon consisting of between 365 and 913 days. Each problem instance is differentiated by the nature of stopping activities, the location of caving level access, and/or the horizon length.

Table 4.3: Problem instances highlighting the number of total activities, stopping activities, caving levels, and horizons lengths

Case	Number of			Horizon [days]
	Total Activities	Stopping Activities	Caving Levels	
1	896	611	-	365
2	1,522	1,062	-	365
3	2,271	380	1	365
4				548
5	2,953	1,062	1	365
6				548
7	6,883	589	2	730
8				913
9	7,356	1,062	2	730
10				913

For each instance, we consider the option to activate a single stage of refrigeration. Due to tractability issues, CPLEX 12.10 was unable to determine feasible solutions even for the smallest case in a reasonable amount of time; Case 1 resulted in optimality gaps of 10% after 70,225 seconds respectively, and refrigeration was not activated. Therefore, we employ the specialized solver OMP to determine better-quality solutions to larger instances within an acceptable amount of run time. Table 4.4 details these results with respect to *(i)* size of each instance, *(ii)* the time at which refrigeration is activated during the schedule, *(iii)* the resulting solution time after solving the linear program to optimality and employing heuristic (\mathcal{H}), and *(iv)* the resulting optimality gap. The solver’s propagated early starts reduce the theoretical problem size by about 37%, on average. Refrigeration is activated in all but the smallest instance, and at varying times during the horizon. Solution times range from between a few seconds to 8 hours, where longer solution times generally correspond to larger instances. On average, the time spent solving the linear programming relaxation constitutes 95% of the solution time; heuristic (\mathcal{H}) accounts for the other 5%. Gaps fall under 10% for all but two instances, averaging 5% for these eight. Two instances have larger gaps (about 12% and 15%) particularly due to the ability of the linear programming relaxation to activate only a small portion of refrigeration and incurring the commensurately small costs; however, given that the instances are unsolvable in their

monolithic instantiations, even these results represent significant improvements.

Table 4.4: Solution details of the respective cases

Case	Variable Count		Refrigeration Activation [day]	Solution Time [seconds]*	Optimality Gap [%]
	Theoretical	Practical [†]			
1	731,798	491,358	-	14	0.35
2	960,806	620,912	8	252	15.34
3	1,235,689	661,226	84	165	7.97
4	2,154,900	1,328,460	82	634	12.89
5	1,485,616	827,792	86	745	9.49
6	2,530,000	1,619,000	89	2,886	6.47
7	6,643,632	4,309,290	123	10,374	2.83
8	8,806,875	6,021,072	129	12,297	5.12
9	6,989,868	4,592,126	65	16,900	3.15
10	9,989,970	6,390,467	130	25,480	4.10

*Solution time includes linear programming relaxation and heuristic (\mathcal{H}) solve time

[†]Variable count representative of early start pre-processing

4.6.3 Managerial Insights

The results from solving all formulation variants listed in Table 4.3 provide insights to mine planners. For long- and medium-term scheduling such as the situation we consider, the objective function maximizes net present value. A proxy for net present value is total daily haulage, because the tons extracted from the mine are subsequently sent to processing (without the intermediate stage of a stockpile, which is generally absent in underground mining), after which the product is sold. The hauled tons are typically the constraining factor in underground mines because of the rate of production relative to the rate at which other activities (such as blasting or backfilling) occur. For Case 7, Figure 4.8 presents the tons hauled, which acts as the limiting factor in at least some of the time periods over the course of the horizon. However, for the variant in which heat is not constrained, the tons hauled appears to be the limiting factor most of time; this suggests unreasonably high production levels and correspondingly unacceptably high temperatures. At the opposite extreme, the formulation in which we constrain heat but preclude refrigeration exhibits the fewest tons hauled, indicating that without the option to cool the

mine, the schedule extracts less material, lowering the net present value. Employing the option of refrigeration mitigates heat levels while maintaining a fairly high production rate, and represents the most realistic, yet opportunistic, situation. Table 4.5 summarizes.

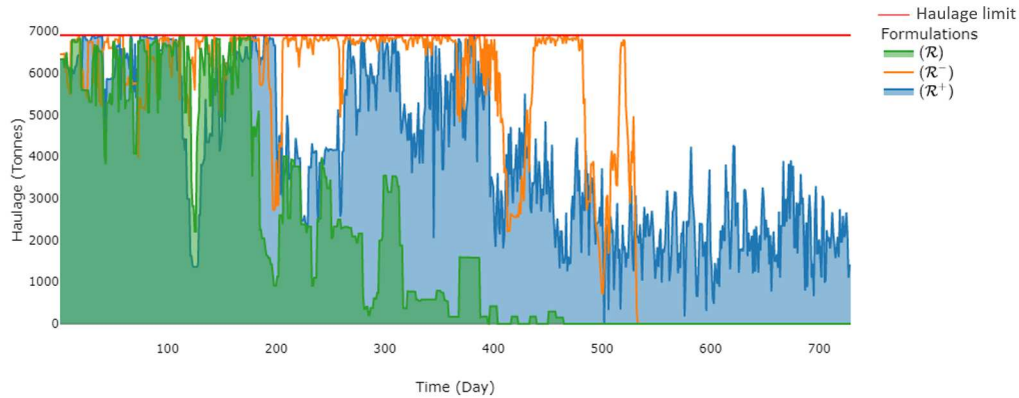


Figure 4.8: Comparison of the respective formulations based on daily haulage, where (\mathcal{R}^-) is the standard formulation, (\mathcal{R}) is the simplistic fix to formulation (\mathcal{R}^-) , and (\mathcal{R}^+) is the proposed formulation

Table 4.5: Comparison of Case 7 formulations and their respective net present value changes

Formulation	Net present value change with respect to the objective value of (\mathcal{R}^-) [%]	Feasibility with respect to temperature
(\mathcal{R}^-)	-	No
(\mathcal{R})	-42.30	Yes
(\mathcal{R}^+)	-12.29	Yes

Figure 4.10 evaluates the temperature levels on the deepest mine level. The solution obtained with (\mathcal{R}^-) for Case 7 violates the typical maximum temperature for normal operation, here 28°C wet-bulb; formulations (\mathcal{R}) and (\mathcal{R}^+) adhere to the heat limits. Without refrigeration, the mine level is too hot to operate; correspondingly, there are no activities on this level in (\mathcal{R}) 's schedule. The refrigeration option exercised in formulation (\mathcal{R}^+) 's schedule lowers the temperature; at the extreme, on day 123 when refrigeration is activated, there is a significant drop in temperature, which remains low until sufficient heat-generating activities are introduced into the schedule.

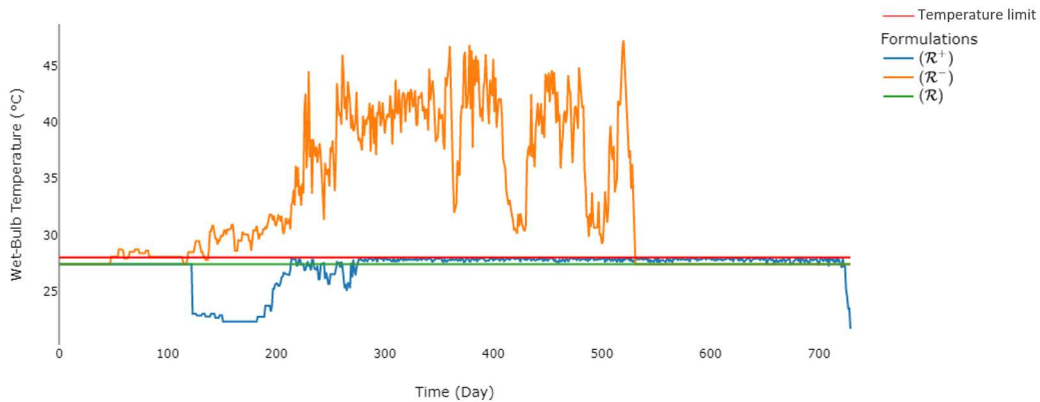


Figure 4.9: Comparison of the respective formulation types based on end-of-day temperature outputs on the lowest level of the mine, where (\mathcal{R}^-) is the standard formulation, (\mathcal{R}) is the simplistic fix to formulation (\mathcal{R}^-) , and (\mathcal{R}^+) is the proposed formulation

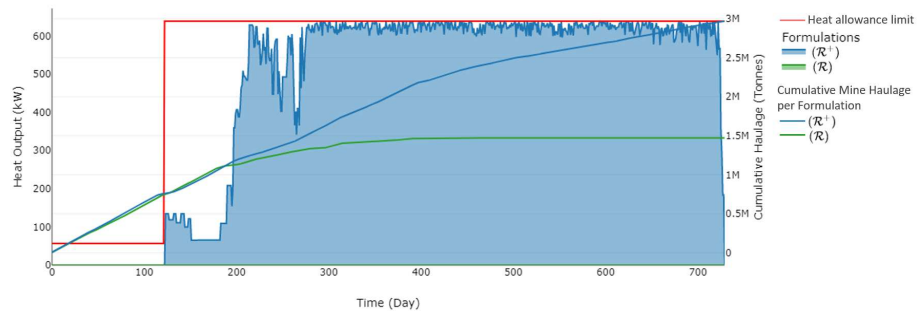


Figure 4.10: Comparison of the remaining heat-feasible schedules based on daily heat output on the lowest level in the mine, where (\mathcal{R}) is the simplistic fix to formulation (\mathcal{R}^-) , and (\mathcal{R}^+) is the proposed formulation

Comparing the formulations that produce the two feasible schedules – (\mathcal{R}^+) and (\mathcal{R}) , the former possesses an advantage over the latter in that the increase of the right-hand side by over 580 kW when refrigeration is activated on day 123 permits greater cumulative haulage, leading to a higher net present value, even though refrigeration costs are incurred.

4.7 Conclusions and Future Research Directions

Underground mine planning is a complex process, critical to providing solutions that appropriately determine realistic execution dates of activities. We provide a detailed mixed

integer programming formulation (\mathcal{O}) of a production scheduling problem that maximizes net present value by considering precedence, resources, and final temperature, where the latter feature is based on heat output at the end of each respective time period while incorporating refrigeration and ventilation at every mine level. We reformulate (\mathcal{O}) as (\mathcal{R}^+), which possesses a classical *RCPSP* structure; this enables us to solve large instances using a decomposition scheme for the linear programming relaxation and a tailored heuristic (\mathcal{H}) to produce integer-feasible solutions. For ten realistic test cases, we obtain solutions, on average, to within 7% of optimality in under two hours, where otherwise instances are intractable. Our solutions provide operationally feasible production schedules with respect to heat accumulation in an underground mine, while weighing the economic trade-offs between the cost incurred for activating refrigeration and the increased production enabled by it.

Future research could accommodate short-term scheduling by modifying (\mathcal{O}) and (\mathcal{R}^+) to incorporate transient effects and seasonal temperature and humidity variations. Finally, our heuristic (\mathcal{H}) creates multiple solutions whose trade-offs could be evaluated by determining when refrigeration is activated.

Acknowledgements

We acknowledge our industry partners who provided data funding and an explanation of the scheduling problem. We thank Professor Marcos Goycoolea from the University of Adolfo Ibañez; Samuel Nichols, Kieran Lewis, Eric Smoorenberg, John Ayaburi, and Aditya Juganda from the Colorado School of Mines; Akshay Chowdu from the South Dakota School of Mines for providing additional insights regarding model formulation. We also thank Dr. Mark Larson and Mr. Donovan Benton from the National Institute of Occupational Safety and Health for their review. This research has been partially funded by the National Institute of Occupational Safety and Health as part of the Mine Ventilation and Safety Research and Capacity Building program, contract number: 0000HCCS-2019-36404, and by the National Agency for Research and Development

(ANID), Chile, Scholarship Program, Becas de Doctorado Nacional: 2017-21180460.

CHAPTER 5

CONCLUSION

Solving large-scale, real-world optimization models can be complex, owing not only to their size, but also to their complexity; these difficulties arise, in particular, in models whose solutions are implemented, as is the case of the models we present in this dissertation. However, with state-of-the-art modeling techniques and modern algorithms and solvers, implementable solutions can be obtained in an operationally acceptable amount of time. Chapter 2 explores the benefits of optimization modeling through a design and dispatch model that integrates distributed energy resources. The detailed integer program minimizes life cycle costs, which include capital costs, operations and maintenance costs, utility costs and incentives. The constraints restrict fuel availability, peak demand accounting, load balancing, storage operations, and technology sizing. A case study analysis demonstrates the ability of the optimization model to determine a cost-minimizing system size and dispatch of distributed energy resources, relative to the application of rules of thumb. For the cases we test, corresponding solutions from the optimization model provide significant savings— amounting to millions of dollars— over a 25-year time horizon.

Chapter 3 examines the benefits of data management, variable redefinition, variable elimination, and constraint reformulation to provide high-quality solutions within an appropriate amount of time for a web-based tool. Due to the size of the mixed integer program (i.e., instances can contain hundreds of thousands of variables and constraints), we tailor our data structures, efficiently handle data, and streamline the formulation through variable redefinition to improve the tractability of the model and provide sufficiently fast solution times for a web-based tool. The enhancements, on average, result in a 2% optimality gap within a ten-minute time limit compared to the un-enhanced formulation that yields solutions with optimality gaps typically 15% or higher in the same amount of time. Future work in this area entails expanding the suite of technologies available for system design and highlighting the model's use for energy systems outside of

the United States, e.g., in sub-Saharan Africa.

Finally, Chapter 4 develops an entirely new paradigm for underground production scheduling that considers ventilation at the level of detail derived from mechanical engineering principles. Our integer program maximizes net present value by scheduling activities based on their precedence requirements, and resources they consume; heat output for each time period is treated as a limiting constraint. We reformulate the model into a classical RESOURCE-CONSTRAINED PROJECT SCHEDULING PROBLEM to enable us to solve large instances using a specialized solver known as OMP. We then tailor a heuristic that uses the solution from the linear-programming relaxation to provide integer-feasible solutions. Future work could explore the trade-offs of near-optimal solutions provided by the heuristic, and could entail transforming the reformulation into a transient, short-term production scheduling model.

As models in heavy industry become more complex, they may exhibit nonlinear problem structures, necessitating solution techniques that may extend beyond state-of-the-art. Currently in literature there are direct translations of some nonlinearities that are straight-forward to implement; in other cases, there are only linear approximations. Moving forward, questions in the development phase of optimization modeling may require determining how nonlinearities should be captured. Additionally, if linear approximations are necessary, the practitioner must determine an acceptable amount of error.

BIBLIOGRAPHY

- Abbey, C. and G. Joos (2005). Short-term energy storage for wind energy applications. In *Industry Applications Conference, 2005. Fourtieth IAS Annual Meeting. Conference Record of the 2005*, Volume 3, pp. 2035–2042. IEEE.
- Acuña, E. I. and I. S. Lowndes (2014). A review of primary mine ventilation system optimization. *Interfaces* 44(2), 163–175.
- Adam, A., E. S. Fraga, and D. J. Brett (2015). Options for residential building services design using fuel cell based micro-CHP and the potential for heat integration. *Applied Energy* 138, 685–694.
- Adwo (2020). Mining truck driving out of underground mine[digital image]. Shutterstock. Accessed: 03/10/2021.
- Agnor, M. (2017). Gold mining underground[digital image]. Shutterstock. Accessed: 03/10/2021.
- Anderson, J. and I. Longson (1986). Optimisation of ventilation and refrigeration in British coal mines. *Mining Engineer* 146, 115–20.
- Anderson, K., D. Olis, B. Becker, L. Parkhill, N. Laws, X. Li, S. Mishra, T. Kwasnik, A. Jeffrey, E. Elgqvist, K. Krah, D. Cutler, A. Zolan, N. Muerdter, R. Eger, A. Walker, C. Hampel, and G. Tomberlin (2021). REopt Lite user manual. Technical Report NREL/TP-7A40-79235, National Renewable Energy Laboratory, Golden, CO (United States).
- Anyenya, G. A., R. J. Braun, K. J. Lee, N. P. Sullivan, and A. M. Newman (2018). Design and dispatch optimization of a solid-oxide fuel cell assembly for unconventional oil and gas production. *Optimization and Engineering* 19(4), 1037–1081.
- Asadi, E., M. G. da Silva, C. H. Antunes, and L. Dias (2012). A multi-objective optimization model for building retrofit strategies using TRNSYS simulations, genopt and matlab. *Building and Environment* 56, 370–378.
- Ashari, M. and C. Nayar (1999). An optimum dispatch strategy using set points for a photovoltaic (PV), diesel and battery hybrid power system. *Solar Energy* 66(1), 1 – 9.
- Atabay, D. (2017). An open-source model for optimal design and operation of industrial energy systems. *Energy* 121, 803–821.
- Atlas Copco (2007). Mining methods in underground mining. *Stockholm: Atlas Copco*.
- Bascompta, M., A. M. Castañón, L. Sanmiquel, and J. Oliva (2016). Heat flow assessment in an underground mine: An approach to improve the environmental conditions. *Dyna* 83(197), 174–179.
- Bienstock, D. and M. Zuckerberg (2010). Solving LP relaxations of large-scale precedence constrained problems. In *International Conference on Integer Programming and Combinatorial Optimization*, pp. 1–14. Springer.

- Blackburn, L., A. Young, P. Rogers, J. Hedengren, and K. Powell (2019). Dynamic optimization of a district energy system with storage using a novel mixed-integer quadratic programming algorithm. *Optimization and Engineering* 20(2), 575–603.
- BloombergNEF (2019). New energy outlook. Technical report, Bloomberg New Energy Finance.
- Bluhm, S., W. Marx, F. Von Glehn, and M. Biffi (2001). VUMA mine ventilation software. *Journal of the Mine Ventilation Society of South Africa* 54(3).
- Booth, S., X. Li, I. Baring-Gould, D. Kollanyi, A. Bharadwaj, and P. Weston (2018). Productive use of energy in african micro-grids: Technical and business considerations.
- Bracco, S., G. Dentici, and S. Siri (2016). DESOD: A mathematical programming tool to optimally design a distributed energy system. *Energy* 100, 298–309.
- Brake, D. and R. Fulker (2000). The ventilation and refrigeration design for Australia’s deepest and hottest underground operation: the Enterprise mine. In *MassMin 2000*, pp. 611–621. Australasian Institute of Mining and Metallurgy.
- Braslavsky, J. H., J. R. Wall, and L. J. Reedman (2015). Optimal distributed energy resources and the cost of reduced greenhouse gas emissions in a large retail shopping centre. *Applied Energy* 155, 120–130.
- Brickey, A. J. (2015). *Underground production scheduling optimization with ventilation constraints*. Ph. D. thesis, Colorado School of Mines. Arthur Lakes Library.
- Brown, G. G. and R. F. Dell (2007). Formulating integer linear programs: A rogues’ gallery. *INFORMS Transactions on Education* 7(2), 153–159.
- Brown, T., J. Hörsch, and D. Schlachtberger (2018). PyPSA: Python for power system analysis. *Journal of Open Research Software* 6(1).
- Buoro, D., P. Pinamonti, and M. Reini (2014). Optimization of a distributed cogeneration system with solar district heating. *Applied Energy* 124, 298–308.
- Burer, M., K. Tanaka, D. Favrat, and K. Yamada (2003). Multi-criteria optimization of a district cogeneration plant integrating a solid oxide fuel cell-gas turbine combined cycle, heat pumps and chillers. *Energy* 28, 497–518.
- Camm, J. D., A. S. Raturi, and S. Tsubakitani (1990). Cutting big M down to size. *Interfaces* 20(5), 61–66.
- Campeau, L.-P. and M. Gamache (2020). Short-term planning optimization model for underground mines. *Computers & Operations Research* 115, 104642.
- Carlyle, M. and C. Eaves (2001). Underground planning at Stillwater Mining Company. *Interfaces* 31(4), 50–60.
- Carpentier, S., M. Gamache, and R. Dimitrakopoulos (2016). Underground long-term mine production scheduling with integrated geological risk management. *Mining Technology* 125(2), 93–102.

- Chasm Consulting (2015). *Ventsim*. Chasm Consulting.
- Chiradeja, P. and R. Ramakumar (2004). An approach to quantify the technical benefits of distributed generation. *IEEE Transactions on Energy Conversion* 19(4), 764–773.
- Chowdu, A., P. Nesbitt, A. Brickey, and A. Newman (2021). Operations research in underground mine planning: A review. *INFORMS Journal on Applied Analytics*, accepted.
- Connolly, D., H. Lund, B. V. Mathiesen, and M. Leahy (2010). A review of computer tools for analysing the integration of renewable energy into various energy systems. *Applied Energy* 87(4), 1059–1082.
- Cuesta, M., T. Castillo-Calzadilla, and C. Borges (2020). A critical analysis on hybrid renewable energy modeling tools: An emerging opportunity to include social indicators to optimise systems in small communities. *Renewable and Sustainable Energy Reviews* 122, 109691.
- Cutler, D., D. Olis, E. Elgqvist, X. Li, N. Laws, N. DiOrio, A. Walker, and K. Anderson (2017a). REopt: A platform for energy system integration and optimization. National Renewable Energy Laboratory, Tech. Rep. NREL/TP-7A40-70022.
- Cutler, D. S., D. R. Olis, E. M. Elgqvist, X. Li, N. D. Laws, N. A. DiOrio, H. A. Walker, and K. H. Anderson (2017b, 9). REopt: A platform for energy system integration and optimization.
- Datamine (2015). *Enhanced Production Scheduler*. Datamine.
- De Mel, I. A., O. V. Klymenko, and M. Short (2020). Balancing accuracy and complexity in optimisation models of distributed energy systems and microgrids: A review. *arXiv e-prints*, arXiv-2008.
- Deru, M., K. Field, D. Studer, K. Benne, B. Griffith, P. Torcellini, B. Liu, M. Halverson, D. Winiarski, M. Rosenberg, et al. (2011). US department of energy commercial reference building models of the national building stock.
- Deswik Mining Consultants (Australia) Pty Ltd (2014). *Deswik.Sched*. Deswik Mining Consultants (Australia) Pty Ltd.
- Deswik Mining Consultants (Australia) Pty Ltd (2018). *Deswik.CAD*.
- DiOrio, N., A. Dobos, and S. Janzou (2015). Economic analysis case studies of battery energy storage with SAM. Technical report, National Renewable Energy Lab, Golden, CO.
- Dobos, A. (2014). Pvwatts version 5 manual. Technical report, National Renewable Energy Lab, Golden, CO.
- Donoghue, A. (2004). Occupational health hazards in mining: an overview. *Occupational Medicine* 54(5), 283–289.
- Donohoo-Vallett, P., P. Gilman, D. Feldman, J. Brodrick, D. Gohlke, R. Gravel, A. Jiron,

- C. Schutte, S. Satyapal, T. Nguyen, P. Scheihing, B. Marshall, and S. Harman (2016). Revolution...now. Technical report, Department of Energy.
- Dorfner, J. and T. Hamacher (2020). urbs: A linear optimisation model for distributed energy systems.
- Draxl, C., A. Clifton, B.-M. Hodge, and J. McCaa (2015). The wind integration national dataset (WIND) toolkit. *Applied Energy* 151, 355–366.
- DSIRE (2020). Database of state incentives for renewables and efficiency. N.C. clean energy technology center at N.C. Accessed: 6/29/2020.
- Dufo-Lopez, R. and J. L. Bernal-Agustin (2005). Design and control strategies of PV-Diesel systems using genetic algorithms. *Solar Energy* 79(1), 33 – 46.
- Dufo-López, R. and J. L. Bernal-Agustín (2005). Design and control strategies of PV-Diesel systems using genetic algorithms. *Solar Energy* 79(1), 33–46.
- El-Khattam, W. and M. M. Salama (2004). Distributed generation technologies, definitions and benefits. *Electric Power Systems Research* 71(2), 119–128.
- Energy Information Administration (2019). Annual energy outlook 2019 – electricity supply, disposition, prices, and emissions. EIA. Accessed: 9/04/2020.
- Freeman, J. M., N. A. DiOrio, N. J. Blair, T. W. Neises, M. J. Wagner, P. Gilman, and S. Janzou (2018). System advisor model (sam) general description (version 2017.9. 5). Technical report, National Renewable Energy Lab, Golden, CO.
- Fuentes-Cortés, L. F. and A. Flores-Tlacuahuac (2018). Integration of distributed generation technologies on sustainable buildings. *Applied Energy* 224, 582–601.
- Gamma Technologies (2017). GT-Power user’s manual, GT-Suite version 2017. *Gamma Technologies*.
- Gertsch, R. E. and R. L. Bullock (1998). *Techniques in Underground Mining: Selections from Underground Mining Methods Handbook*. SME.
- Goodall, G., M. Scioletti, A. Zolan, B. Suthar, A. Newman, and P. Kohl (2019). Optimal design and dispatch of a hybrid microgrid system capturing battery fade. *Optimization and Engineering* 20(1), 179–213.
- Gopalakrishnan, H. and D. Kosanovic (2014). Economic optimization of combined cycle district heating systems. *Sustainable Energy Technologies and Assessments* 7, 91–100.
- Gopalakrishnan, H. and D. Kosanovic (2015). Operational planning of combined heat and power plants through genetic algorithms for mixed 0–1 nonlinear programming. *Computers & Operations Research* 56, 51–67.
- Groissböck, M. (2019). Are open source energy system optimization tools mature enough for serious use? *Renewable and Sustainable Energy Reviews* 102, 234–248.
- Gumerman, E. Z., R. R. Bharvirkar, K. H. LaCommare, and C. Marnay (2003). Evaluation framework and tools for distributed energy resources. Technical report,

- Lawrence Berkeley National Lab.(LBNL), Berkeley, CA (United States).
- Hamilton, W. T., M. A. Husted, A. M. Newman, R. J. Braun, and M. J. Wagner (2020). Dispatch optimization of concentrating solar power with utility-scale photovoltaics. *Optimization and Engineering* 21(1), 335–369.
- Hamrin, H. (1980). *Guide to Underground Mining: Methods and Applications*. Atlas Copco.
- Hartman, H. L. and J. M. Mutmanský (2002). *Introductory Mining Engineering*. John Wiley & Sons.
- Hartman, H. L., J. M. Mutmanský, R. V. Ramani, and Y. J. Wang (2012). *Mine Ventilation and Air Conditioning*. John Wiley & Sons.
- Hilpert, S., C. Kaldemeyer, U. Krien, S. Günther, C. Wingenbach, and G. Plessmann (2018). The open energy modelling framework (oemof)-a new approach to facilitate open science in energy system modelling. *Energy Strategy Reviews* 22, 16–25.
- Hirwa, J., O. Ogunmodede, A. Zolan, and A. Newman (2020). Optimizing design and dispatch of a renewable-combined heat and power energy system. Working Paper, Colorado School of Mines.
- Hollermann, D. E., M. Goerigk, D. F. Hoffrogge, M. Hennen, and A. Bardow (2020). Flexible here-and-now decisions for two-stage multi-objective optimization: Method and application to energy system design selection. *Optimization and Engineering*, 1–27.
- Howells, M., H. Rogner, N. Strachan, C. Heaps, H. Huntington, S. Kypreos, A. Hughes, S. Silveira, J. DeCarolis, M. Bazillian, et al. (2011). OSeMOSYS: The open source energy modeling system: An introduction to its ethos, structure and development. *Energy Policy* 39(10), 5850–5870.
- Howes, M. (2011). Ventilation and cooling in underground mines. *Mining and Quarrying* 74, 45–46.
- Huang, S., G. Li, E. Ben-Awuah, B. O. Afum, and N. Hu (2020). A robust mixed integer linear programming framework for underground cut-and-fill mining production scheduling. *International Journal of Mining, Reclamation and Environment* 34(6), 397–414.
- Huster, W. R., A. M. Schweidtmann, and A. Mitsos (2019). Working fluid selection for organic rankine cycles via deterministic global optimization of design and operation. *Optimization and Engineering*, 1–20.
- Hustrulid, W. A. and R. C. Bullock (2001). *Underground Mining Methods*. Society for Mining, Metallurgy, and Exploration, Littleton, CO.
- IBM ILOG (2020). CPLEX optimizer 12.10.
- IEEE (2020). Ieee recommended practice for sizing lead-acid batteries for stationary applications.

- Johnson, T. B. (1968). Optimum open pit mine production scheduling. Technical report, DTIC Document.
- Karlsson, K. and P. Meibom (2008). Optimal investment paths for future renewable based energy systems—using the optimisation model Balmorel. *International Journal of Hydrogen Energy* 33(7), 1777–1787.
- Katsigiannis, Y. and P. Georgilakis (2008). Optimal sizing of small isolated hybrid power systems using tabu search. *Journal of Optoelectronics and Advanced Materials* 10(5), 1241.
- Kerr, T. (2008). Evaluating the benefits of greater global investment in combined heat and power. International Energy Agency.
- Khodayari, F. and Y. Pourrahimian (2019). Long-term production scheduling optimization and 3D material mixing analysis for block caving mines. *Mining Technology* 128(2), 65–76.
- Klein, S., W. Beckman, J. Mitchell, J. Duffie, N. Duffie, T. Freeman, J. Mitchell, J. Braun, B. Evans, J. Kummer, et al. (2004). Trnsys 16—a TRaNsient system simulation program, user manual.
- Klotz, E. and A. M. Newman (2013a). Practical guidelines for solving difficult linear programs. *Surveys in Operations Research and Management Science* 18(1-2), 1–17.
- Klotz, E. and A. M. Newman (2013b). Practical guidelines for solving difficult mixed integer linear programs. *Surveys in Operations Research and Management Science* 18(1-2), 18–32.
- Koivisto, M., J. Gea-Bermúdez, and P. Sørensen (2019). North Sea offshore grid development: Combined optimisation of grid and generation investments towards 2050. *IET Renewable Power Generation* 14(8), 1259–1267.
- Krug, R., V. Mehrmann, and M. Schmidt (2020). Nonlinear optimization of district heating networks. *Optimization and Engineering*, 1–37.
- Kuchta, M., A. Newman, and E. Topal (2004). Implementing a production schedule at LKAB’s Kiruna mine. *Interfaces* 34(2), 124–134.
- Kutchka, M., A. M. Newman, and E. Topal (2003). Production scheduling at LKAB’s Kiruna mine using mixed-integer programming. *Mining Engineering* 55(4), 35–40.
- Lambert, B., A. Brickey, A. Newman, and K. Eurek (2014). Open-pit block-sequencing formulations: a tutorial. *Interfaces* 44(2), 127–142.
- Lambert, T., P. Gilman, and P. Lilienthal (2006). Micropower system modeling with HOMER. *Integration of Alternative Sources of Energy* 1(1), 379–385.
- Larson, M. (2021). Private communication. National Institute of Occupational Safety and Health.
- Lazaro, P. and M. Momayez (2020). Heat stress in hot underground mines: a brief

- literature review. *Mining, Metallurgy & Exploration*, 1–12.
- Lee, K.-H., D.-W. Lee, N.-C. Baek, H.-M. Kwon, and C.-J. Lee (2012). Preliminary determination of optimal size for renewable energy resources in buildings using RETScreen. *Energy* 47(1), 83–96.
- Lerchs, H. and I. F. Grossmann (1965). Optimum design of open-pit mines. *Transactions CIM* 58, 47–54.
- Lian, J., Y. Zhang, C. Ma, Y. Yang, and E. Chaima (2019). A review on recent sizing methodologies of hybrid renewable energy systems. *Energy Conversion and Management* 199, 112027.
- Lockhart, E., X. Li, S. Booth, J. Salasovich, D. Olis, J. Elsworth, and L. L. (2019). Comparative study of techno-economics of lithium-ion and lead-acid batteries in microgrids and sub-saharan africa. NREL/TP-7A40-73238.
- Lopes, T. V. F. (2017). Underground mine production scheduling using OMP solver: Analysis of modifications to an integer programming model and implementation of a sliding time window heuristic. Master’s thesis, South Dakota School of Mines and Technology, Rapid City.
- Loulou, R., G. Goldstein, K. Noble, et al. (2004). Documentation for the MARKAL family of models. *Energy Technology Systems Analysis Programme*, 65–73.
- Lund, H. and A. N. Andersen (2005). Optimal designs of small CHP plants in a market with fluctuating electricity prices. *Energy Conversion and Management* 46(6), 893–904.
- Maeng, H., K. Andersen, and A. Andersen (2002). EnergyPRO users guide.
- Magri, E. and A. Unsted (1976). Mine production, ventilation and refrigeration planning—a unified approach via mathematical programming. *IFAC Proceedings Volumes* 9(5), 91–104.
- Marks, J. (1980). Refrigeration economics at the Star mine - introduction. Society for Mining, Metallurgy & Exploration.
- Martinez, M. and A. Newman (2011a). A solution approach for optimizing long-and short-term production scheduling at LKAB’s Kiruna mine. *European Journal of Operational Research* 211(1), 184–197.
- Martinez, M. and A. M. Newman (2011b). Using decomposition to optimize long- and short-term production scheduling at LKAB’s Kiruna Mine. *European Journal of Operational Research* 211(1), 184–197.
- Mashayekh, S., M. Stadler, G. Cardoso, and M. Heleno (2017). A mixed integer linear programming approach for optimal DER portfolio, sizing, and placement in multi-energy microgrids. *Applied Energy* 187, 154–168.
- McPherson, M. J. (2012). *Subsurface ventilation and environmental engineering*. Springer Science & Business Media.

- Merkel, E., R. McKenna, and W. Fichtner (2015a). Optimisation of the capacity and the dispatch of decentralised micro-CHP systems: A case study for the UK. *Applied Energy* 140, 120–134.
- Merkel, E., R. McKenna, and W. Fichtner (2015b). Optimisation of the capacity and the dispatch of decentralised micro-CHP systems: A case study for the UK. *Applied Energy* 140, 120–134.
- Mine Ventilation Services Inc. (2014). *VnetPC Pro+*. Mine Ventilation Services, Inc.
- MineRP (2015). *EPS Schedule Optimisation Tool*. MineRP.
- Mischler, S. E. and J. F. Colinet (2009). Controlling and monitoring diesel emissions in underground mines in the United States. In *Mine Ventilation: Proceedings of the Ninth International Mine Ventilation Congress, New Delhi, India*, Volume 2, pp. 879–888.
- Mishra, S., J. Pohl, N. Laws, D. Cutler, T. Kwasnik, W. Becker, A. Zolan, K. Anderson, D. Olis, and E. Elgqvist (2021). Computational framework for behind-the-meter DER techno-economic modeling and optimization – REopt Lite. *Energy Systems* (submitted).
- Morais, H., P. Kadar, P. Faria, Z. A. Vale, and H. Khodr (2010). Optimal scheduling of a renewable micro-grid in an isolated load area using mixed-integer linear programming. *Renewable Energy* 35(1), 151 – 156.
- Muñoz, G. (2012). Modelos de optimización lineal entera y aplicaciones a la minería. Master’s thesis, Dept. Math. Engineering, Universidad de Chile, Santiago, Chile.
- Muratori, M., E. Elgqvist, D. Cutler, J. Eichman, S. Salisbury, Z. Fuller, and J. Smart (2019). Technology solutions to mitigate electricity cost for electric vehicle DC fast charging. *Applied Energy* 242, 415–423.
- Nasution, E. F., J. Shadiq, H. S. Purnomo, and J. F. Socaningrumline (2019). Bali energy planning: Optimization of energy resources for electrical generation 2019-2028. In *2019 2nd International Conference on High Voltage Engineering and Power Systems (ICHVEPS)*, pp. 085–090. IEEE.
- National Renewable Energy Laboratory (2002). How to size a grid-connected solar electric system. Accessed: 10/03/2020.
- National Renewable Energy Laboratory (2020). NREL’s PVWatts Calculator. <https://pvwatts.nrel.gov/>.
- Nehring, M., E. Topal, M. Kizil, and P. Knights (2010). An investigation to integrate optimum long-term planning with short planning in underground mine production scheduling. In *Mine Planning and Equipment Selection Conference*, pp. 1–13. Fremantle, Western Australia.
- Nehring, M., E. Topal, M. Kizil, and P. Knights (2012). Integrated short-and medium-term underground mine production scheduling. *Journal of the Southern African Institute of Mining and Metallurgy* 112(5), 365–378.

- Neto, P. B. L., O. R. Saavedra, and D. Q. Oliveira (2020). The effect of complementarity between solar, wind and tidal energy in isolated hybrid microgrids. *Renewable Energy* 147, 339–355.
- Newman, A. and M. Kuchta (2007). Using aggregation to optimize long-term production planning at an underground mine. *European Journal of Operational Research* 176(2), 1205–1218.
- Newman, A., E. Rubio, R. Caro, A. Weintraub, and K. Eurek (2010). A review of operations research in mine planning. *Interfaces* 40(3), 222–245.
- Nichols, S., G. Bogin, and A. Newman (2019). Simulation of the impact of environmental conditions in underground mines on truck and loader engine efficiency and emissions. In *SME Annual Conference & Expo and CMA 121st National Western Mining Conference*, pp. 716–721. SME.
- Nieto, A. (2011). Key deposit indicators (KDI) and key mining method indicators (KMI) in underground mining method selection. *Transaction of the Society of Mining, Metallurgy, and Engineering* 328, 381–396.
- Office of Energy Efficiency and Renewable Energy (2020). Commercial reference buildings.
- Ogunmodede, O., K. Anderson, D. Cutler, and A. Newman (2021). Optimizing design and dispatch of a renewable energy system. *Applied Energy* 287, 116527.
- Oluleye, G., J. Allison, N. Kelly, and A. D. Hawkes (2018). An optimisation study on integrating and incentivising thermal energy storage (TES) in a dwelling energy system. *Energies* 11(5), 1095.
- Ong, S. and R. McKeel (2012). National utility rate database. In *World Renewable Energy Forum. Conference Record of the 2012*, pp. 1–7.
- O’Shaughnessy, E., D. Cutler, K. Ardani, and R. Margolis (2018). Solar plus: Optimization of distributed solar PV through battery storage and dispatchable load in residential buildings. *Applied Energy* 213, 11–21.
- OSTI (2020). REopt Lite Web Tool: Capabilities and Features. <https://www.nrel.gov/docs/fy20osti/76420.pdf>.
- O’Sullivan, D., A. Brickey, and A. Newman (2015). Is open pit production scheduling ‘easier’ than its underground counterpart? *Mining Engineering* 67(4), 68–73.
- O’Sullivan, D. and A. M. Newman (2014). Extraction and backfill scheduling in a complex underground mine. *Interfaces* 44(2), 204–221.
- Patsios, C., B. Wu, E. Chatzinikolaou, D. J. Rogers, N. Wade, N. P. Brandon, and P. Taylor (2016). An integrated approach for the analysis and control of grid connected energy storage systems. *Journal of Energy Storage* 5, 48–61.
- Perera, A. T. D., V. M. Nik, D. Mauree, and J.-L. Scartezzini (2017). Electrical hubs: An effective way to integrate non-dispatchable renewable energy sources with minimum impact to the grid. *Applied Energy* 190, 232–248.

- Pffenninger, S., J. DeCarolis, L. Hirth, S. Quoilin, and I. Staffell (2017). The importance of open data and software: Is energy research lagging behind? *Energy Policy* 101, 211–215.
- Pruitt, K. A., R. J. Braun, and A. M. Newman (2013a). Establishing conditions for the economic viability of fuel cell-based, combined heat and power distributed generation systems. *Applied Energy* 111, 904–920.
- Pruitt, K. A., R. J. Braun, and A. M. Newman (2013b). Evaluating shortfalls in mixed-integer programming approaches for the optimal design and dispatch of distributed generation systems. *Applied Energy* 102, 386–398.
- Pruitt, K. A., S. Leyffer, A. M. Newman, and R. J. Braun (2014). A mixed-integer nonlinear program for the optimal design and dispatch of distributed generation systems. *Optimization and Engineering* 15(1), 167–197.
- REopt development team (2020). REopt user manual. Accessed: 6/23/2020.
- Ringkjøb, H.-K., P. M. Haugan, and I. M. Solbrekke (2018). A review of modelling tools for energy and electricity systems with large shares of variable renewables. *Renewable and Sustainable Energy Reviews* 96, 440–459.
- Rivera, O., A. J. Brickey, D. Espinoza, M. Goycoolea, and E. Moreno (2016). The OMP guide. In *Technical Report*. Universidad Adolfo Ibañez.
- Rong, A. and R. Lahdelma (2007). CO₂ emissions trading planning in combined heat and power production via multi-period stochastic optimization. *European Journal of Operational Research* 176(3), 1874–1895.
- Scioletti, M. S., A. M. Newman, J. K. Goodman, A. J. Zolan, and S. Leyffer (2017). Optimal design and dispatch of a system of diesel generators, photovoltaics and batteries for remote locations. *Optimization and Engineering* 18(3), 755–792.
- Sebutsoe, T. and C. Musingwini (2017). Characterizing a mining production system for decision-making purposes in a platinum mine. *Journal of the Southern African Institute of Mining and Metallurgy* 117(2), 199–206.
- Sengupta, M., Y. Xie, A. Lopez, A. Habte, G. Maclaurin, and J. Shelby (2018). The national solar radiation database (NSRDB). *Renewable and Sustainable Energy Reviews* 89, 51–60.
- Shah, M., D. Cutler, J. Maguire, Z. Peterson, X. Li, J. Pohl, and J. Reyna (2020). Metrics and analytical frameworks for valuing energy efficiency and distributed energy resources in the built environment.
- Sharma, V. (2015). *Longterm schedule optimization of an underground mine under geotechnical and ventilation constraints using SOT*. Ph. D. thesis, Laurentian University of Sudbury.
- Siddiqui, A., C. Marnay, R. Firestone, and N. Zhou (2005, July). Distributed generation with heat recovery and storage. Technical Report LBNL-58630, Lawrence Berkeley

National Laboratory.

- Silvente, J., G. M. Kopanos, E. N. Pistikopoulos, and A. Espuña (2015). A rolling horizon optimization framework for the simultaneous energy supply and demand planning in microgrids. *Applied Energy* 155, 485–501.
- Smith, M., I. Sheppard, and G. Karunatillake (2003). Using MIP for strategic life-of-mine planning of the lead/zinc stream at Mount Isa mines. In *Proceedings of the 31st International APCOM Symposium, Cape Town, South Africa*, pp. 465–474.
- Sotoudeh, F., M. Nehring, M. Kizil, P. Knights, and A. Mousavi (2020). Production scheduling optimisation for sublevel stoping mines using mathematical programming: A review of literature and future directions. *Resources Policy* 68, 101809.
- Sousa, J., O. R. Saavedra, and S. L. Lima (2018). Decision making in emergency operation for power transformers with regard to risks and interruptible load contracts. *IEEE Transactions on Power Delivery* 33, 1556–1564.
- Stadler, M., M. Groissböck, G. Cardoso, and C. Marnay (2014). Optimizing distributed energy resources and building retrofits with the strategic DER-CAModel. *Applied Energy* 132, 557–567.
- Theo, W. L., J. S. Lim, W. S. Ho, H. Hashim, and C. T. Lee (2017). Review of distributed generation (DG) system planning and optimisation techniques: Comparison of numerical and mathematical modelling methods. *Renewable and Sustainable Energy Reviews* 67, 531–573.
- Thevenard, D., G. Leng, and S. Martel (2000). The RETscreen model for assessing potential PV projects. In *Conference Record of the Twenty-Eighth IEEE Photovoltaic Specialists Conference-2000 (Cat. No. 00CH37036)*, pp. 1626–1629. IEEE.
- Trick, M. (2005). Formulations and reformulations in integer programming. In *International conference on integration of artificial intelligence (AI) and operations research (OR) techniques in constraint programming*, pp. 366–379. Springer.
- Trout, L. (1995). Underground mine production scheduling using mixed integer programming. In *25th International APCOM Symposium Proceedings*, pp. 395–400.
- Twaha, S. and M. A. Ramli (2018). A review of optimization approaches for hybrid distributed energy generation systems: Off-grid and grid-connected systems. *Sustainable Cities and Society* 41, 320–331.
- Upadhyay, S. and M. Sharma (2014). A review on configurations, control and sizing methodologies of hybrid energy systems. *Renewable and Sustainable Energy Reviews* 38, 47–63.
- Vimmerstedt, L. J., S. Akar, C. R. Augustine, P. C. Beiter, W. J. Cole, D. J. Feldman, P. Kurup, E. J. Lantz, R. M. Margolis, T. J. Stehly, et al. (2019). 2019 annual technology baseline. Technical report, National Renewable Energy Lab, Golden, CO.
- Wagner, H. (2013). The management of heat flow in deep mines. *Mining Report* 149(2),

88–100.

- Wang, G. and H. Hijazi (2018). Mathematical programming methods for microgrid design and operations: a survey on deterministic and stochastic approaches. *Computational Optimization and Applications* 71(2), 553–608.
- Weber, C., F. Marechal, D. Favrat, and S. Kraines (2006). Optimization of an SOFC-based decentralized polygeneration system for providing energy services in an office-building in Tokyo. *Applied Thermal Engineering* 26, 1409–1419.
- Welder, L., D. S. Ryberg, L. Kotzur, T. Grube, M. Robinius, and D. Stolten (2018). Spatio-temporal optimization of a future energy system for power-to-hydrogen applications in Germany. *Energy* 158, 1130–1149.
- Wiese, F., R. Bramstoft, H. Koduvere, A. P. Alonso, O. Balyk, J. G. Kirkerud, Å. G. Tveten, T. F. Bolkesjø, M. Münster, and H. Ravn (2018). Balmorel open source energy system model. *Energy Strategy Reviews* 20, 26–34.
- Wiser, R. H. and M. Bolinger (2019). 2018 wind technologies market report.
- Wood Mackenzie Power and Renewables and the Energy Storage Association (ESA) (2019). U.S. energy storage monitor: Q3 2019 full report.
- Zakrzewski, T. (2017). *Advancing Design Sizing and Performance Optimization Methods for Building Integrated Thermal and Electrical Energy Generation Systems*. Ph. D. thesis, Illinois Institute of Technology.
- Zhang, H., R. Hauta, and L. Fava (2017). Mine schedule optimisation with ventilation constraints: a case study. In *Proceedings of the First International Conference on Underground Mining Technology*, pp. 145–152. Australian Centre for Geomechanics.
- Zhao, B., X. Zhang, P. Li, K. Wang, M. Xue, and C. Wang (2014). Optimal sizing, operating strategy and operational experience of a stand-alone microgrid on dongfushan island. *Applied Energy* 113, 1656–1666.
- Zolan, A., M. Scioletti, D. Morton, and A. Newman (2020). Decomposing loosely coupled mixed-integer programs for optimal microgrid design. *INFORMS Journal on Computing*, accepted.

APPENDIX A

SUPPLEMENTAL DATA FOR CHAPTER 2

A.1

Figures A.1 and A.2 show the hourly schedule for energy and demand time-of-use periods, respectively, for the utility rate tariff applied to San Diego. In this example, tariffs vary by month of year, hour of day, and weekday versus weekend. Hourly or sub-hourly real-time energy and demand prices can also be specified for sites where utility rates vary in every time step.

Figure A.1: San Diego Utility Tariiff Energy TOU period schedule (Ong and McKeel, 2012)

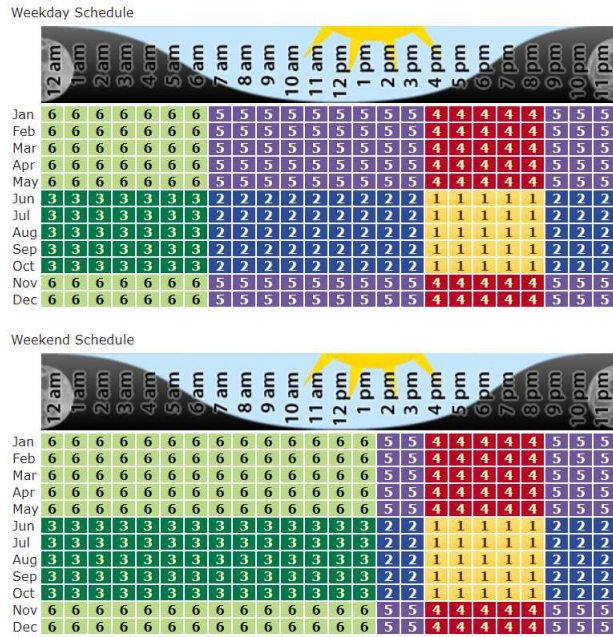
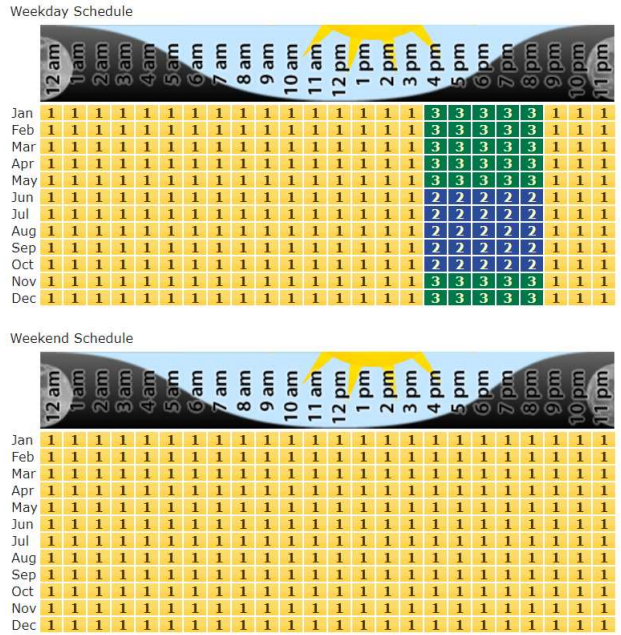


Figure A.2: San Diego Utility Tarriff Demand TOU period schedule (Ong and McKeel, 2012)



A.1.1 Renewable Energy

We model hourly production factors for wind and solar resource for one year. Figure A.3 shows hourly variability in production factors. Solar production factors follow similar daily and seasonal patterns at each location; however, wind production factors exhibit pronounced variability. The hourly variations in production factors affect the calculation of the value of the generated electricity based on its timing.

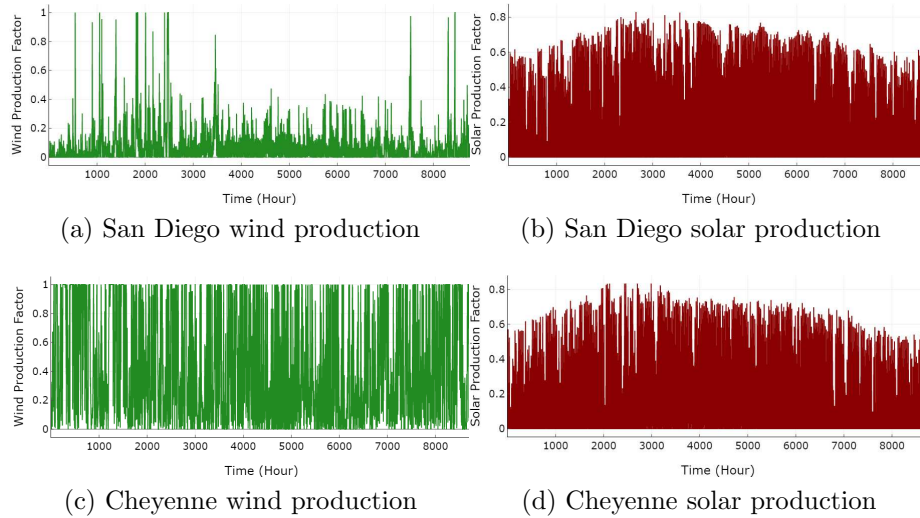
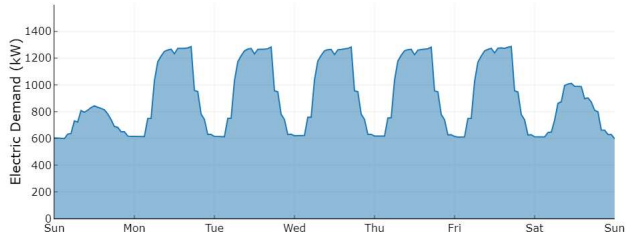


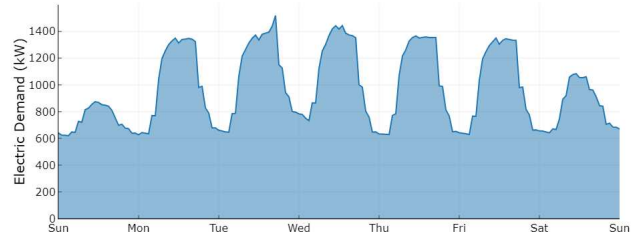
Figure A.3: Each location’s wind and solar production factors over the course of a representative year

A.1.2 Load Profile

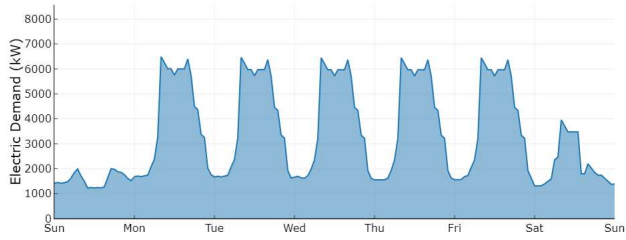
We model hourly load data for one year. The load for one winter and one summer week in each location in Figure A.4 demonstrates the profile variability. The hospital load profile exhibits less variability between minimum and maximum load than the campus Deru et al. (2011). The climate zones of the selected locations also impact the seasonal variability of the load profiles.



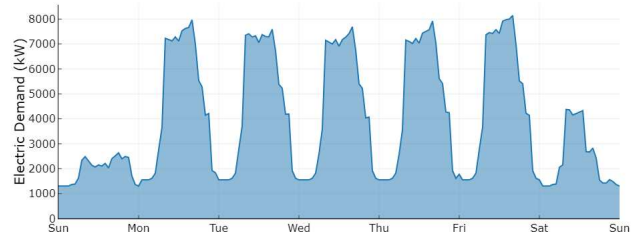
(a) San Diego, week in winter



(b) San Diego, week in summer



(c) Cheyenne, week in winter



(d) Cheyenne, week in summer

Figure A.4: Each location's electric demand for a week in the winter and summer

A.1.3 Technical and Economic Parameters

We assume a standard set of technical and economic parameters for both case study sites, as shown in Tables A.1 and A.2.

Table A.1: Renewable energy parameters used in (\mathcal{R})

PV parameters	Value	Reference
Array type	Rooftop, Fixed	Dobos (2014)
Array azimuth	180°	Dobos (2014)
Array tilt	10°	Dobos (2014)
DC-to-AC size ratio	1.2	Dobos (2014)
System losses	14%	Dobos (2014)
Capital cost	\$1,600/kW	Vimmerstedt et al. (2019)
O&M cost	\$16/kW	Vimmerstedt et al. (2019)
Federal incentive percentage	26%	DSIRE (2020)
Depreciation schedule	5-year MACRS*	DSIRE (2020)
<hr/>		
Wind parameters	Value	Reference
Size class	Midsized (101-999 kW)	Wiser and Bolinger (2019)
Capital cost	\$4,440/kW	Wiser and Bolinger (2019)
O&M cost	\$40/kW	Wiser and Bolinger (2019)
Federal incentive percentage	18%	DSIRE (2020)
Depreciation schedule	5-year MACRS*	DSIRE (2020)
<hr/>		
Battery parameters	Value	Reference
Rectifier efficiency	96%	Patsios et al. (2016)
Round-trip efficiency	97.5%	Patsios et al. (2016)
Inverter efficiency	96%	Patsios et al. (2016)
Minimum state of charge	20%	Patsios et al. (2016)
Initial state of charge	50%	[-]
Battery life	10 years	DiOrto et al. (2015)
Energy capacity cost	\$420/kWh	Wood Mackenzie Power and Renewables and the Energy Storage Association (ESA) (2019)
Energy replacement cost	\$200/kWh	Wood Mackenzie Power and Renewables and the Energy Storage Association (ESA) (2019)
Power capacity cost	\$840/kW	Wood Mackenzie Power and Renewables and the Energy Storage Association (ESA) (2019)
Power replacement cost	\$410/kW	Wood Mackenzie Power and Renewables and the Energy Storage Association (ESA) (2019)
O&M cost	\$0/kW	[-]
Federal incentive percentage	0%†	DSIRE (2020)
Depreciation schedule	7-year MACRS*	DSIRE (2020)

†Assume the battery can charge from the grid, eliminating the incentive

*MACRS: Modified Accelerated Cost Recovery System

Table A.2: System-wide parameters used in (\mathcal{R})

General economic parameters	Value	Reference
Electricity cost escalation rate	2.3%	Energy Information Administration (2019)
Host discount rate	8.3%	Vimmerstedt et al. (2019)
Host effective tax rate	26%	Vimmerstedt et al. (2019)
O&M cost escalation rate	2.5%	Vimmerstedt et al. (2019)
Analysis period	25 years	Vimmerstedt et al. (2019)
Net metering limit	0 kW	[-]
Wholesale rate	0 \$/kWh	[-]

APPENDIX B

SUPPLEMENTAL FORMULATION FOR CHAPTER 3

B.1 Appendix

We provide here additional notation not given (or used) in the body of the document, but that appears in the following constraints.

Sets

\mathcal{K}	Subdivisions of power rating
\mathcal{S}	Power rating segments
\mathcal{V}	Net metering regimes

Subsets and Indexed Sets

\mathcal{M}^{lb}	Look-back months considered for peak pricing
$\mathcal{T}_u \subseteq \mathcal{T}$	Technologies that may access electrical energy sales pricing tier u
$\mathcal{U}^c \subseteq \mathcal{U}^s$	Electrical energy curtailment pricing tiers
$\mathcal{U}^{\text{nm}} \subseteq \mathcal{U}^s$	Electrical energy sales pricing tiers used in net metering
$\mathcal{U}^s \subseteq \mathcal{U}$	Electrical energy sales pricing tiers

Parameters for Costs and their Functional Forms

c^{amc}	Utility annual minimum charge	[\$]
------------------	-------------------------------	------

Power Rating and Fuel Limit Parameters

b_c^σ	Minimum power rating for technology class c	[kW]
$b_{tks}^{\sigma s}$	Minimum power rating for technology t , subdivision k , segment s	[kW]
$\bar{b}_{tks}^{\sigma s}$	Maximum power rating for technology t , subdivision k , segment s	[kW]

Binary Variables

Z_{mn}^{dmt}	1 If tier n has allocated demand during month m ; 0 otherwise	[unitless]
Z_{de}^{dt}	1 if tier e has allocated demand during time-of-use period d ; 0 otherwise	[unitless]
Z_v^{nmil}	1 If generation is in net metering interconnect limit regime v ; 0 otherwise	[unitless]
Z_t^{pi}	1 If production incentive is available for technology t ; 0 otherwise	[unitless]
Z_{mu}^{ut}	1 If demand tier u is active in month m ; 0 otherwise	[unitless]

The following constraints, when combined with those given in §3.3, form the monolith ($\widehat{\mathcal{R}}$) that considers combined heat and power technologies in addition to the original renewable technologies. These constraints and their corresponding descriptions are taken directly from Ogunmodede et al. (2021) and are included here for completeness.

B.1.1 Production Incentives

$$X_t^{\text{pi}} \leq \min \left\{ \bar{v}_t \cdot Z_t^{\text{pi}}, \sum_{h \in \mathcal{H}} \Delta \cdot i_t^{\text{r}} \cdot f_t^{\text{pi}} \cdot f_{th}^{\text{p}} \cdot f_t^{\text{li}} \cdot X_{th}^{\text{rp}} \right\} \quad \forall t \in \mathcal{T} \quad (\text{B.1a})$$

$$X_t^{\sigma} \leq \bar{v}_t^{\sigma} + M \cdot (1 - Z_t^{\text{pi}}) \quad \forall t \in \mathcal{T} \quad (\text{B.1b})$$

Constraint (B.1a) calculates total production incentives, if available, for each technology. Constraint (B.1b) sets an upper bound on the size of system that qualifies for production incentives, if production incentives are available.

B.1.2 Power Rating

$$X_t^{\sigma} \leq \bar{b}_t^{\sigma} \cdot \sum_{s \in \mathcal{S}_{tk}} Z_{tks}^{\sigma s} \quad \forall c \in \mathcal{C}, t \in \mathcal{T}_c, k \in \mathcal{K}_t \quad (\text{B.2a})$$

$$\sum_{t \in \mathcal{T}_c, s \in \mathcal{S}_{tk}} Z_{tks}^{\sigma s} \leq 1 \quad \forall c \in \mathcal{C}, k \in \mathcal{K} \quad (\text{B.2b})$$

$$\sum_{t \in \mathcal{T}_c} X_t^{\sigma} \geq \bar{b}_c^{\sigma} \quad \forall c \in \mathcal{C} \quad (\text{B.2c})$$

$$X_{th}^{\text{rp}} = X_t^{\sigma} \quad \forall t \in \mathcal{T}^{\text{td}}, h \in \mathcal{H} \quad (\text{B.2d})$$

$$X_{th}^{\text{rp}} \leq f_{th}^{\text{ed}} \cdot X_t^{\sigma} \quad \forall t \in \mathcal{T} \setminus \mathcal{T}^{\text{td}}, h \in \mathcal{H} \quad (\text{B.2e})$$

$$\underline{b}_{tk_s}^{\sigma_s} \cdot Z_{tk_s}^{\sigma_s} \leq X_{tk_s}^{\sigma_s} \leq \bar{b}_{tk_s}^{\sigma_s} \cdot Z_{tk_s}^{\sigma_s} \quad \forall t \in \mathcal{T}, k \in \mathcal{K}_t, s \in \mathcal{S}_{tk} \quad (\text{B.2f})$$

$$\sum_{s \in \mathcal{S}_{tk}} X_{tk_s}^{\sigma_s} = X_t^\sigma \quad \forall t \in \mathcal{T}, k \in \mathcal{K}_t \quad (\text{B.2g})$$

Constraint (B.2a) permits nonzero power ratings only for the selected technology and corresponding subdivision in each class. Constraint (B.2b) allows at most one technology to be chosen for each subdivision in each class. Constraint (B.2c) limits the power rating to the minimum allowed for a technology class. Constraint (B.2d) prevents renewable technologies from turning down; rather, they must provide output at their nameplate capacity. Constraint (B.2e) limits rated production from all non-renewable technologies to be less than or equal to the product of the power rating and the derate factor for each time period. Constraint (B.2f) imposes both lower and upper limits on power rating of a technology, allocated to a subdivision in a segment, and constraint (B.2g) sums the segment sizes to the total for a given technology and subdivision.

B.1.3 Load Balancing and Grid Sales

$$\begin{aligned} \sum_{t \in \mathcal{T}^e} (f_{th}^p \cdot f_t^l \cdot X_{th}^{\text{rp}}) + \sum_{b \in \mathcal{B}^e} X_{bh}^{\text{dfs}} + \sum_{u \in \mathcal{U}^p} X_{uh}^g = \sum_{t \in \mathcal{T}^e} \left(\sum_{b \in \mathcal{B}^e} X_{bth}^{\text{pts}} + \sum_{u \in \mathcal{U}_t^s} X_{tuh}^{\text{ptg}} \right) \\ + \sum_{u \in \mathcal{U}^{\text{sb}}} X_{uh}^{\text{stg}} + X_h^{\text{gts}} + \sum_{t \in \mathcal{T}^{\text{ec}}} X_{th}^{\text{tp}} / \eta^{\text{ec}} + \delta_h^{\text{d}} \quad \forall h \in \mathcal{H}^g \end{aligned} \quad (\text{B.3a})$$

$$\begin{aligned} \sum_{t \in \mathcal{T}^e} (f_{th}^p \cdot f_t^l \cdot X_{th}^{\text{rp}}) + \sum_{b \in \mathcal{B}^e} X_{bh}^{\text{dfs}} = \sum_{b \in \mathcal{B}^e, t \in \mathcal{T}^e} \left(X_{bth}^{\text{pts}} + \sum_{u \in \mathcal{U}^c} X_{tuh}^{\text{ptg}} \right) \\ + \sum_{t \in \mathcal{T}^{\text{ec}}} X_{th}^{\text{tp}} / \eta^{\text{ec}} + \delta_h^{\text{d}} \quad \forall h \in \mathcal{H} \setminus \mathcal{H}^g \end{aligned} \quad (\text{B.3b})$$

$$\sum_{u \in \mathcal{U}^p} X_{uh}^g \geq X_h^{\text{gts}} \quad \forall h \in \mathcal{H}^g \quad (\text{B.3c})$$

$$\sum_{b \in \mathcal{B}^e} X_{bh}^{\text{dfs}} \geq \sum_{u \in \mathcal{U}^{\text{sb}}} X_{uh}^{\text{stg}} \quad \forall h \in \mathcal{H}^g \quad (\text{B.3d})$$

$$\Delta \cdot \sum_{h \in \mathcal{H}^g} \left(X_{uh}^{\text{stg}} + \sum_{t \in \mathcal{T}_u} X_{tuh}^{\text{ptg}} \right) \leq \bar{\delta}_u^{\text{gs}} \quad \forall u \in \mathcal{U}^{\text{sb}} \cap \mathcal{U}^{\text{nm}} \quad (\text{B.3e})$$

$$\Delta \cdot \sum_{h \in \mathcal{H}^g, t \in \mathcal{T}_u} X_{tuh}^{\text{ptg}} \leq \bar{\delta}_u^{\text{gs}} \quad \forall u \in \mathcal{U}^{\text{nm}} \setminus \mathcal{U}^{\text{sb}} \quad (\text{B.3f})$$

Constraint (B.3a) balances load by requiring that the sum of power (*i*) produced, (*ii*)

discharged from storage, and (iii) purchased from the grid is equal to the sum of (i) the power charged to storage, (ii) the power sold to the grid from in-house production or storage, (iii) the power charged to storage directly from the grid, (iv) any additional power consumed by the electric chiller (where this is an additional term relative to the original model (\mathcal{R})), and (v) the electrical load on site. Constraint (B.3b) provides an analogous load-balancing requirement for hours in which the site is disconnected from the grid due to an outage (and contains the same additional term relative to the original model (\mathcal{R})). Constraint (B.3c) restricts charging of storage from grid production to the grid power purchased for each hour. Similarly, constraint (B.3d) restricts the sales from the electrical storage system to its rate of discharge in each time period. Constraints (B.3e) and (B.3f) restrict the annual energy sold to the grid at net-metering rates; only one of these is implemented in each case according to user-specified options. While a collection of pre-specified technologies may contribute to net-metering rates in both cases, constraint (B.3e) allows storage to contribute to net-metering while constraint (B.3f) does not.

B.1.4 Rate Tariff Constraints

Net Metering

$$\sum_{v \in \mathcal{V}} Z_v^{\text{nmil}} = 1 \quad (\text{B.4a})$$

$$\sum_{t \in \mathcal{T}_v} f_t^{\text{d}} \cdot X_t^{\sigma} \leq i_v^{\text{n}} \cdot Z_v^{\text{nmil}} \quad \forall v \in \mathcal{V} \quad (\text{B.4b})$$

$$\Delta \cdot \sum_{h \in \mathcal{H}^{\text{g}}} \left(\sum_{u \in \mathcal{U}^{\text{nm}}, t \in \mathcal{T}_u} X_{tuh}^{\text{ptg}} + \sum_{u \in \mathcal{U}^{\text{nm}} \cap \mathcal{U}^{\text{sb}}} X_{uh}^{\text{stg}} \right) \leq \Delta \cdot \sum_{u \in \mathcal{U}^{\text{p}}, h \in \mathcal{H}^{\text{g}}} X_{uh}^{\text{g}} \quad (\text{B.4c})$$

Constraint (B.4a) limits the net metering to a single regime at a time. Constraint (B.4b) restricts the sum of the power rating of all technologies to be less than or equal to the net metering regime. Constraint (B.4c) ensures that energy sales at net-metering rates do not exceed the energy purchased from the grid.

Monthly Total Demand Charges

$$\Delta \cdot \sum_{h \in \mathcal{H}_m} X_{uh}^g \leq \bar{\delta}_u^{\text{tu}} \cdot Z_{mu}^{\text{ut}} \quad \forall m \in \mathcal{M}, u \in \mathcal{U}^{\text{P}} \quad (\text{B.5a})$$

$$Z_{mu}^{\text{ut}} \leq Z_{m,u-1}^{\text{ut}} \quad \forall u \in \mathcal{U}^{\text{P}} : u \geq 2, m \in \mathcal{M} \quad (\text{B.5b})$$

$$\bar{\delta}_{u-1}^{\text{tu}} \cdot Z_{mu}^{\text{ut}} \leq \Delta \cdot \sum_{h \in \mathcal{H}_m} X_{u-1,h}^g \quad \forall u \in \mathcal{U}^{\text{P}} : u \geq 2, m \in \mathcal{M} \quad (\text{B.5c})$$

Constraint (B.5a) limits the quantity of electrical energy purchased from the grid in a given month from a specified pricing tier to the maximum available. Constraint (B.5b) forces pricing tiers to be charged in a specific order, and constraint (B.5c) forces one pricing tier's purchases to be at capacity if any charges are applied to the next tier.

Peak Power Demand Charges: Months

$$X_{mn}^{\text{dn}} \leq \bar{\delta}_n^{\text{mt}} \cdot Z_{mn}^{\text{dmt}} \quad \forall n \in \mathcal{N}, m \in \mathcal{M} \quad (\text{B.6a})$$

$$Z_{mn}^{\text{dmt}} \leq Z_{m,n-1}^{\text{dmt}} \quad \forall n \in \mathcal{N} : n \geq 2, m \in \mathcal{M} \quad (\text{B.6b})$$

$$\bar{\delta}_{n-1}^{\text{mt}} \cdot Z_{mn}^{\text{dmt}} \leq X_{m,n-1}^{\text{dn}} \quad \forall n \in \mathcal{N} : n \geq 2, m \in \mathcal{M} \quad (\text{B.6c})$$

$$\sum_{n \in \mathcal{N}} X_{mn}^{\text{dn}} \geq \sum_{u \in \mathcal{U}^{\text{P}}} X_{uh}^g \quad \forall m \in \mathcal{M}, h \in \mathcal{H}_m \quad (\text{B.6d})$$

Constraint (B.6a) limits the energy demand allocated to each tier to no more than the maximum demand allowed. Constraint (B.6b) forces monthly demand tiers to become active in a prespecified order. Constraint (B.6c) forces demand to be met in one tier before the next demand tier. Constraint (B.6d) defines the peak demand to be greater than or equal to all of the demands across the time horizon, where an equality is actually induced by the sense of the objective function. A user-defined option precludes CHP technology production from reducing peak demand; if selected, constraint (B.6d) becomes:

$$\sum_{n \in \mathcal{N}} X_{mn}^{\text{dn}} \geq \sum_{u \in \mathcal{U}^{\text{P}}} X_{uh}^g + \sum_{t \in \mathcal{T}^{\text{CHP}}} \left(f_{th}^{\text{p}} \cdot f_t^{\text{l}} \cdot X_{th}^{\text{rp}} - \sum_{b \in \mathcal{B}^{\text{h}}} X_{bth}^{\text{pts}} - \sum_{u \in \mathcal{U}_i^{\text{s}}} X_{tuh}^{\text{ptg}} \right) \quad \forall m \in \mathcal{M}, h \in \mathcal{H}_m$$

Peak Power Demand Charges: Time-of-Use Demand and Ratchet Charges

$$X_{de}^{\text{de}} \leq \bar{\delta}_e^{\text{t}} \cdot Z_{de}^{\text{dt}} \quad \forall e \in \mathcal{E}, d \in \mathcal{D} \quad (\text{B.7a})$$

$$Z_{de}^{\text{dt}} \leq Z_{d,e-1}^{\text{dt}} \quad \forall e \in \mathcal{E} : e \geq 2, d \in \mathcal{D} \quad (\text{B.7b})$$

$$\bar{\delta}_{e-1}^{\text{t}} \cdot Z_{de}^{\text{dt}} \leq X_{d,e-1}^{\text{de}} \quad \forall e \in \mathcal{E} : e \geq 2, d \in \mathcal{D} \quad (\text{B.7c})$$

$$\sum_{e \in \mathcal{E}} X_{de}^{\text{de}} \geq \max \left\{ \sum_{u \in \mathcal{U}^{\text{p}}} X_{uh}^{\text{g}}, \delta^{\text{lp}} \cdot X^{\text{plb}} \right\} \quad \forall d \in \mathcal{D}, h \in \mathcal{H}_d \quad (\text{B.7d})$$

$$X^{\text{plb}} \geq \sum_{n \in \mathcal{N}} X_{mn}^{\text{dn}} \quad \forall m \in \mathcal{M}^{\text{lb}} \quad (\text{B.7e})$$

Constraints (B.7a)-(B.7d) correspond to constraints (B.6a)-(B.6d), respectively, but pertain to a type of charge not related to monthly use, but rather to time of use within a month. These *ratchet charges* are implemented using constraints (B.7d). The charge applied for each time-of-use period is a linearizable function of the greater of the peak electrical demand during that period (as given by the first term on the right-hand side of (B.7d)) and a fraction of the peak demand that occurs over a collection of months (known as *look-back months*) during the year (as given by the second term on the right-hand side of (B.7d)). Constraint (B.7e) ensures the peak demand over the set of look-back months is no lower than the peak demand for each look-back month. In this way, charges are based not only on use in a given month, but also on a fraction of use over the last several months, and becomes relevant when this latter use is high relative to current use. If CHP technologies are not allowed to reduce peak demand, constraint (B.7d) becomes:

$$\sum_{e \in \mathcal{E}} X_{de}^{\text{de}} \geq \sum_{u \in \mathcal{U}^{\text{p}}} X_{uh}^{\text{g}} + \sum_{t \in \mathcal{T}^{\text{CHP}}} \left(f_{th}^{\text{p}} \cdot f_t^{\text{l}} \cdot X_{th}^{\text{rp}} - \sum_{b \in \mathcal{B}^{\text{h}}} X_{bth}^{\text{pts}} - \sum_{u \in \mathcal{U}_t^{\text{s}}} X_{tuh}^{\text{ptg}} \right) \quad \forall d \in \mathcal{D}, h \in \mathcal{H}_d$$

B.1.5 Minimum Utility Charge

$$X^{\text{mc}} \geq c^{\text{amc}} - \underbrace{\left(\Delta \cdot \sum_{u \in \mathcal{U}^{\text{p}}, h \in \mathcal{H}^{\text{g}}} c_{uh}^{\text{g}} \cdot X_{uh}^{\text{g}} \right)}_{\text{Grid Energy Charges}} + \underbrace{\sum_{d \in \mathcal{D}, e \in \mathcal{E}} c_{de}^{\text{r}} \cdot X_{de}^{\text{de}}}_{\text{Time-of-Use Demand Charges}} + \underbrace{\sum_{m \in \mathcal{M}, n \in \mathcal{N}} c_{mn}^{\text{rm}} \cdot X_{mn}^{\text{dn}}}_{\text{Monthly Demand Charges}} -$$

$$\Delta \cdot \underbrace{\left(\sum_{h \in \mathcal{H}^g} \left(\sum_{u \in \mathcal{U}^{sb}} c_{uh}^e \cdot X_{uh}^{stg} + \sum_{t \in \mathcal{T}, u \in \mathcal{U}_t^s} c_{uh}^e \cdot X_{tuh}^{ptg} \right) \right)}_{\text{Energy Export Payment}} \quad (\text{B.8})$$

Constraint (B.8) enforces a minimum payment to the utility provider, which is a fixed constant less charges incurred from grid energy, time-of-use demand and monthly demand payments, plus sales from exports to the grid.

B.1.6 Non-negativity

$$X^{plb}, X^{mc} \geq 0 \quad (\text{B.9a})$$

$$X_t^\sigma, X_t^{pi} \geq 0 \quad \forall t \in \mathcal{T} \quad (\text{B.9b})$$

$$X_{tuh}^{ptg} \geq 0 \quad \forall u \in \mathcal{U}, t \in \mathcal{T}_u, h \in \mathcal{H} \quad (\text{B.9c})$$

$$X_{uh}^{stg}, X_{uh}^g \geq 0 \quad \forall u \in \mathcal{U}, h \in \mathcal{H} \quad (\text{B.9d})$$

$$X_{de}^{de} \geq 0 \quad \forall d \in \mathcal{D}, e \in \mathcal{E} \quad (\text{B.9e})$$

$$X_{mn}^{dn} \geq 0 \quad \forall m \in \mathcal{M}, n \in \mathcal{N} \quad (\text{B.9f})$$

$$X_h^{gts} \geq 0 \quad h \in \mathcal{H} \quad (\text{B.9g})$$

$$X_b^{bkW}, X_b^{bkWh} \geq 0 \quad b \in \mathcal{B} \quad (\text{B.9h})$$

$$X_{tks}^{\sigma s} \geq 0 \quad \forall t \in \mathcal{T}, k \in \mathcal{K}, s \in \mathcal{S}_{tk} \quad (\text{B.9i})$$

$$X_{bth}^{pts} \geq 0 \quad \forall b \in \mathcal{B}, t \in \mathcal{T}, h \in \mathcal{H} \quad (\text{B.9j})$$

$$X_{bh}^{se}, X_{bh}^{dfs} \geq 0 \quad \forall b \in \mathcal{B}, h \in \mathcal{H} \quad (\text{B.9k})$$

$$X_{th}^{rp}, X_{th}^f, X_{th}^{fb}, X_{th}^{tpb}, X_{th}^{tp}, X_{th}^{ptw} \geq 0 \quad \forall t \in \mathcal{T}, h \in \mathcal{H} \quad (\text{B.9l})$$

B.1.7 Integrality

$$Z_v^{nmil} \in \{0, 1\} \quad \forall v \in \mathcal{V} \quad (\text{B.10a})$$

$$Z_{tks}^{\sigma s} \in \{0, 1\} \quad \forall t \in \mathcal{T}, k \in \mathcal{K}, s \in \mathcal{S}_{tk} \quad (\text{B.10b})$$

$$Z_t^{pi} \in \{0, 1\} \quad \forall t \in \mathcal{T} \quad (\text{B.10c})$$

$$Z_{th}^{\text{to}} \in \{0, 1\} \quad \forall t \in \mathcal{T}, h \in \mathcal{H} \quad (\text{B.10d})$$

$$Z_{de}^{\text{dt}} \in \{0, 1\} \quad \forall d \in \mathcal{D}, e \in \mathcal{E} \quad (\text{B.10e})$$

$$Z_{mn}^{\text{dmt}} \in \{0, 1\} \quad \forall m \in \mathcal{M}, n \in \mathcal{N} \quad (\text{B.10f})$$

$$Z_{mu}^{\text{ut}} \in \{0, 1\} \quad \forall m \in \mathcal{M}, u \in \mathcal{U} \quad (\text{B.10g})$$

Finally, constraints (B.9) ensure all of the variables in our formulation assume non-negative values. In addition to non-negativity restrictions, constraints (B.10) establish the integrality of the appropriate variables.

APPENDIX C

NECESSARY PERMISSIONS FOR REPRODUCTION

C.1 Image Permissions

Permission to Use Images for Dissertation and Academic Journal Article ✕ 🖨️ 📄

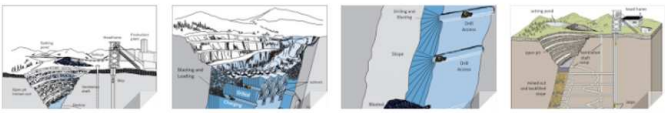
Oluwaseun Ogunmodede
to tomas.vilen 📧 Thu, Feb 25, 11:38 AM ☆ ↶ ⋮

Hello Tomas,

I am a Ph.D. candidate at the Colorado School of Mines and I came across these images attached. May I please ask for permission to use them in my dissertation and academic journal that I plan on submitting soon? If so, how would you like me to cite and reference the images? I hope to hear from you soon.

Thanks,
Oluwaseun Ogunmodede

4 Attachments 📎 🔄



Tomas Vilen
to me Thu, Feb 25, 11:57 PM ☆ ↶ ⋮

God Morning

And thank's for asking Oluwaseun, if you use them with a reference it is okay

Good luck and have a nice day

Best regards,

Tomas Vilen
R&D Fagersta

Epiroc

Rock Drilling Tools division
Epiroc Drilling Tools AB

Figure C.1: Permission granted for Figures 4.1, 4.2a, and 4.2b by Epiroc

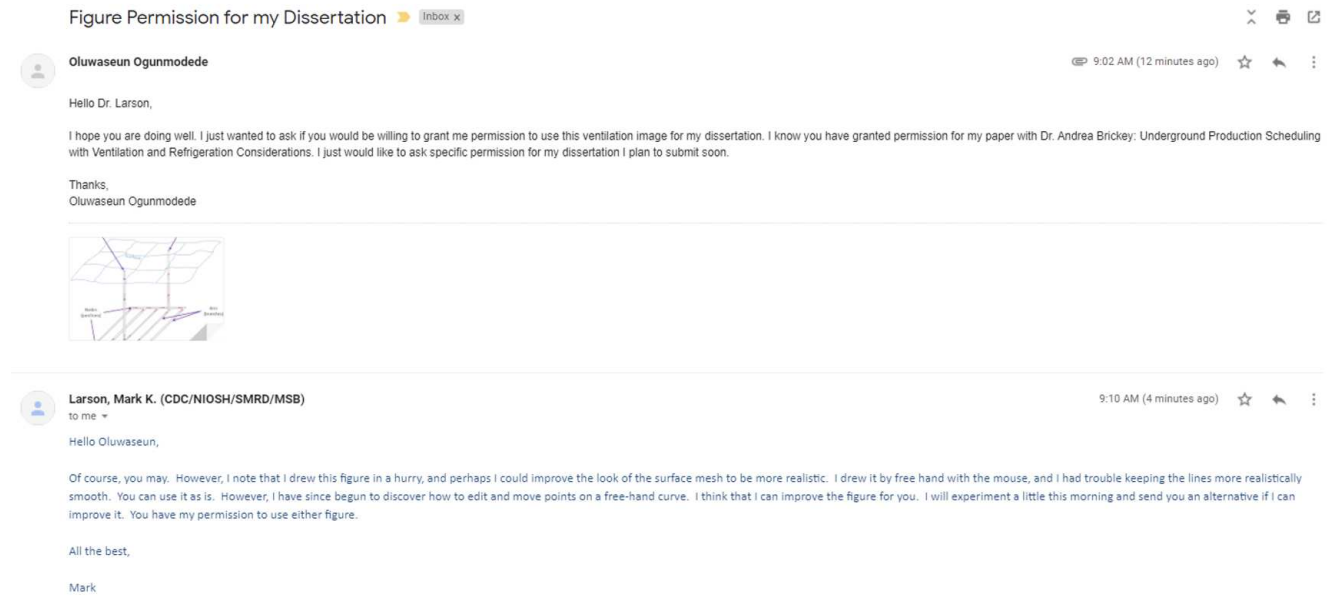


Figure C.2: Permission granted for Figure 4.3 by Dr. Mark Larson

C.2 Co-Author Permissions

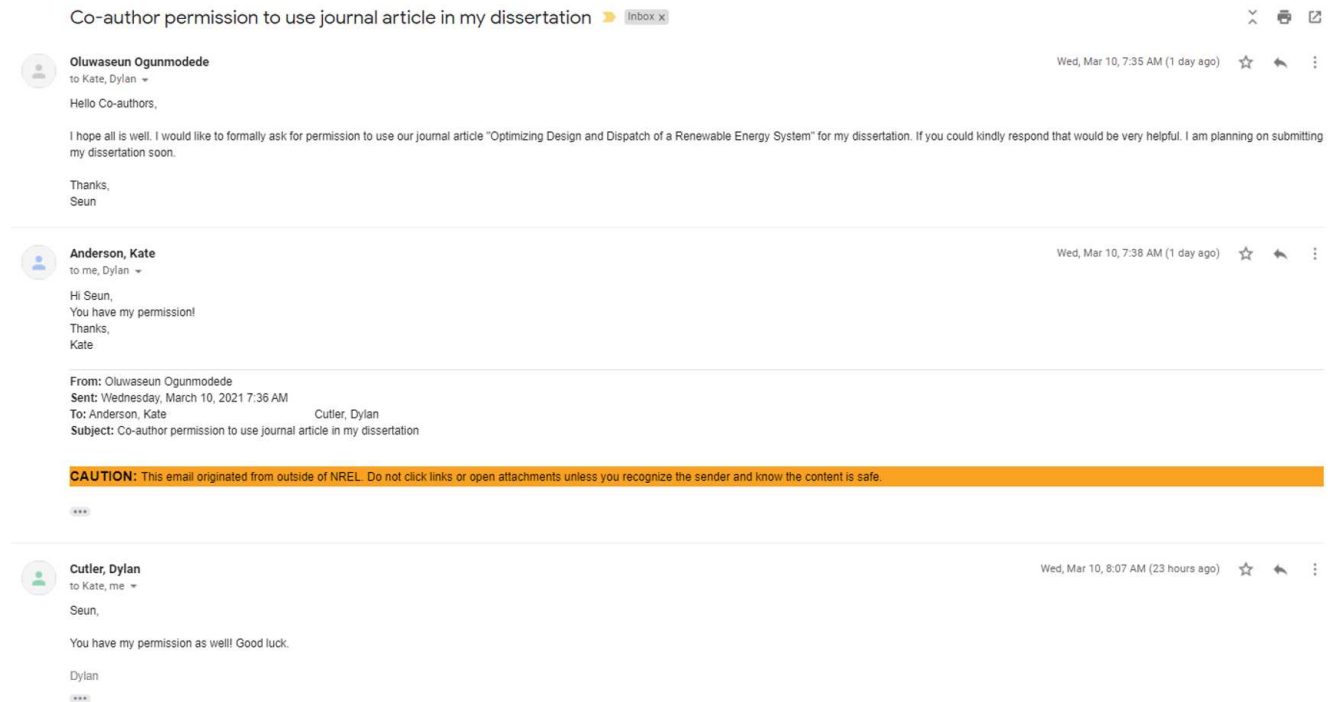


Figure C.3: Permission granted for use of Chapter 2 by co-authors Kate Anderson and Dylan Cutler



Figure C.4: Permission granted for use of Chapter 3 by co-authors Dr. Alexander Zolan and Jusse Hirwa

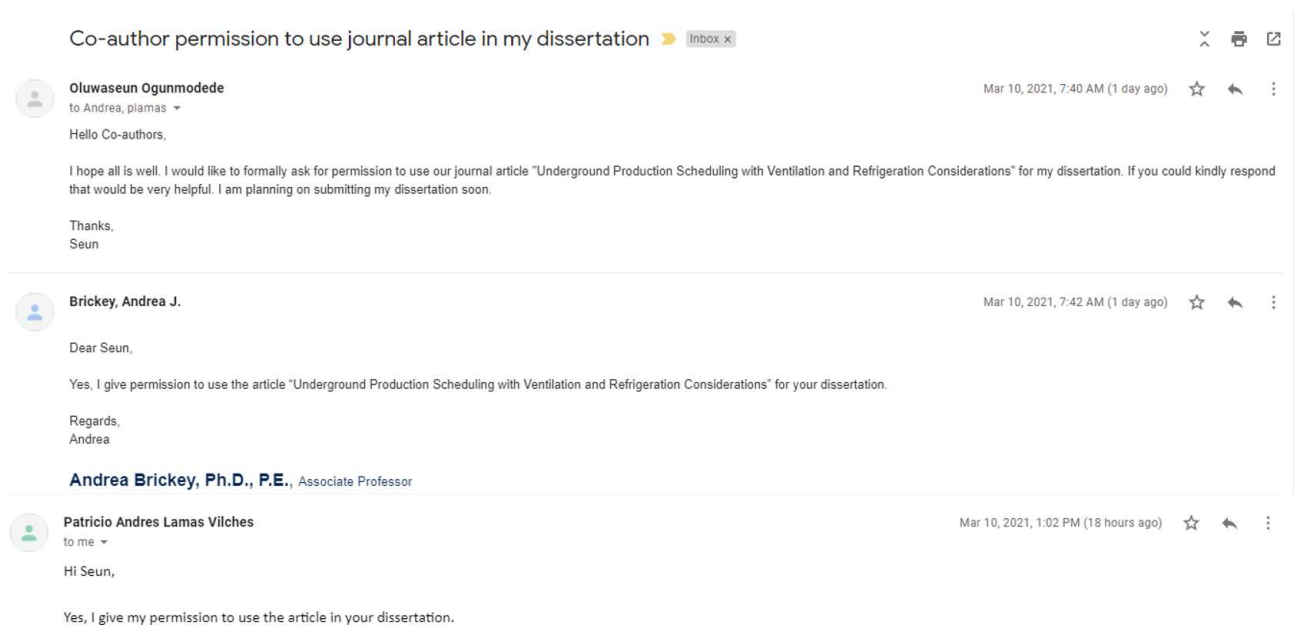



Figure C.5: Permission granted for use of Chapter 4 by co-authors Dr. Andrea Brickey and Patricio Lamas

C.3 Publisher Permissions



APPLIED ENERGY

Optimizing design and dispatch of a renewable energy system
Author: Oluwaseun Ogunmodede, Kate Anderson, Dylan Cutler, Alexandra Newman
Publication: Applied Energy
Publisher: Elsevier
Date: 1 April 2021
© 2021 Elsevier Ltd. All rights reserved.

Journal Author Rights

Please note that, as the author of this Elsevier article, you retain the right to include it in a thesis or dissertation, provided it is not published commercially. Permission is not required, but please ensure that you reference the journal as the original source. For more information on this and on your other retained rights, please visit: <https://www.elsevier.com/about/our-business/policies/copyright#Author-rights>

Figure C.6: Permission not required for use of Chapter 2 by Publisher Elsevier